



Chair of Drilling and Completion Engineering

Master's Thesis



Real-Time Monitoring of Cement  
Hydration to Verify TOC and Well  
Integrity

Elisabeth Csar, BSc

September 2019



## EIDESSTATTLICHE ERKLÄRUNG

Ich erkläre an Eides statt, dass ich diese Arbeit selbständig verfasst, andere als die angegebenen Quellen und Hilfsmittel nicht benutzt, und mich auch sonst keiner unerlaubten Hilfsmittel bedient habe.

Ich erkläre, dass ich die Richtlinien des Senats der Montanuniversität Leoben zu "Gute wissenschaftliche Praxis" gelesen, verstanden und befolgt habe.

Weiters erkläre ich, dass die elektronische und gedruckte Version der eingereichten wissenschaftlichen Abschlussarbeit formal und inhaltlich identisch sind.

Datum 10.09.2019

Elisabeth Csar

Unterschrift Verfasser/in  
Elisabeth, Csar  
Matrikelnummer: 01235381



# Abstract

Primary cementing is critical to zonal isolation and well integrity. Besides, cement plugs are used for several operations in the oil and gas industry, such as lost circulation control, formation testing, directional/sidetrack drilling, zonal isolation, and well abandonment. Set cement may be too soft or not in the planned location and hence fail to provide hydraulic seal and lead to well integrity and safety issues. This could be due to a number of issues, including contamination with wellbore fluids, ineffective displacement, and casing eccentricity.

This thesis focuses on continuous monitoring real-time data during the hydration process of cement to be able to determine the phase of hydration process, to define the exact location of the cement, to establish contaminated parts of cement and prove a competent/imperfect well barrier.

Electrical conductivity measurements could be an indication of how the cement slurry is hydrating and the degree of contamination. Several tests with different levels of mud contamination were performed and analyzed. In addition, experiments with fiber-optic sensing to measure strain and temperature changes during cement slurry hydration were conducted. Both the electrical conductivity and fiber-optic measurements are able to identify degree of hydration and also level of contamination. The lab setup, test procedure, data, analysis, and results are presented and discussed. These measurements, analysis, and application would significantly improve the accuracy of cement jobs, and operational performance in the oil and gas industry.

Benefits to the industry from continuous monitoring and evaluation are discussed. In addition, recommendations for future work and conclusions can be found in the last chapter of the thesis.



# Zusammenfassung

Die primäre Zementierung ist für die zonale Isolation und die Integrität der Bohrlöcher von entscheidender Bedeutung. Darüber hinaus werden Zementbrücken für verschiedene Vorgänge in der Öl- und Gasindustrie verwendet, wie z.B. für die Kontrolle bei Zirkulationsverlust, Formationsprüfungen, Richtungs-/Ablenkungsbohrungen, zonale Isolation und für die Stilllegung von Bohrlöchern. Ausgehärteter Zement ist möglicherweise zu weich oder nicht an der geplanten Stelle und bietet daher keine hydraulische Abdichtung und kann deshalb zu Problemen mit der Integrität und Sicherheit des Bohrloches führen. Dies könnte auf eine Reihe von Problemen zurückzuführen sein, wie zum Beispiel Kontamination durch Bohrlochflüssigkeiten, erfolglose Flüssigkeitsverdrängung und Rohrexzentrizität.

Diese Arbeit befasst sich mit der kontinuierlichen Überwachung von Echtzeitdaten während des Aushärtungsprozesses von Zement, um die Phase des Hydratationsprozesses zu bestimmen, die genaue Position des Zements zu definieren, kontaminierte Zementteile festzustellen und eine fehlerlose/unvollständige Bohrlochsperrung nachzuweisen.

Messungen der elektrischen Leitfähigkeit könnten Aufschluss über die Hydratisierung und Verunreinigung des Zements geben. Es wurden mehrere Tests mit unterschiedlichem Verschmutzungsgrad durchgeführt und analysiert. Zusätzlich wurden Experimente mit Glasfasertechnik zur Messung von Dehnungs- und Temperaturänderungen während der Hydratation von Zement durchgeführt. Sowohl die elektrische Leitfähigkeit als auch die faseroptischen Messungen sind in der Lage, den Hydratationsgrad und den Verschmutzungsgrad zu bestimmen. Der Laboraufbau, das Testverfahren, die Daten, die Analysen und die Ergebnisse werden vorgestellt und diskutiert. Diese Messungen, Analysen und Anwendungen würden die Genauigkeit von Zementbrücken und die Unternehmensleistung in der Öl- und Gasindustrie erheblich verbessern.

Die Vorteile einer kontinuierlichen Überwachung und Evaluierung für die Industrie werden erörtert. Empfehlungen für zukünftige Arbeiten und Schlussfolgerungen befinden sich im letzten Kapitel der Arbeit.





# Acknowledgements

I would like to acknowledge everyone who played a role in my academic accomplishments. First of all, I would like to reward my gratitude to my supervisor and mentor at the Mining University of Leoben, Univ.-Prof. MBA PhD Ravi Krishna for his support, guidance and patient advices throughout the research process and also to my parents and friends, who supported me with love and understanding throughout the entire duration of my study. Without you, I could never have reached this current level of success.

Thank you all for your unwavering support!

*Glück Auf!*



# Contents

<b>Chapter 1 Introduction</b> .....	<b>1</b>
<b>Chapter 2 Off-Bottom Cement Plugs</b> .....	<b>3</b>
2.1 Setting procedure .....	3
2.2 Reasons for installing a cement plug.....	5
2.2.1 Lost circulation control .....	6
2.2.2 Sidetracking and directional drilling .....	7
2.2.3 Testing operations .....	8
2.2.4 Well control .....	9
2.2.5 Wellbore stability .....	9
2.2.6 Well or zone abandonment .....	9
<b>Chapter 3 The Challenge</b> .....	<b>11</b>
3.1 Contamination of cement slurry .....	12
3.1.1 Improper well fluid removal.....	13
3.1.2 Insufficient slurry volume .....	13
3.1.3 Poor job execution.....	14
3.1.4 Poor slurry design .....	14
3.1.5 Incorrect well parameter.....	14
3.2 Project objectives .....	14
<b>Chapter 4 Fiber Optic Cable</b> .....	<b>15</b>
4.1 Structure of fiber-optics.....	15
4.2 How fiber-optics work .....	16
4.2.1 Types of fiber-optic cables .....	17
4.2.2 Temperature and strain measurement .....	18
4.3 Applications of fiber-optic sensors by TU Graz.....	20
<b>Chapter 5 Portland Cement</b> .....	<b>23</b>
5.1 Phenomenology of cement hydration .....	23
5.1.1 The five main phases of hydration.....	23
5.1.2 Electrical resistivity/conductivity of a concrete.....	26
5.1.3 Shrinkage of concrete .....	28
<b>Chapter 6 Experiments</b> .....	<b>29</b>
6.1 Experiment 1: Resistivity measurement of a concrete .....	29

Contents

- 6.1.1 Equipment..... 29
- 6.1.2 Experiment setup ..... 30
- 6.2 Experiment 2: Different mud-cement ratios ..... 35
  - 6.2.1 Equipment..... 36
  - 6.2.2 Slurry design..... 43
  - 6.2.3 Experiment 2.1: 100% Cement slurry ..... 47
  - 6.2.4 Experiment 2.2: 100% cement slurry + 0,6% of cement mass starch..... 48
  - 6.2.5 Experiment 2.3: 90% Cement slurry + 10% Mud ..... 50
  - 6.2.6 Experiment 2.4: 70% cement slurry + 30% mud..... 51
  - 6.2.7 Experiment 2.5: 50% cement slurry + 50% mud..... 52
  - 6.2.8 Experiment 2.6: 30% cement slurry + 70% mud..... 54
  - 6.2.9 Experiment 2.7: 10% cement slurry + 90% mud..... 55
  - 6.2.10 Experiment 2.8: 100% mud ..... 56
  - 6.2.11 Result ..... 57
- 6.3 Experiment 3: Fiber optic cable measurement ..... 59
  - 6.3.1 Equipment..... 59
  - 6.3.2 Experiment 3.1: Stable base fluid – competent cement plug ..... 62
  - 6.3.3 Experiment 3.2: Unstable base fluid – contaminated cement plug ..... 77
- Chapter 7 Recommendations for future work ..... 89**
- Chapter 8 Conclusion ..... 91**

# Chapter 1 Introduction

Pumping slurry of cement needed additives and water down the casing, tubing or drill pipe to a predetermined spot in the well is defined as a well-cementing operation. There are two main categories named primary cementing and remedial cementing, whereby each process fulfills a different function.

Primary cementing operation is performed immediately after the casing is in place, whereas remedial cementing includes any other cement operations performed either during drilling operation or during the production period.

The main purpose of primary cementing operations is to provide zonal isolation between subsurface formations, to prevent fluid migration between different zones, to hold the casing in place and to bond, protect and support the casing. Whereas remedial cementing refers to the two following broad categories:

- Squeeze cementing
- Plug cementing

The second case will be discussed in detail since my thesis focuses on off-bottom cement plugs (OBCP).

(“Cementing Operations -” 2018),(Narendra Kumar Dewangan 2015)

According to a case study from Halliburton, problems related to cement plugs are the fifth most important influencing factor on hours spent on non-productive time (NPT). Hence, increasing the success rate of cement plugs would be a possibility to decrease NPT significantly.

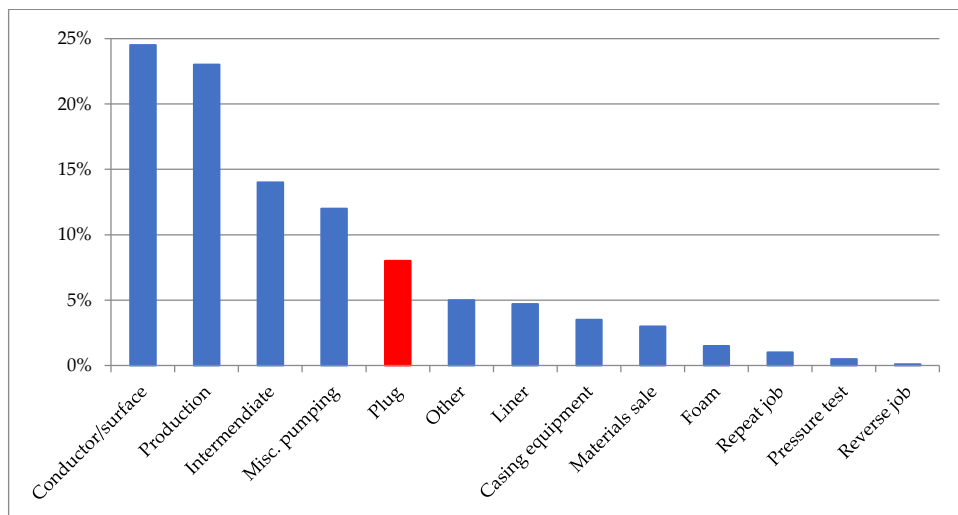


Figure 1: NPT hours for several operations (Souza, Sasso, and Munoz 2017)

## Introduction

Already many studies have been done to improve the success rate of cement plugs on the first attempt.

My studies focus on continuous monitoring parameters which are significantly changing during the hydration process of cement to determine the phase of hydration process, to define the exact location of the cement, to establish contaminated parts of cement and in the end to prove a competent/imperfect well barrier.

After intensive research and discussions, conductivity, temperature, and strain were selected to be monitored. Application of electrical conductivity measurements for quality control during cement slurry placement, curing and beyond could characterize the quality of the cement. Moreover, fiber-optic sensing could substantially improve the accuracy of cement plugs, and operational performance in the oil and gas industry since the provided real-time data, and the information give a deep insight into the real-time operations and predictive modeling. These measurements will provide long term monitoring and therefore assure safety, well integrity, and environmental protection. Finally, the well could be ultimately abandoned and furthermore, time would be saved, which decreases the costs significantly.

The thesis covers a detailed literature review with the focus on the necessity of cement plug and reasons for cement plug contamination. Moreover, the function and application of fiber-optics are discussed. To be able to interpret the results of the experiments, the phenomenology of cement hydration is reviewed. For the experimental part, the change in conductivity of different contaminated cement samples was measured and compared. Afterward, tests with fiber-optic sensors to monitor temperature and strain changes were performed.

## Chapter 2 Off-Bottom Cement Plugs

The remedial cementing technique, known as plug cementing, refers to the method of placing the cement slurry across a selected interval in an open or cased hole to create a reliable wellbore seal or “plug”. The purpose is to inhibit fluid communication, either between a formation and the surface or between different layers. Therefore, the mechanic and hydraulic seal must be guaranteed.

In addition, to the crucial well parameters required to perform a primary cement job including depth, wellbore geometry, temperature, formation pressure, formation characteristics, fluid properties, fluid mechanics and chemistry influence, further factors such as displacement efficiency, slurry stability, and fluid compatibilities have to be considered for a proper cement plug design.

(Salahub and Ripley 1980), (“Preview-Ceme.Pdf” n.d.), (“Remedial Cementing -” 2015), (Narendra Kumar Dewangan 2015)

### 2.1 Setting procedure

The balanced cement plug method based on the concept of balanced hydrostatic is the most common technique to install an off-bottom cement plug. This operation requires equilibrium between the hydrostatic pressure at the end of the cement string and the hydrostatic pressure in the annulus.

The necessary volume to balance hydrostatic for both sides must be calculated based on the well schematic, pipe’s dimensions, open hole or casing size and height of cement plug. As can be seen in Figure 2, it is necessary to under displace a few barrels to allow the cement to migrate down during pulling out of the hole, which as well reduces the risk of swabbing effect.

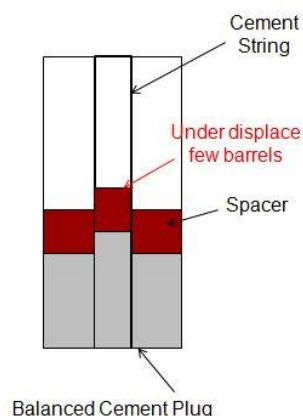


Figure 2: Under displaced balanced cement plug (DrillingFormulas.Com | 2011)

Setting procedure

The depth of a cement plug depends on specific parameters such as the type of job, required height to meet specifications and on the operator experience. The length can vary from a few hundred feet to several hundred feet. A small stinger is recommended as the swabbing effect will be minimized.

The standard procedure to set a cement plug requires pumping a spacer or chemical wash ahead of and behind the cement slurry. For the plug base, the cementing string, also known as cement stinger, has to be lowered to the desired depth. Afterward, spacer, cement slurry and again spacer will be pumped one after another. Finally, the stinger can be slowly pulled out, and the excess cement can reverse out.

Unfortunately, this procedure cannot be performed when an off-bottom cement plug is required as no solid base, which supports the cement's weight, is present. Therefore the biggest challenge for installing an off-bottom cement plug is the heavier cement compared to the mud. According to physics, the denser slurry on the top will always tend to migrate through the lighter fluid beneath. Therefore, the densities of the two liquids should not differ too much to guarantee success. A stable mud-cement interface is as well fundamental to prevent mixing of liquids. If the resistance of the cement slurry is too low, it would diffuse with the mud and results in an incompetent plug which has to be replaced. Figure 3 shows an ideal case of an off-bottom cement plug compared to a failed plug due to unstable viscous pill base and lighter mud below.

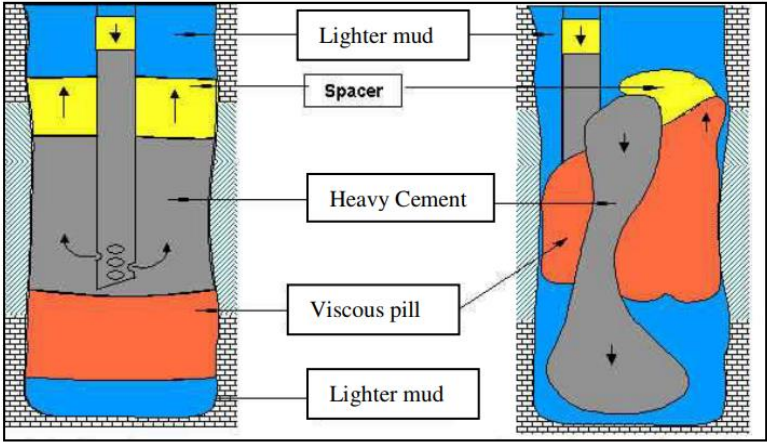


Figure 3: Ideal case of OBCP versus fluid mixing due to the unstable base and lighter mud underneath (N. Gupta, Bogaerts, and Arshad 2014)

This problem is less critical in deviated wells, although the length of the competent cement is reduced because of the presence of slump angle. Usually, the first attempt fails and builds the base for the second try, which will lead to increasing non-productive time.



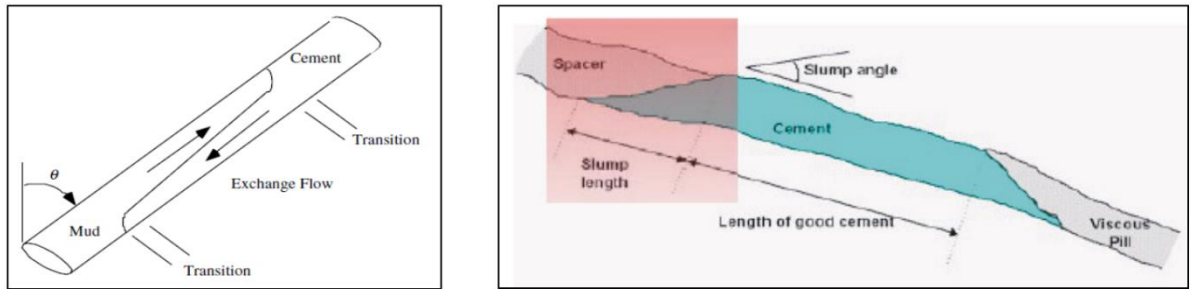


Figure 4: OBCP in deviated well –reduced effective length of competent cement and slump angle (N. Gupta, Bogaerts, and Arshad 2014)

To avoid fluid contamination and failure of off-bottom cement plugs, it is crucial to pump a base fluid before pumping spacer and cement slurry. For instance, a usual base for OBCP is a high viscous pill which consists of a mixture of water and a substance that thickens it. The additive is usually bentonite but could also be any suitable material such as cellulose, potato, or oatmeal. A viscous fluid can support the solids in the cement and hence creates the base for the cement slurry.

The stinger will be lowered beneath the planned bottom depth of the plug, and the viscous pill will be pumped to install a cement plug. Afterward, the operation follows the typical procedure of setting a balanced cement plug. Attention must be paid since the more viscous the fluid, the more difficult to pump.

Other methods like reactive chemical pills, more substantial fluid below the cement, bridge plugs, expandable packers, or cement support tool can as well be utilized as a base. The most common method is using a viscous pill as a base since trajectory, space, cost, and the absence of a casing limit the usage of mechanical devices.

The optimum length of a cement plug is critical to define. A too-short plug would increase the possibility of cement contamination. On the other hand, a too-long plug would induce the risk of suck pipe.

The setting of an off-bottom cement plug is often considered as one of the simplest operations performed on a well. Unfortunately, a competent cement plug that satisfies the required conditions at the first attempt is not often obtained.

(DrillingFormulas.Com | 2011),("Balanced-Plug Method. Basic Calculations" 2019),(N. Gupta, Bogaerts, and Arshad 2014),(Harestad 2018)

## 2.2 Reasons for installing a cement plug

There are various reasons why setting a cement plug is necessary for the oil and gas industry such as lost circulation control, sidetracking/directional drilling, formation testing, well control, wellbore stability, zonal isolation, and plug and abandonment.

(Halliburton n.d.),(Salahub and Ripley 1980)

## 2.2.1 Lost circulation control

The uncontrolled flow of partial or complete drilling fluid into the surrounding formation during drilling operations and therefore a reduction or absence of fluid flow up the annulus is known as lost circulation. This phenomenon appears when the total formation pressure is less than the total exerted pressure against the formation. There are three classifications of lost circulation:

- **Seepage loss** will only affect the drilling operation slightly or not at all, as only a minimal volume, less than 20 bbl/hr [3 m<sup>3</sup>/hr], of drilling fluid enters the formation.
- **Partial loss** is indicated by a specific volume loss of the drilling mud into the formation, but some of the fluid still returns to the surface. Besides the loss of the mud, another challenge known as ballooning is induced by this phenomenon. However, partial losses will typically not result in a well control situation as fluid remains inside the borehole.
- **Total loss** is the most crucial scenario, as no drilling mud is returning to the surface. Thus, the whole volume of fluid enters the formation. The mud level inside the borehole will drop down to an unknown level, decreasing the hydrostatic pressure at the bottom, which can induce a kick and in the worst case can result in a blowout. As the hole will not be stabilized any longer formation breakouts and collapse of the well could also be a common consequence of a total loss problem.

Lost circulation zones can result from drilling-induced fractures by excessive downhole pressures, chemically induced formation instability, natural fractures, cavernous or high permeable formations.

(Mohan Doshi 2014),("Lost Circulation - Schlumberger Oilfield Glossary" n.d.),("Lost Circulation -" 2015),(DrillingFormulas.Com | 2014),(Fidan, Babadagli, and Kuru 2004)

In some cases, loss circulation materials (LCM) do not achieve to stop drilling fluid loss and are therefore not able to help regain full returns of the circulation fluids to surface. Hence, an alternative is to use cement plugs for non-producing zones.

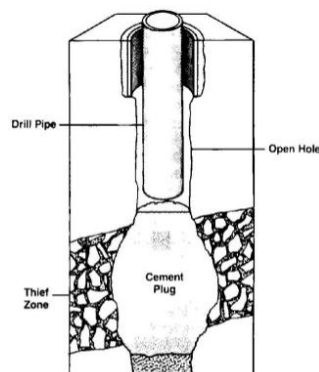


Figure 5: Cement plug at thief zone (Narendra Kumar Dewangan 2015)

The two conventional methods commonly used to seal loss circulation zones are the balanced plug method and the drift plug method. The main difference between these two procedures is the position of placing the cement slurry. The balanced plug method refers to spotting the cement into and above the loss zone compared to the drift plug method where the cement slurry is placed above the thief zone and will drift downwards as one single mass of cement as can be seen in Figure 6. After drilling back through the plug, the operation can finally continue.

(Ng'ang'a 2014),("Remedial Cementing -" 2015)

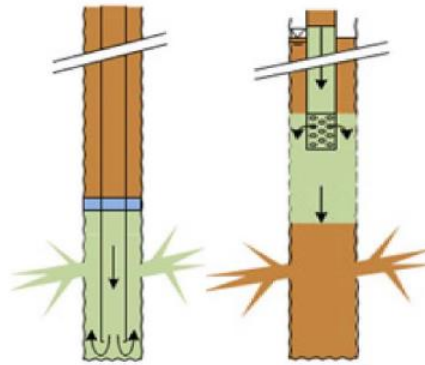


Figure 6: Balanced plug method and drift plug method (Ng'ang'a 2014)

## 2.2.2 Sidetracking and directional drilling

However, much more demanding are the stresses appearing on a cement plug for sidetracking, directional drilling or testing operations. These plugs, known as kick-off plugs, have to be harder than the formation since the bit will always focus on the path of least resistance. Commonly, open hole sidetracks are kicked off from such cement plugs.

During a drilling operation, it can be necessary to guide the drill bit in the desired direction due to unrecoverable stuck bottom hole assembly or to ensure that the drilling target is reached. Geological structures can as well require a sidetracking operation. For these reasons, a cement plug is installed to support the mechanical whipstock and thus initiate directional drilling.

(Salahub and Ripley 1980),(Ng'ang'a 2014),("Clear Directional - Tools" n.d.)

## Reasons for installing a cement plug

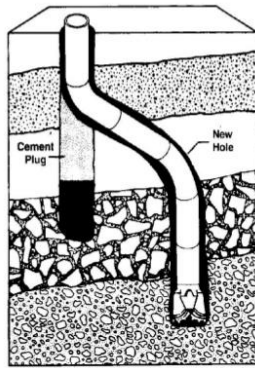


Figure 7: Cement plug for directional drilling and sidetracking/whipstocking  
(Narendra Kumar Dewangan 2015)

A pilot hole must be drilled to create space to install such a required kick-off plug. Once the pilot hole is drilled, a cement plug extending several meters above and below the KOP has to be installed. The cement often needs more than 24 hours to cure to assure a competent strength which must exceed the formation's compressive strength. As soon as the cement has set, a directional BHA is applied to kick off the well. The success of the operation depends on the reliability of the cement plug. Unfortunately, the cement integrity often fails and lead to a restart of the procedure which means drilling out the cement, tripping out of the hole, mixing a new cement slurry, setting a new plug, waiting for the fresh plug to set and try again to finally kick-off. All this requires additional time and will lead to increasing costs.

(Bruton et al. 2014)

### 2.2.3 Testing operations

Especially when the interval to be tested is considerably off the bottom, and other techniques of isolating the zone are not possible or feasible, a cement plug is necessary to create the base for open-hole formation test tools. Furthermore, a cement plug is required when only an individual section needs to be investigated.

(Halliburton n.d.),("Remedial Cementing -" 2015)

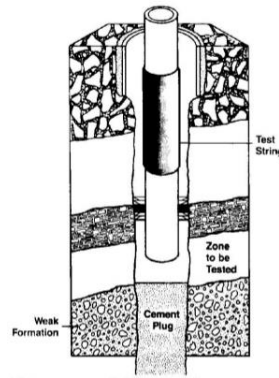


Figure 8: Cement plug for zonal isolation for testing operation (Narendra Kumar Dewangan 2015)

### 2.2.4 Well control

Another purpose of setting cement plugs is for well control operations. In case of no remaining margin between the pore and fracture pressure during the drilling, the drill string cannot be lifted without risk of causing an uncontrolled flow to the surface or a crossflow from a high pressured zone into a weak or low pressured area.

(“Remedial Cementing -” 2015)

### 2.2.5 Wellbore stability

In many cases, unstable formations result in breakouts or elliptical hole shapes during drilling. Hence, cement plugs can be installed to support formation integrity and near-wellbore stresses, which are subsequently drilled out. A cement sheath will be left in place to prevent further damage to the formation and to reconstruct the original shape and diameter of the well. The outcome will be a stabilized well with improved annular velocities.

(“Remedial Cementing -” 2015)

### 2.2.6 Well or zone abandonment

Necessities such as seal a dry hole, seal depleted zones, seal non-commercial zones or wellbores and temporary well or zone abandonment require cement plugging. The aim is to prevent any communication of fluids between two zones, especially hydrocarbon migration and drainage of freshwater into lower zones. Cement plugs for permeable zones need to observe special requirements, which vary for different areas.

(Salahub and Ripley 1980),(“Preview-Ceme.Pdf” n.d.)

Reasons for installing a cement plug

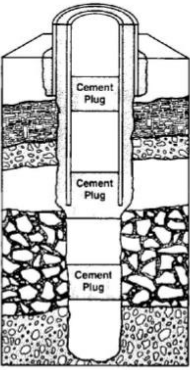


Figure 9: Cement plug for well abandonment (Narendra Kumar Dewangan 2015)

## Chapter 3 The Challenge

To keep the cement in the required place until it stopped migrating and formed a solid cement plug is the crucial challenge of setting an off-bottom cement plug. The transition period is the most critical period for gas migration since microchannels could be formed. The ideal case to prevent any contamination is a right angle setting cement which means the compressive strength increases rapidly and builds a 90° curve at a particular time.

There are various reasons why setting a cement plug off-bottom during or after a drilling operation could be necessary. However, it is widespread that the plug is not found where it is supposed to be. Contamination of the slurry can inhibit the cement from hardening and can impact the final position and lead to an unstable well barrier. In general, a proper cement barrier is often not discovered and leads to plug failures, even if the cement is in place. A reason for this is that many times no hydraulic seal can be achieved due to too soft cement plugs resulting from contaminated cement slurry. Thus, microchannels and cracks could be generated, leading to unwanted fluid migration. Besides the hydraulic seal failure, it is not possible to kick-off from a soft kick off plug as the cement in the wellbore should be harder to drill than the surroundings. Therefore enough hardening time must be provided to reach sufficient compressive strength before continuing with the sidetracking operation.

(Årebråt n.d.),(Salahub and Ripley 1980)

The oil and gas industry commonly uses the balanced cement plug method to install an off-bottom cement plug. Even though this procedure is already applied for decades and various reasons, it is still challenging. Installing a balanced off-bottom cement plug is known as one of the most unpredictable and time-consuming operations during drilling or plug and abandonment. This operation as well represents a considerable cost component and is particularly challenging compared to other cement jobs.

Based on research, the failure rate for the installation of a cement plug is very high; approximately only 25 % of cement plugs are set successfully at the first try. Usually, two or three attempts are necessary to provide a competent cement plug.

The statistics of setting cement plugs may be distorted as some companies may have different definitions on how to measure the success/failure rate. For example, sometimes the success is only measured by yes or no without considering the number of attempts and regardless of how many days were needed to meet the objective. To achieve a meaningful result, it is essential to measure the values based on a successful plug at first attempt.

If one takes into account that often ten to twenty consecutive plugs are required for one single sidetrack operation and each of them needs about eight hours hardening time this cement operation remains one of the most essential problems for the industry that has a great potential to be improved.

To avoid any incidents and future problems related to well integrity a perfect and intact well barrier is crucial. However, safety is not the only problem that plays an important role as well non-productive time will increase significantly. The necessity of performing one job twice or even more often require additional rig time and material which will than result in high costs.

(Harestad 2018),(Rommetvedt 2018)

### 3.1 Contamination of cement slurry

A well-recognized problem in the oil and gas industry is the placing of an off-bottom cement plug. The probability of success is high if the cement contamination is minimized. When the cement slurry is mixed with fluids like spacer, mud, or formation fluid, the cement is defined as contaminated. Since the setting properties such as thickening time and compressive strength development are affected, the time of waiting on cement (WOC) will be increased and can lead to an unstable cement plug that does not achieve well integrity anymore. In such cases, the operation has to be repeated.

In general, it is known that the contamination of cement is more severe when using oil-based mud (OBM) or synthetic-based mud (SBM).

The setting procedure of a balanced off-bottom cement plug is already described in the previous chapter. It is almost impossible to install a cement plug above a lighter fluid. Therefore, a viscous pill that works as a base will be pumped ahead. A common problem is the downward movement of the cement slurry as the denser fluid always tends to migrate downwards. The result of a failed base fluid can be seen in Figure 10. The heavier cement is moving down, and all the liquids will be mixed, the cement will be contaminated and prohibited to cure. The cement operation failed and has to be repeated.

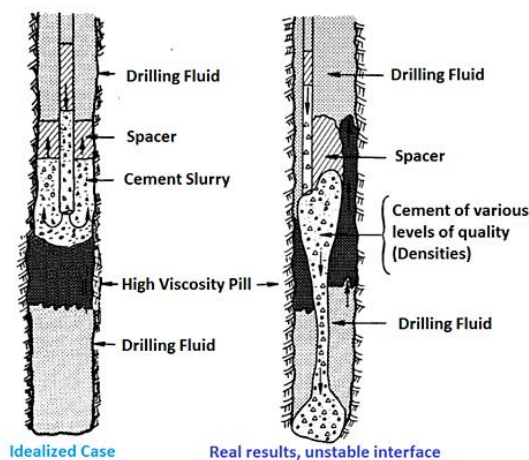


Figure 10: Downward movement of cement slurry (Diaz 2017)



Various reasons for cement contamination are discussed below.

(N. D. Gupta et al. 2014)

### 3.1.1 Improper well fluid removal

Spacers and flushes are useful displacement aids and always pumped ahead of the cement slurry and after the drilling fluid. The main objective of these fluids is to entirely displace the drilling fluid from the annulus and thereby prevent mixing of the drilling fluid with the cement slurry. Moreover, it is necessary to prepare the wellbore to receive cement to successfully achieve a hydraulic seal and zonal isolation. Hence, the surface must be cleaned to guarantee an adequate and proper bond between the cement and the surface of the casing or formation. For this purpose, flushes are used to disperse and thin drilling fluid particles.

Spacers and flushes can be designed for water-based or oil-based mud and play an essential role in successful cementing operations since already a thin layer of drilling fluid can prevent cement slurry from forming a good bond with the surroundings.

(“Spacers and Flushes - Halliburton” n.d.), (“Pre-Flushes and Spacers | Trican Well Service” n.d.), (“Spacers and Flushers in Cementing - PetroWiki” n.d.)

Improper well fluid removal induces the risk of a mud filter cake on the walls. It can result in channeling, which leads to cement contamination and causes problems in obtaining a competent hydraulic barrier. Therefore an impeccable well fluid removal over the whole planned setting interval is crucial to guarantee an intact cement plug.

Parameter such as hole quality, wellbore preparation, dogleg severity, fluid properties like rheology and density, the application of spacer and much more factors influence the well fluid removal and must be considered and optimized before the drilling and cementing job.

### 3.1.2 Insufficient slurry volume

Another common reason for cement plug failure is the use of inadequate slurry Volume. Even though running a caliper log before cementing operations is necessary to obtain accurate information about hole size and well path conditions, it is often not performed due to time and cost reasons. Without a caliper run, the required cement slurry volume cannot be estimated.

In case of not knowing the desired volume of cement, often a higher excess volumes of cement is pumped. This method is not reliable and frequently leads to cement plug failures.

### 3.1.3 Poor job execution

The job execution is essential for the operation and does not depend on the equipment used or how the activity is planned. Due to the small volumes compared to the present mud volume, the operator has to understand the hydraulics very well to install an excellent and successful cement plug. It is crucial that the operator pulls out of the hole (POOH) slowly while the stinger is inside the cement to prevent swabbing, which induces cement contamination due to the mixing of the fluids. Under displacing a few barrels of cement will as well avoid swabbing effect, allow pulling dry by enabling the cement to migrate downwards in the stinger during POOH.

### 3.1.4 Poor slurry design

The slurry design has to be performed individually and must fulfill all special requirements for each planned cement plug. Parameters such as thickening time, slurry pumping properties, and fluid loss properties can be adjusted by adding special additives. The main objective of a proper cement slurry design is to prevent cement contamination.

### 3.1.5 Incorrect well parameter

Supplying the laboratory with correct and accurate well parameters is the most crucial part of the cement operation. The previous tests in the laboratory under real conditions ensure the cement slurry performs as required. If the parameters used during the test in the laboratory differ from the real ones, the cement slurry will highly probable not be useful for the application. A common unwanted effect is often inhibition of the hydration process of the cement.

(Diaz 2017), (Årebråt n.d.), (N. D. Gupta et al. 2014)

## 3.2 Project objectives

Nowadays, there is no method available to continuously monitor meaningful parameters during the hydration process of the cement slurry. By collecting specific data, important decisions could be made earlier as contamination of cement could be detected after a short period. Moreover, an intact and perfect cement barrier could be proven by monitoring the hydration process.

Therefore the main objective of this master thesis is to evaluate meaningful parameters and find the best method to monitor these values.

As temperature, strain, and resistivity/conductivity changes are significantly affected by the hydration process of cement, these parameters were chosen to be monitored.

# Chapter 4 Fiber Optic Cable

In the 1950s, fiber cables were initially developed in the medical industry for endoscopes. About ten years later, engineers managed to transmit telephone calls with the use of this new technology. Nowadays, the application of fiber-optic cables becomes indispensable in our industry as they can carry massive amounts of information down a glass or plastic pipe at the speed of light. Furthermore, they can transmit data over long distances, provide reliability, save a lot of space, are immune to interference, and are relatively cheap. These days, the cables are used in a versatile range of application in various sectors and steadily replacing copper wires in terms of data transmission. For instance, they are applied at computer networks, broadcasting, medical scanning, automotive industry, lighting, and decorations, military equipment, and geotechnical monitoring.

(Woodford 2018),(FS.COM 2014),(jesseyang 2017)

## 4.1 Structure of fiber-optics

In Figure 11, components of a fiber-optic cable can be seen.

- The **core** is tiny (measured in microns) and transports the optical data signal. It is made up of one continuous strand of glass and is the physical component that includes the light transmission area of the fiber-optic.
- The **cladding** consists of a different type of glass compared to the core of providing a different refractive index. It is wrapped around the outside of the core and its primary purpose it is to create the necessary reflection to keep the light in the pipe.
- A thick plastic layer surrounding the cladding is known as the **coating**. It has the main function to protect the fiber core.
- To prevent the core against damage during installation or from being crushed, **strengthening fibers** cover the coating.
- The **outer jacket** exists as well for protection purpose and represents the outermost layer of a fiber-optic.

(FS.COM 2014)

## How fiber-optics work

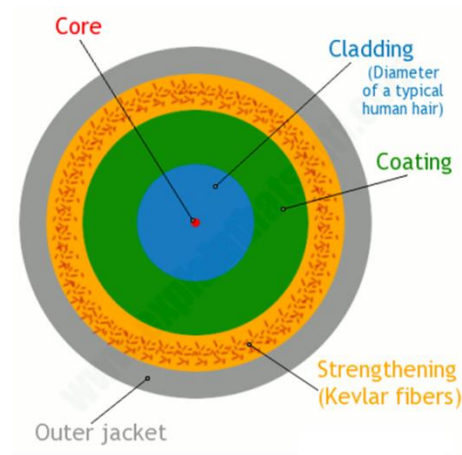


Figure 11: Internal construction of fiber-optic cable (Woodford 2018)

## 4.2 How fiber-optics work

Optical fibers are composed of a few or several hundred incredibly thin strands of glass or plastic where one strand is less than a tenth as thick as a human hair. The strand forms the inner part of the cable, which is known as the core. About 25 000 telephone calls can be carried by one strand without any problems. The enormous amount of information is converted from electrical information into a series of light pulses. The coded beam of light travels down the fiber-optic cable by repeatedly bouncing, like a bobsleigh going down an ice run, off the walls. At the end of the cable, the pulses of light have to be converted to electrical information again.

One phenomenon that keeps the light inside the pipe is known as total internal reflection where light is reflected by the glass, similar to a mirror. It occurs when the light hits the glass at an angle of less than  $42^\circ$ . As light does not always travel with such a shallow angle, there is as well a component of the fiber-optic responsible for keeping the light inside the glass pipe called cladding. This is another glass layer with a lower refractive index wrapped around the outside of the core and can be seen in Figure 12.

(Woodford 2018)

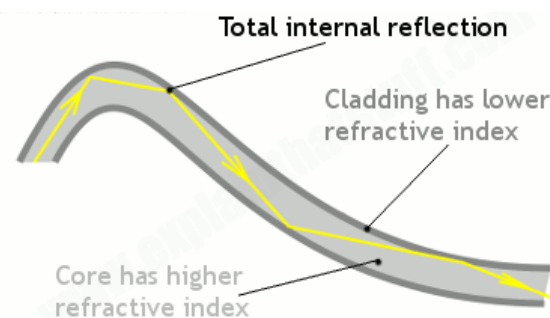


Figure 12: Total internal reflection of light (Woodford 2018)

## 4.2.1 Types of fiber-optic cables

Light signals can be carried down an optical-fiber in different modes. Therefore, three different optical-fiber cables are conventionally known as single-mode fiber, multi-mode fiber, and plastic optical fiber (POF).

A **single-mode fiber** consists of a core that measures about 5-10 microns in diameter and is one of the simplest types of fiber-optic cables. The light beams travel straight down the middle of the optical fiber in a very tight space due to the relatively small core and narrow diameter. The light signals do not bounce off the edges, which result in a high transmission rate and as well provide ranges over 100 km. Typical applications are, for instance, cable TV, telephone signals, and the internet. A disadvantage is the high costs.

(Woodford 2018),(FS.COM 2014)

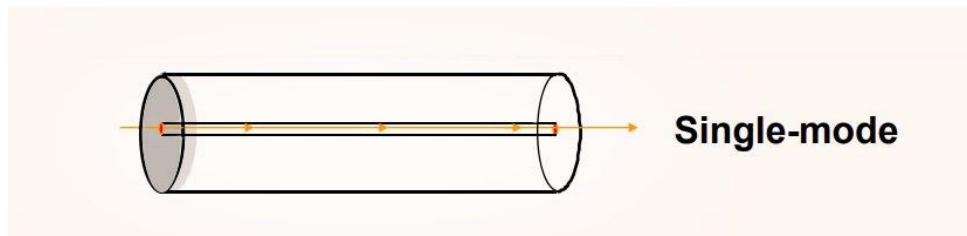


Figure 13: Single-mode optical-fiber (FS.COM 2014)

Since the **multi-mode cable** is about ten times thicker compared to a single-mode fiber, the light signals have more space and therefore allowed to follow a variety of different paths as can be seen in Figure 14. Due to the bigger size of the optical fiber and the short-range (<900 meters) of information transport, they are cheaper than single-mode cables. The field of application is usually to link computer networks together.

(Woodford 2018),(FS.COM 2014)

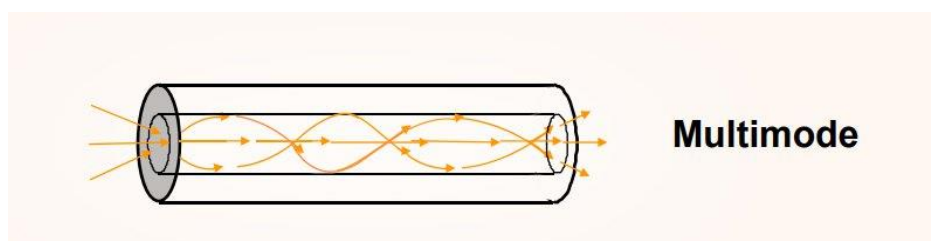


Figure 14: Multi-mode optical fiber (FS.COM 2014)

The **plastic-optical fiber** is about 1 mm in diameter, which provides enough space to couple lots of light beams from sources and connectors without any necessity of high

precision. Hence they are cheap, easy to cut with a razor blade, and simple to install due to the plastic. For these reasons, plastic-optical fibers are becoming more and more critical for the industry.

(FS.COM 2014)

## 4.2.2 Temperature and strain measurement

All methods of measuring strain or temperature have in common that they all rely in some way on the properties of light.

### 4.2.2.1 Strain

To be able to measure strain, a Fiber Bragg Grating (FBG) is inscribed into the optical fiber, as can be seen in Figure 15. It can be described as a pattern of material interferences where the slices are placed at a predetermined interval. Furthermore, the refractive index of the obstructions is different compared to the rest of the fiber and therefore reflect the light differently. Hence, these thin slices are responsible for reflecting specific wavelengths of the transmitted light beams, while others pass through. With a change in strain, that lead to compression or elongation of the fiber-optic, the intervals of the slices are influenced as well. As a result, the time of light signals to travel back and the wavelength is changing when strain is applied on the cable since the refracting index changes too.

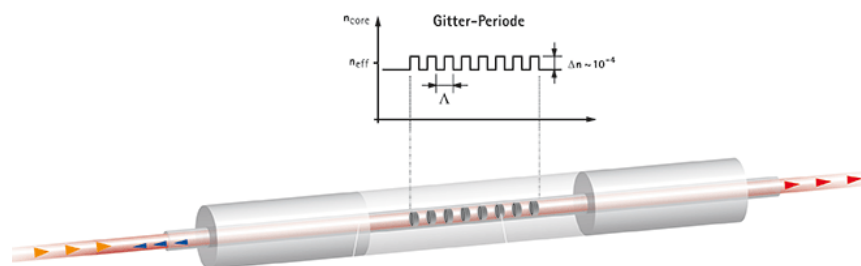


Figure 15: Fiber Bragg Grating (“How Does an Optical Strain Gauge Work?” 2018)

One Fiber Bragg Grating measures about 5 millimeters in length and the material interferences can only be seen under a microscope. Therefore, many individual strain sensors can be installed in one long fiber cable.

The integrator is a device that continuously sends out light in different wavelengths one after another. The light beams travel through the fiber where the FBG reflects some and force them to move back to the integrator whereas the rest is refracted when reaching the end of the cable. To differ between the signals of different sensors, the FBGs have distinct periods.

As the length of the fiber is also affected by temperature variations, temperature compensation is crucial to differentiate between changing strain or temperature. Certain possibilities are available:

- **Temperature sensor next to strain sensor:** If a temperature sensor is placed next to a strain sensor, data can be compared and mathematically compensated by subtracting the temperature effects.
- **Push-pull configuration of two FBGs:** This installation allows compression at one FBG and stretching on the other one as soon as the FBGs are under strain. In contrast to the temperature where the effect of lengthening is identical for both situations, the influence of mechanical stress differs. Mathematical compensation becomes possible since the FBG under traction experiences a positive strain and the other one a negative strain.
- **Encapsulation of fiber:** A mechanical apparatus encases the fiber and expands in the opposite direction of the tested material. Since stress will be applied to the FBG, this case causes cancellation of the temperature effects.

The purpose of most strain measurements is to allow an analysis of the mechanical stresses in the material. For instance, a fiber-optic cable installed in the wall of a tunnel gives you information about stresses in the material of the walls as it is strained due to vibrations or other motions. Continuous measurement of strain provides new details on necessary maintenance as weak points or fissures are immediately detected.

(“How Does an Optical Strain Gauge Work?” 2018)

#### 4.2.2.2 Temperature

To measure temperature along a fiber, several different systems are available.

- **Fiber-Bragg-Grating (FBG):** The function of this method was already discussed above.
- **Optical Backscatter Reflectometry (OBR):** This system is based on a combination of Fiber-Bragg-Grating and Raman-based optical frequency domain reflectometry (OFDR). Small structural imperfections, which can be influenced by temperature, change the amplitude of the backscattered light in an unmodified glass. Isothermal reflection amplitudes are stored at a reference temperature and compared with the local ones. By inscribing FBG structures, the signal-to-noise ratio can be improved.
- **Raman-based optical time-domain reflectometry (OTDR):** A laser source is integrated into the interrogator, and conventional glass fiber is used. The measured position and Raman amplitude are localized by the traveling time of the backscattered light. By evaluating the Stokes and the anti-Stokes amplitudes, the temperature can be calculated almost independent of mechanical stress.
- **Raman-based optical frequency domain reflectometry (OFDR):** Compared to the OTDR, the OFDR system is using amplitude-modulated laser source with a

sweepable modulation frequency. Therefore, the localization is done in the frequency domain. Afterward, for the point localization, the frequency-dependent backscattered Raman amplitudes are converted back into the time domain.

The most elaborate measurement for temperature is optical backscatter reflectometry and is used in fiber cables shorter than 500 m. The difference between the Raman and the Brillouin spectrum of the backscattered light can be seen in the sensitivity for mechanical stress and temperature. The Raman technique is highly sensitive to heat compared to the Brillouin spectrum, which is similarly susceptible to mechanical stress and temperature. OTDR and OFDR systems are available for both frequencies. These systems can be used in cables up to 50 km, including over 10000 sensor segments per fiber. Usually, these systems are applied for mechanical and/or thermal observation in tunnels, pipelines or in objects that extend over a wide area.

Today, FBG is known as the most resistant temperature measurement with multiple glass fiber sensors.

(Dosky et al. 2013)

## 4.3 Applications of fiber-optic sensors by TU Graz

The TU-Graz is monitoring infrastructure objects with fiber-optic sensors since 2001. Until now, they have embedded more than 50 km of sensing cable into bridges, tunnels, shafts, pipelines, ships, piles, anchors and beams. The objective is to monitor strain and temperature within different objects.

(“IGMS - Fiber Optic Sensors” n.d.)

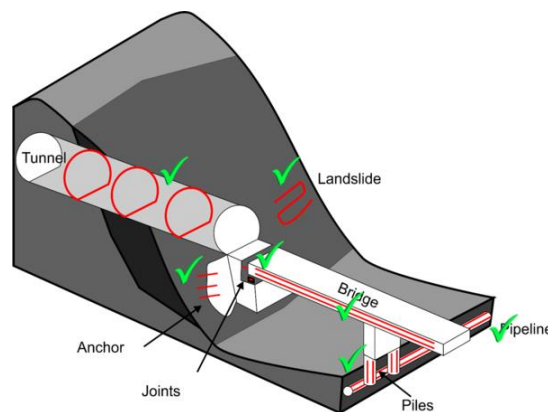


Figure 16: Fiber-optic sensors in civil infrastructure objects (“IGMS - Fiber Optic Sensors” n.d.)

To further describe their applications, more in-depth insight into the installation of fiber-optic cables in modern tunneling will be given.



Ensuring a safe construction to guarantee a long lifetime of the tunnel is the most relevant factor in modern tunneling. Therefore geotechnical deformation monitoring became an integral part of this industry. Ancient technics such as total stations or terrestrial laser scanner for displacement measuring at the inner lining surface and vibrating wire sensors to monitor internal deformations are not able to deliver a competent picture of the capacity within the tunnel lining. For this reason, fiber-optic measurements that allow in-situ deformation monitoring in tunnels were developed by IGMS. Two different sensing systems for backscattering are available. For instance, Rayleigh systems provide a very high spatial resolution of about 10mm, whereby they generate impeccable new information. Moreover, the utilization grade of the segment at about 6000 positions can be observed by installing up to 60 m long sensing cables into precast tunnel lining segments. The detection of cracks can be guaranteed by the high measurement resolution of about 1  $\mu\text{m}/\text{m}$ , which is proven based on the camera system and vibrating wire sensors.

As already proven in several field installations at the Semmering Base Tunnel, a modified system can be installed in the shotcrete lining and used to monitor a geological interference zone in the area of the working face. This application provides autonomous monitoring during the setting process of the shotcrete and can as well measure for several weeks in the de long term during the further excavation of the tunnel.

(“IGMS - Distributed Fiber Optic Sensing in Tunneling” n.d.)



# Chapter 5 Portland Cement

The most common cement used in the oil and gas industry is known as portland cement since its attributes make it ideal for cementing operations. The American Petroleum Institution (API) differs between class A, C, G, or H cement, depending on the chemical composition. Portland cement is not just drying out but generates compressive strength through hydration, which describes chemical reactions between the cement compounds and the water. For this reason, portland cement hardens in the air as well as in a liquid surrounding area. Moreover, it generates low permeable cement once it sets.

(Aitcin 2016)

## 5.1 Phenomenology of cement hydration

Limestone and clay (or shale) are the essential components of Portland cement. The raw meal, which consists of precise proportions of these two materials, is transformed into clinker through the complex pyroprocessing.

Cement hydration strongly depends on the fineness of the cement particles since the reaction always starts with the ionic species at the surface. This means a finer cement is more reactive. However, Portland cement creates mechanical bonds, liberates a certain amount of heat, and cause a contraction of the absolute volume of the cement paste when it is hydrating.

By heating the raw meal to a temperature of about 1450 °C four minerals with the essential characteristic to create bonds, as they react with water, are formed. All four materials together form the Portland clinker.

- Tricalcium silicate (Alite)  $\text{SiO}_2$  3CaO (C<sub>3</sub>S)
- Dicalcium silicate (Belite)  $\text{SiO}_2$  2CaO (C<sub>2</sub>S)
- Tricalcium aluminate  $\text{Al}_2\text{O}_3$  3CaO (C<sub>3</sub>A)
- Tetracalcium ferroaluminate 4CaO  $\text{Al}_2\text{O}_3$   $\text{Fe}_2\text{O}_3$  (C<sub>3</sub>AF)

The silicate phase is represented by  $\text{SiO}_2$  3CaO and  $\text{SiO}_2$  2CaO, whereby  $\text{Al}_2\text{O}_3$  3CaO and 4CaO  $\text{Al}_2\text{O}_3$   $\text{Fe}_2\text{O}_3$  constitute the aluminous phase.

To form Portland cement usually gypsum or another form of calcium sulfate is added to the Portland clinker to prevent  $\text{Al}_2\text{O}_3$  3CaO from hydrating too fast.

### 5.1.1 The five main phases of hydration

The mixture of water and Portland cement induces a chemical reaction, that is responsible for the setting and hardening process of the cement. It is mostly exothermic and therefore produces heat.

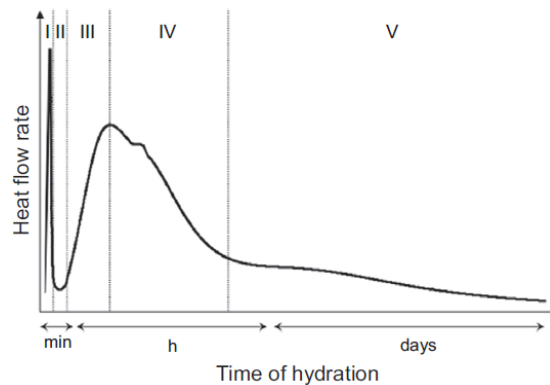


Figure 17: Different phases of the hydration of Portland cement (Aïtcin 2016)

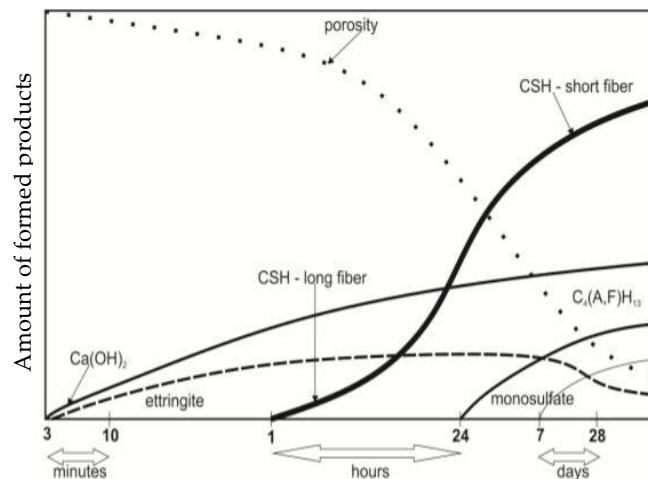


Figure 18: Formed products of hydration of Portland cement (Franus, Panek, and Wdowin 2015)

Sulfates and gypsum immediately dissolve when mixing clinker and water and form an alkaline and sulfate-rich solution.

### Phase I: Initial reactions

The most reactive material of the main clinker is  $\text{Al}_2\text{O}_3 \cdot 3\text{CaO}$ . In phase I, it reacts with water and forms an aluminum-rich gel layer which response to the sulfate solution. As a result, small rod-like crystals of ettringite are formed (Figure 18). Furthermore, tricalcium silicate reacts by releasing calcium ions and heat. This reaction lasts typically only a few minutes after adding the water but is strongly exothermic, as can be seen in Figure 17.

### Phase II: Induction/Dormant phase

In phase II, a slow dissolution can be recognized. The formed ettringite hinders  $\text{Al}_2\text{O}_3 \cdot 3\text{CaO}$  reactions, almost no heat evolution can be seen, and the slurry remains liquid phase. This period can take from several minutes to about two hours. The concrete can

be placed up to perhaps half-way of the dormant period since afterward the slurry becomes too stiff to be workable. At the end of this phase, the setting of cement can be recognized.

### Phase III: Accelerating phase

In this period, the reaction rate is increased significantly, which can also be seen in the rising temperature. The duration is about 3-12 hours after adding water. Silicate hydrate (C-S-H) and calcium hydroxide/hydrated lime (portlandite) are formed, developing compressive strength of the concrete due to the beginning reaction of Alite and Belite in the cement. The peak between phase III and IV emerge from the main hydration of tricalcium silicate, which is responsible for the early strength (~first seven days). The reaction of dicalcium silicate is slower and contributes only to the compressive strength at later times. The size of the anhydrous particles decreases, and the individual grains on the surface respond. The hydration of tricalcium aluminate continues as well.

### Phase IV: Decelerating phase

The duration of this phase is about 10-24 hours after adding water. Long ettringite is formed due to the secondary hydration of silicate. Now, C-S-H products form as well in the inside of the shell. The densification of the formed hydrate layer slows down the reaction. The little peak in phase IV indicates the sulfate depletion point increasing the hydration of tricalcium aluminate. Porosity decreases as the particles water space are filled up.

### Phase V: Slowdown

Due to the composed gypsum, ettringite reacts with tricalcium silicate and decomposes to monosulfate. Moreover, further C-S-H products are formed which fill the spaces more and more between shell and grain. This phase can last to several days.

(“Cement Hydration” n.d.), (Aïtcin 2016), (“Concrete: Scientific Principles” n.d.), (“Rak-82\_3131\_cement\_hydration\_-\_new.Pdf” n.d.)

In the first three days of the hydration process, 50% of heat is generated and in the first seven days, even 80%. In the table below, the approximate heat development of each reaction is listed.

(Swaddiwudhipong, Chen, and Zhang 2002)

Compound specific heat of hydration (cal/g)			
C <sub>3</sub> S	53%	120 cal/g	520,1 kJ/kg
C <sub>2</sub> S	22%	62 cal/g	259,4 kJ/kg
C <sub>3</sub> A	9%	320 cal/g	1338,9 kJ/kg
C <sub>4</sub> AF	10%	100 cal/g	418,4 kJ/kg

Table 1: Compound specific heat of hydration (Swaddiwudhipong, Chen, and Zhang 2002), (“Table 1 . Chemical Composition of Ordinary Portland Cement.” n.d.)

## Phenomenology of cement hydration

To calculate the total generated heat due to the chemical reaction, the following equation can be used.

$$\Delta Q = m * c * \Delta T \quad (1)$$

where:

$\Delta Q$  is the energy [J]

$m$  is the mass [kg]

$c$  is the specific heat capacity [ $\frac{J}{kg \cdot K}$ ]

$\Delta T$  is the change of temperature [-]

### 5.1.2 Electrical resistivity/conductivity of a concrete

The application of electrical resistivity measurements for quality control of concretes becomes more and more important in the industries since the characterization of fresh concrete is essential for guaranteeing the quality of the cement. Moreover, meaningful information about the microstructure, setting time mechanical strength and moisture content can be generated, and evaluations of concrete durability can be made.

The **electrical resistivity**  $\rho$  describes the resistance to the flow of electric current through a specific specimen. It is an inherent characteristic of concrete and does not depend on the geometry of the tested specimen. As can be seen in equation (20), electrical resistivity is computed based on measuring electrical resistance.

(FPrimeC 2017),(Obla et al. 2018)

$$\rho = R * \frac{A}{l} \quad (2)$$

where:

$\rho$  is the specific electrical resistivity of a uniform specimen [ $\Omega m$ ]

$R$  is the electrical resistance of a uniform specimen [ $\Omega$ ]

$l$  is the length of the specimen [m]

$A$  is the cross-sectional area of the specimen [ $m^2$ ]

The ability to transport electrical current through a medium is known as **electrical conductivity**  $\sigma$ . It is the reciprocal of the resistivity and measured in siemens per meter.

(“Resistivity and Electrical Conductivity” 2017)

$$\sigma = \frac{1}{\rho} \quad (3)$$

where:

$\rho$  is the specific electrical resistivity of a uniform specimen [ $\Omega\text{m}$ ]

$\sigma$  is the conductivity of a uniform specimen [ $\frac{\text{S}}{\text{m}}$ ]

The electrical resistivity value of concrete depends on ionic conduction through water-filled capillary pores. Porosity and liquid solution conductivity are mainly controlling the electrical conduction for porous media.

The porosity of concrete can be influenced by:

- Water/cement ratio
- Mineral admixture
- Chemical admixture
- Cement components
- Curing time
- Aggregate proportion
- Compaction condition
- Curing condition

(Wei 2004)

Typical conductivity of water

- Ultrapure water:  $5,5 \times 10^{-6}$  S/m
- Drinking water: 0,005 – 0,05 S/m
- Seawater: 5 S/m

(“Water Conductivity - Lenntech” n.d.)

During the first chemical reaction, ions are released and dissolved. A slight temperature increase can be recognized during this dissolution process, whereas the electrical conductivity increases rapidly (Figure 19). At the end of the dormant period, the conductivity decreases significantly since the ions form compounds.

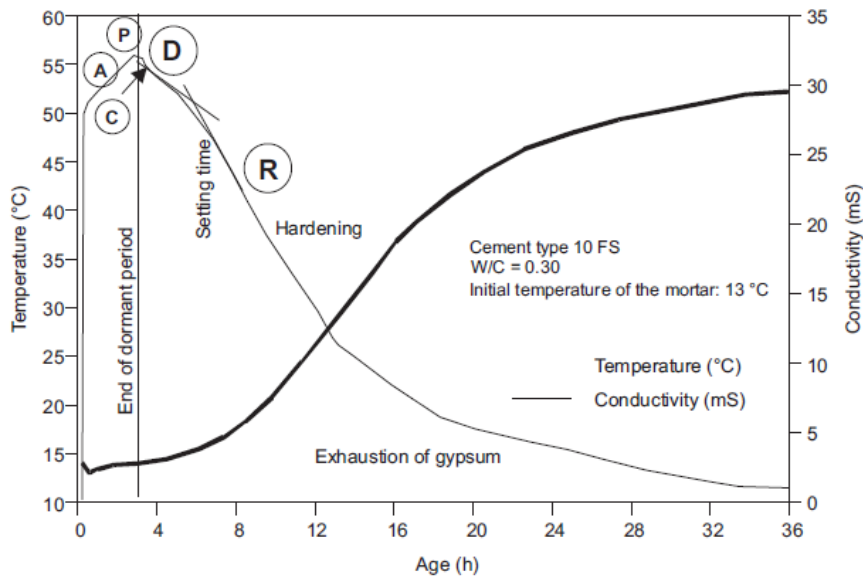


Figure 19: Heat and electrical conductivity development during the hydration of cement (Aïtcin 2016)

Since temperature, strain, and conductivity change significantly during the hydration process of concrete, these parameters were selected to be further investigated.

### 5.1.3 Shrinkage of concrete

From the volumetric point of view, concrete is not a stable material. The apparent volume changes, usually decrease, based on its hardening conditions. When concrete is only partially saturated, shrinkage is a result of the displacement of water in the capillary network.

The four different types of shrinkage:

- **Plastic shrinkage** is known as the evaporation of water from the surface directly after mixing the slurry. This phenomenon occurs after placing and before hardening of the cement. Plastic shrinkage cracking takes place when the rate of evaporation exceeds the amount of bleeding water rising to the surface.
- **Chemical shrinkage:** Chemical reactions lead to the binding of water into hydrates, which result in a volume loss. This process appears in any cement slurry independent of its w/c ratio.
- **Drying shrinkage** develops when water evaporates from cured concrete but does not occur in a downhole environment.
- **Autogenous shrinkage** only appears in low w/c slurries and forms due to the hydration of cement itself. The volume occupied by the product is less compared to the ingredients and therefore induces shrinkage. It is not related to any outside influence, such as drying. Hence, autogenous shrinkage will develop even if the cement is placed in a sealed box.

(Aïtcin 2016)



# Chapter 6 Experiments

## 6.1 Experiment 1: Resistivity measurement of a concrete

According to research, alternating current is preferably used than direct current for measuring the resistance of an electrolytic solution.

A chemical reaction will be induced by sending current through an electrolyte. The initial conductivity cannot be measured any longer as this reaction alters the composition of the solution. Compared to direct current, alternating current sends equal current in both directions over a specified period. Therefore the chemical reactions will be balanced since they occur in both directions. Even if chemical reactions take place, the concentration of ions in the solution will remain constant, and no change in the chemical composition will be recognized.

Therefore, the main objective of this experiment was to visualize the influence of direct current on a liquid medium.

(Govind Balaji 2018)

### 6.1.1 Equipment

- Multimeter UNIGOR 390, applying direct current to the system
- LCR meter 879B, applying alternating current to the system
- Resistivity meter model 88C
- Laboratory power supply
- Laptop for data logging
- Plastic Container (V=1,9l) with two electrodes (screws)



Figure 20: First experiment setup

## 6.1.2 Experiment setup

First, 1.5 liters of tap water was filled into the plastic container. The clamps for the current transmission were placed at the screws, and the ends were plugged at the multimeter. This device was supplied by a laboratory power supply and connected with the computer for data logging. The multimeter was coded to send each 20 seconds the measured value to the network. The generated data were prepared, and diagrams were created with excel.

Figure 21 shows a stable resistance at the beginning and as expected a decrease of resistance after adding 10 grams of Salt. The value stabilized again, and the test was ended after 15 minutes.

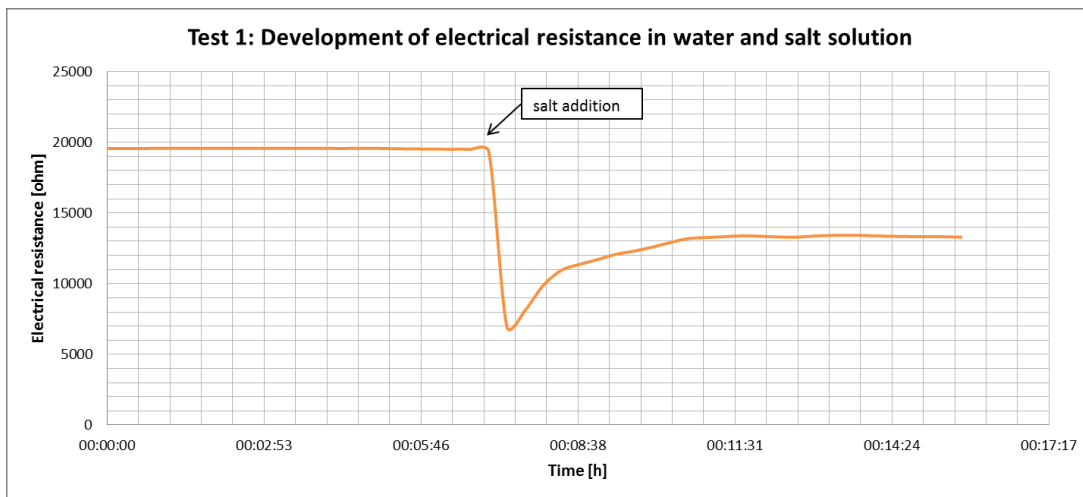


Figure 21: Test 1: Development of electrical resistance in a water and salt solution

According to ("C01bc.Pdf" n.d.) the standard value for tap water is around 20 [ $\Omega m$ ]. Therefore, the data measured by the multimeter are too high. A resistivity meter model 88C was used to prove the falsity. Since this device is showing the specific resistivity [ $\Omega m$ ], the data from the multimeter had to be converted by using equation (44).

$$x = 19550 \Omega * \frac{0,00213 m^2}{0,06 m} \quad (4)$$

$$x = 550704,23 \Omega m$$

If we compare the value from equation (4) with the reading from the resistivity meter, which was 27,5  $\Omega m$ , we can see a big difference which proves the malfunctions of the multimeter.

$$27,5 \Omega m \neq 550704,23 \Omega m \quad (5)$$

The cross-section was not easy to define since the current field in a liquid medium between two little electrodes is never homogeneous as can be seen in Figure 22.

(Sebastian 2013)

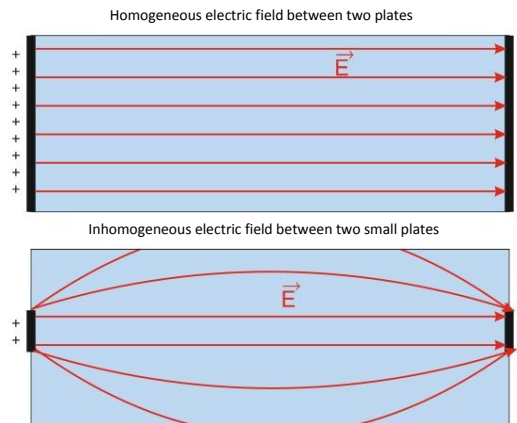


Figure 22: Difference of using screws versus plates (Sebastian 2013)

The diameter of the screws head was 1,5 cm.

$$A = \frac{\pi * d^2}{4} \quad (6)$$

$$A = 0,000177 m^2$$

where:

$A$  is the cross-sectional area of the specimen [ $m^2$ ]

$d$  is the diameter of the specimen [ $m$ ]

An LCR meter 879B, which measures with alternating current and therefore provides accurate values, was used to calculate the real cross-section. 773,4  $\Omega$  were displayed on the LCR meter. The actual cross-section was defined by equating the value from the resistivity meter with the value from the LCR meter

$$27,5 \Omega m = 773,4 \Omega * \frac{y}{0,06 m} \quad (7)$$

$$y = 0,00213 m^2$$

## Experiment 1: Resistivity measurement of a concrete

As expected, the real cross-section is larger due to the phenomenon of inhomogeneity. To prevent inaccuracy due to the inhomogeneous electric field, plates were used instead of screws for experiment 2.

To prove the changing chemical composition of the solution, further experiments were performed.

The next day, the test was repeated without adding salt. The same setup with the same screws was used once again. In Figure 23, a slight decline of the line can already be detected after one hour, but still, the values were nearly stable. The test was stopped after about two and a half hours.

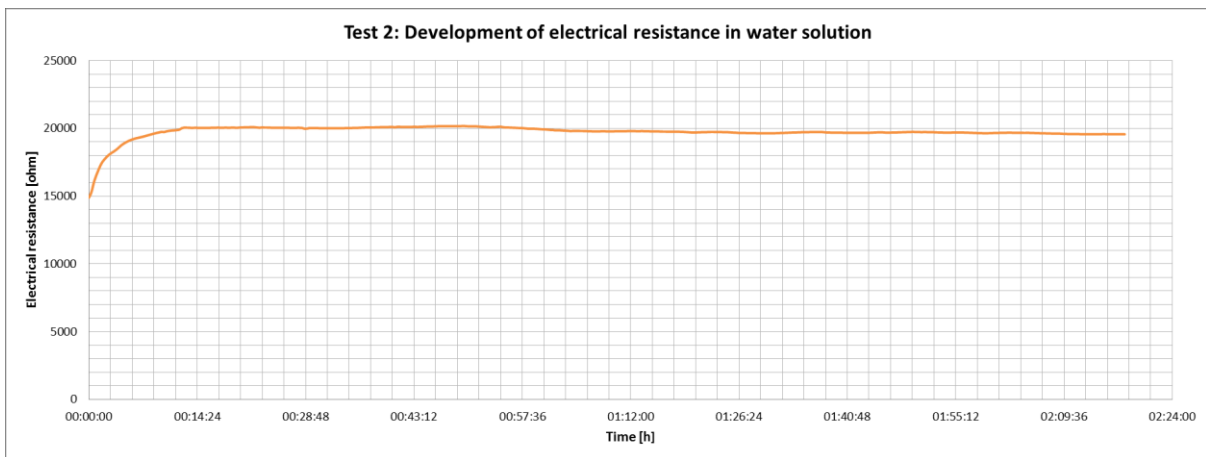


Figure 23: Test 2: Development of electrical resistance in a water solution

The following day, the test was performed again, and still, the same screws were used.

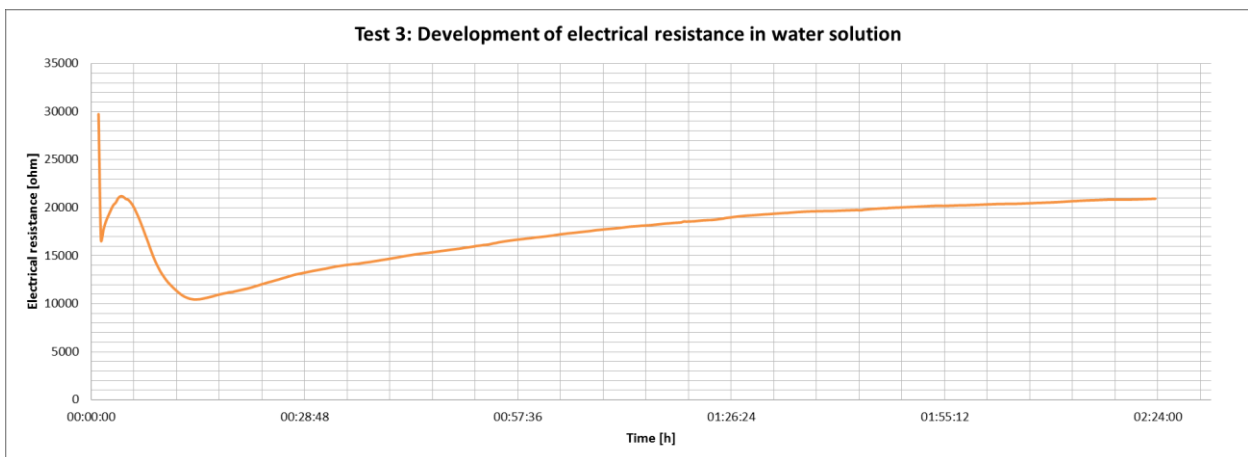


Figure 24: Test 3: Development of electrical resistance in a water solution

According to the data logging, the values did not stabilize any longer. Ions accumulate on the surface of the screws, and therefore, the concentration of ions in the solution is

changing, hence affecting the resistance values. This phenomenon occurs as a result of applying direct current on an electrolyte as one screw is working as a cathode and the other one as an anode.

After the test, the ion accumulation could already be seen on the surface of the screws.



Figure 25: Used screws compared to a new one

One last test was performed on the fourth day, using the utilized screws. As can be seen in Figure 26, the values were much lower compared to the measurement of the days before. Moreover, the values increased with time due to the changing chemical composition.

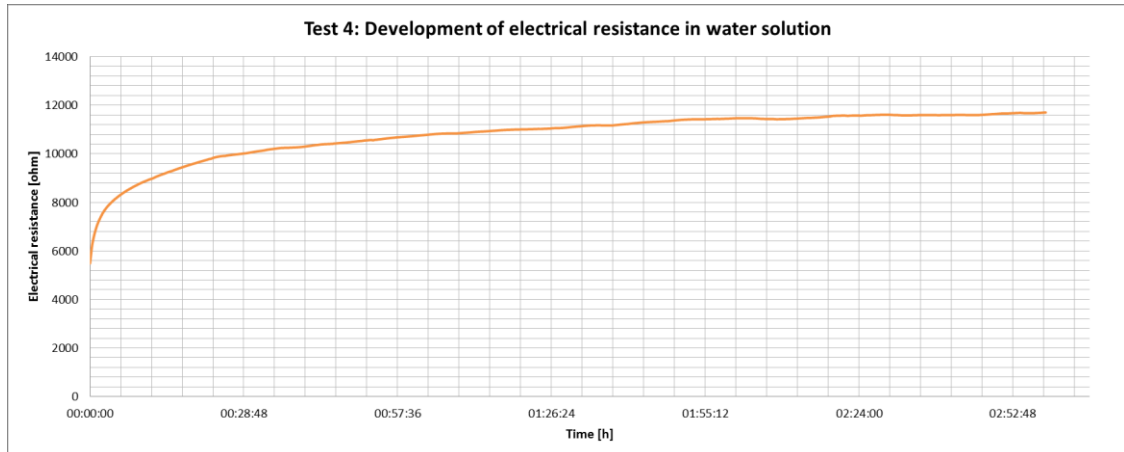


Figure 26: Test 4: Development of electrical resistance in a water solution

Another test was performed using the same setup but changing the multimeter to an LCR Meter 879B since this device sends alternating current through the solution.

Experiment 1: Resistivity measurement of a concrete

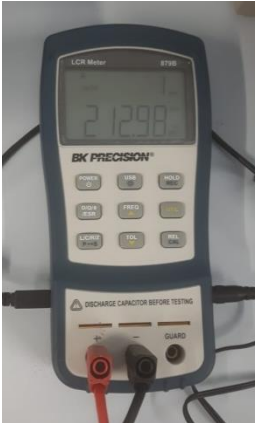


Figure 27: LCR Meter 879B

A clear difference can be seen in the next picture compared to the graphs from the multimeter. Accurate and stable, and values have been generated by this device.

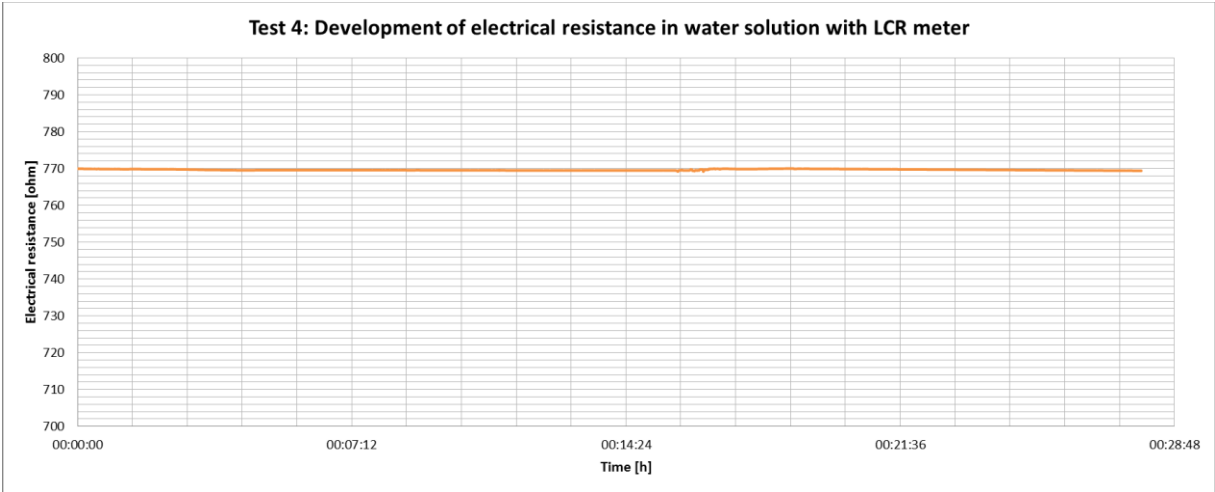


Figure 28: Development of electrical resistance in a water solution with LCR meter

## 6.2 Experiment 2: Different mud-cement ratios

These experiments intended to monitor the resistivity behavior of contaminated cement slurry. The contamination by mud was increased from 0% to 100%.

The cement and mud slurry was designed by the “cement and mud calculation” excel developed by Emanuel Hofer. The mass of cement and water is calculated automatically by inputting the desired values in the green boxes.

A cement slurry must show a water-cement ratio at least equal to 0,42 to reach full hydration. The water-cement ratio in my case is:

$$\frac{w}{c} = \frac{1025,51}{2431,87} = 0,422 \quad (8)$$


Cement Slurry Preparation									
Slurry volume (cc)	Slurry density, ps (SG)	Cement density, pc (SG)	Water density, pw (kg/l)	Vol. of added liquid (gal)	Density of added liquid (kg/l)	Mass of added solid (kg)	Density of added solid (kg/l)	Cement mass (g)	Water mass (g)
1800	1,920768307	3,15	0,9976	0	0	0	0	2431,873398	1025,509555
									
Convert kg/m³ to SG			<b>CONVERSION</b>	Convert ppg to SG			The program uses SG to calculate the required cement and water mass, therefore use the conversion table to convert from Kg/m³ or ppg to SG		
Density [kg/m³]	1000	[kg/m³]		Density [ppg]	16	[ppg]			
Density [SG]	1	[SG]		Density [SG]	1,92	[SG]			
Results									
To prepare the slurry, you need following masses of cement and water:				Neat Glass G Cement	2.431,87	[g]	2,43	[kg]	
				Water	1.025,51	[g]	1,03	[kg]	

Table 2: Cement slurry preparation table

Experiment 2: Different mud-cement ratios

Polymer Mud Calculation	How much Polymer Mud do you want to mix?		
	10	[liter]	
	<b>Results</b>		
	K2CO3 (weight agent and inhibitor)	0,8	800
	S-ES Bio XG- Xanthan Gum (viscosity agent)	0,03	30
	S-ES Pac LV (fluid loss agent)	0,14	140
	Citric Acid (pH control)	0,01	10
Bentonite Mud Calculation	How much Bentonite Mud do you want to mix?		
	10	[liter]	
	<b>Results</b>		
	Bentonite	0,8	800
Weight up Calculation	What is your desired mud weight?		
	13	[ppg]	
	What is the initial mud weight?		
	8,8	[ppg]	
	<b>Results</b>		
	Quantity of Barite	8,0	7999,83

Table 3: Mud slurry preparation table

6.2.1 Equipment

- Scale, Kern FCB

This equipment was used to weigh the different compounds, necessary for the slurries.



Figure 29: Scale

- Constant Speed Mixer, Chandler Engineering

This device was used to mix the cement and mud slurry for the experiments after API Standards. According to ("TREX-06235.Pdf" n.d.), the API Standards require mixing for 15 seconds at 12000 r/min.





Figure 30: Constant Speed Mixer, Chandler Engineering

- Heidolph RZR 2051 electronic Mixer

This mixer was used when a large volume of mud or cement slurry was required.



Figure 31: Heidolph Mixer

- Pressurized Gravity Balencometer

To measure density, according to API Standards, a pressurized gravity balencometer was used. First, the container was filled with mud, closed and filled/pressurized with additional mud over the top inlet. Afterward, it was balanced, and the value was read off in [ppg].

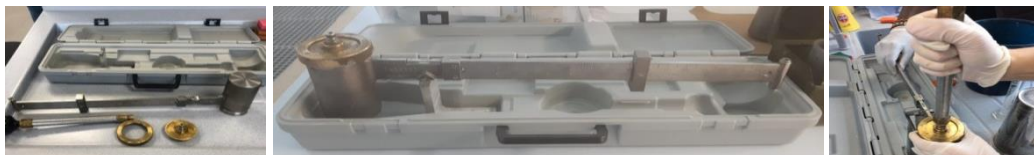


Figure 32: Pressurized Gravity Balencometer

## Experiment 2: Different mud-cement ratios

- Baroid Mud Balance

The cement density was also measured with a baroid mud balance and compared with the values from the pressurized gravity Balancometer. The values slightly differed by approximately -0,5 ppg.



Figure 33: Baroid Mud Balance

- Fann Rational Viscometer, Chandler Engineering

This device was used to determine the rheology of the fluid under atmospheric pressure. The container was filled with the substance to a certain level and lifted. The shear stress ( $\tau$ ) was read off the dial of the Fann Viscometer at different shear rates ( $\gamma$ ).

According to ("Viscometer\_Info2.Pdf" n.d.), the shear stress reading of the dial of the Fann Viscometer has to be corrected by multiplying it with 1,065 to obtain lb/100 ft<sup>2</sup>, whereas the shear rate reading of the Fann Viscometer must be multiplied by 1,703 to convert it from rpm to s<sup>-1</sup>.



Figure 34: Fann Rational Viscometer, Chandler Engineering

Rheology is known as the science of deformation and flow of the material. Drilling mud and cement, for instance, show a complex flow behavior and can therefore not be safely extrapolated from one series of flow conditions to another. A rheological characterization under process conditions is necessary, as they do not behave in a classical or "Newtonian" manner.

It is essential to study the rheological model of drilling mud and cement as it simulates the characteristics of the substance under dynamics conditions. Key factors such as equivalent circulating density, pressure drops in the system, and hole cleaning efficiency can be determined.

The different rheological models are shown in Figure 35.

A straight line through the origin representing a consistency curve is known as the Newtonian fluid model. Its viscosity is equal to the slope of the curve. Typical, a Newtonian fluid model can be applied for water, salt solution, and light oil.

For example, a Bingham Plastic model is commonly used to describe the characteristics of concrete. This model assumes that the shear rate is a straight-line function of the shear stress. The Yield Point or threshold stress is the intersection point with the y-axis. The slope of the function equals to the plastic viscosity. In the case of a Bingham Plastic fluid shear reading of 600 minus 300 gives us already the result in cp without any conversion, since all conversion factors, needed to convert the measured values of the Fann Viscometer to cp, including the shear rate reading makes up approx. 1. The Bingham Plastic Fluid 600 minus 300 shear stress reading times 1 gives the same result as when simply subtracting  $\theta 300$  from  $\theta 600$ .

This is very helpful in the field, because it provides a rapid overview of the viscosity of your drilling fluid, without the need for many calculations. Therefore, plastic viscosity (PV) can be quickly calculated by subtracting the reading at 600 rpm from the reading at 300 rpm at the corresponding temperature.

$$\tau = \tau_{\gamma} + \mu_p * \gamma$$

$$\mu_p = \theta 600 - \theta 300 \quad (9)$$

$$\tau_{\gamma} = \theta 300 - \mu_p$$

where:

$\tau$  is the shear stress  $\left[ \frac{lb}{100ft^2} \right]$

$\tau_{\gamma}$  is the yield point  $\left[ \frac{lb}{100ft^2} \right]$

$\gamma$  is the shear rate  $\left[ \frac{1}{s} \right]$

$\mu_p$  is the plastic viscosity [cp]

$\theta 600$  is the shear stress reading a 600 rpm  $\left[ \frac{lb}{100ft^2} \right]$

$\theta 300$  is the shear stress reading a 300 rpm  $\left[ \frac{lb}{100ft^2} \right]$

The Power-law model can be described by the following exponential equation:

$$\tau = K * \gamma^n \quad (10)$$

## Experiment 2: Different mud-cement ratios

$$n = \frac{\log \frac{\theta_2}{\theta_1}}{\log \frac{\omega_2}{\omega_1}}$$

$$K = \frac{\theta_1}{\omega_1^n}$$

where:

$K$  is the consistency index  $\left[ \frac{lb \cdot s}{100 ft^2} \right]$

$n$  is the flow behavior index

$\theta_1$  is the shear stress at 300rpm  $\left[ \frac{lb}{100 ft^2} \right]$

$\theta_2$  is the shear stress at 600rpm  $\left[ \frac{lb}{100 ft^2} \right]$

$\omega_1$  is the shear rate at 300 rpm  $\left[ \frac{1}{s} \right]$

$\omega_2$  is the shear rate at 600 rpm  $\left[ \frac{1}{s} \right]$

This method is another fluid model to characterize a non-Newtonian fluid where the shear stress is zero at zero shear reading.

The Herschel Bulkley model, also known as the modified Power-law model, is commonly used to describe the characteristics of drilling mud. The following equation defines the model:

$$\tau = \tau_y + K * \gamma^n$$

$$n = \frac{\log \frac{(\theta_2 - \theta_0)}{(\theta_1 - \theta_0)}}{\log \frac{\omega_2}{\omega_1}} \quad (11)$$

$$K = \frac{(\theta_1 - \theta_0)}{\omega_1^n}$$

where:

$\theta_0$  is the shear stress at 3 rpm  $\left[ \frac{lb}{100 ft^2} \right]$

The intersection point with the y-axis is called Yield Point.  $n$  equals one for Newtonian fluids as they show zero shear stress at zero shear rate, whereas for drilling fluid it is less than one. Compared to the Newtonian fluid, the drilling fluid does not have a constant viscosity value. Moreover, some internal resistance has to be overcome to move the drilling fluid from the static condition.

The PV can as well be determined by plotting shear rate vs. shear stress (log vs. log by Power-Law or Herschel Buckley), performing a linear regression and calculating the slope.

(“Viscometer\_Info2.Pdf” n.d.),(DrillingFormulas.Com | n.d.)

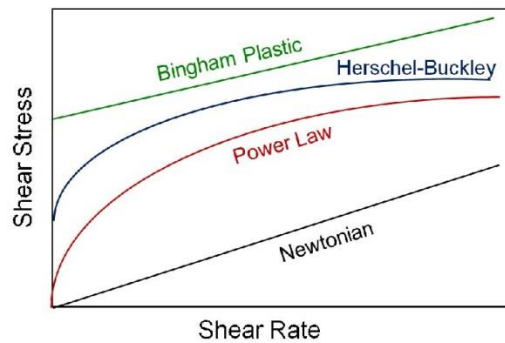


Figure 35: Rheological models (Montgomery 2013)

To choose the right model for the fluid, the regression coefficients have to be compared by plotting shear stress vs. shear rate and performing different regressions. The higher the factor, the better the regression fits.

A critical parameter to perform a competent drilling job is to know the gel strength of the drilling mud as it demonstrates the ability of the fluid to suspend drilled solid and weighting material when circulation has stopped. To determine the gel strength a 10 seconds / 10 minutes test can be performed with the Fann Viscometer. The viscometer has to be set to 600 rpm till the value stabilized. Afterward, the device has to be switched off for 10 seconds and then turned on with 3 rpm again. The number has to be read off. The same procedure has to be done for 10 minutes.

We differentiate between three types of gel strengths.

- The **Progressive gel strength** is increasing with time and requires high pump pressure to brake circulation. In such a case, the gelation of the mud rapidly gains strength with time. It results from an excessive concentration of solids and can be determined by a 30 min gel strength test.
- A high initial gel strength which increases only slightly with time is known as **High Flat gel strength**. Less pump pressure is required to break circulation once it is static.
- A gel strength which is nearly identical from initial to final indicates a **Low Flat gel strength**. These substances are simple to pump and does not cause any problems after static condition.

(“Progressive Gels - Schlumberger Oilfield Glossary” n.d.)

## Experiment 2: Different mud-cement ratios

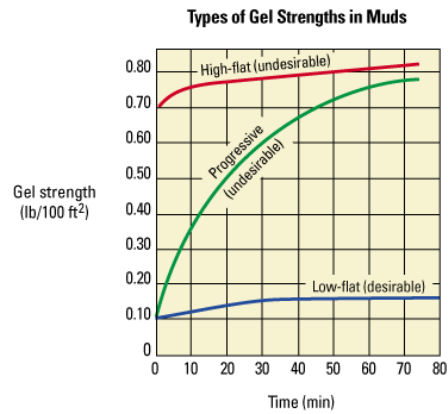


Figure 36: Types of gel strengths in muds (“Progressive Gels - Schlumberger Oilfield Glossary” n.d.)

- LCR Meter 879B, applying alternating current to the system

This device can be seen in Figure 27. As already mentioned, it sends alternating current through the system and can be used to measure the inductance (L), capacitance (C), or resistance (R).

- Resistivity Meter Model 88C

The resistivity meter was already used in Experiment 1. By filling the pipette with the investigating substance and selecting the appropriate scale, the resistivity can be determined in [ $\Omega m$ ].



Figure 37: Fann Rational Viscometer

- Laptop for data logging

- Plastic container (V=1,9l) with two electrodes (aluminum plates)



Figure 38: Plastic container with electrodes

- CT-scan

Generall can be said, the denser the substance, the more radiation is absorbed and the brighter the color on the CT-scan, whereas the lighter material absorbs less radiation.



Figure 39: CT-scan

## 6.2.2 Slurry design

### 6.2.2.1 Bentonite mud

Fifteen liters of mud was mixed previous to all the experiments. The design, which was based on Table 3, and rheological data can be seen below.

<b>Bentonite mud (15 liters)</b>	
<i>Water</i>	<i>15 l</i>
<i>Bentonite</i>	<i>1200 g</i>

Table 4: Mud design for experiment 2

<b>Rheological Data</b>	
<i>Density</i>	<i>8,3 ppg</i>
<i>Initial Temperature</i>	<i>24,4 °C</i>

Experiment 2: Different mud-cement ratios

Shear Rate [1/s]		Shear Stress [lb/100ft <sup>2</sup> ]	
5,11		55,38	
10,22		73,49	
51,09		123,54	
102,18		137,39	
170,3		149,1	
340,6		164,01	
510,9		175,73	
1021,8		213	
<b>Flow behavior index</b>		<b>0,2409</b>	
10 seconds / 10 minutes Gel Strength			
Rotational Speed [rpm]	<u>10 sec Gel Strength</u> [lb/100ft <sup>2</sup> ]	<u>10 min Gel Strength</u> [lb/100ft <sup>2</sup> ]	
3	60	70	

Table 5: Rheological data of mud for experiment 2

As expected, the Power-Law model fits best when plotting the rheological data of the bentonite mud. The flow behavior index n can be read off the exponential equation.

$$\tau = K * \gamma^n = 39,208 * \gamma^{0,2409} \tag{12}$$

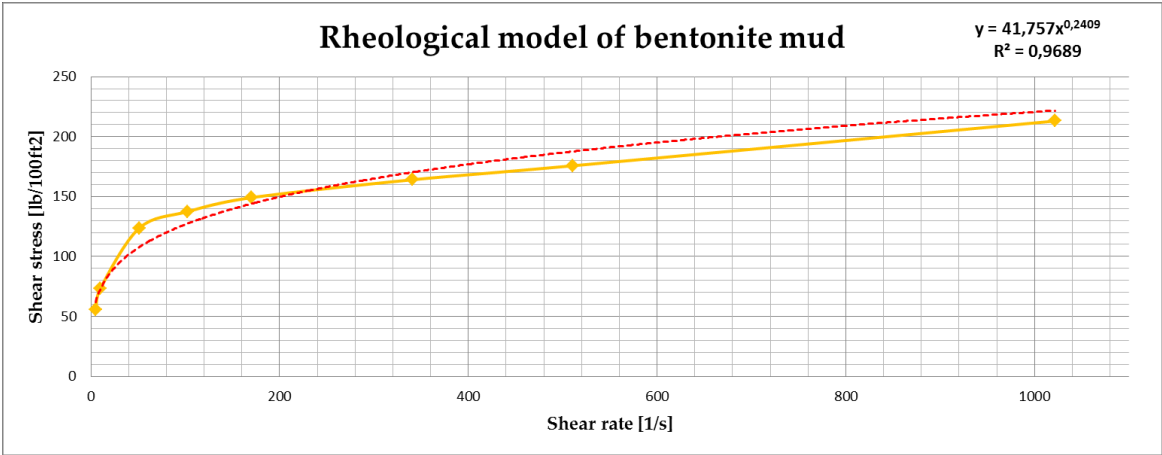


Figure 40: Rheological model of bentonite mud

Due to the high shear stress values and the slight change between the values of the 10 sec gel strength and 10 min gel strength test, the slurry is characterized as a high flat gel.



### 6.2.2.2 Cement slurry

A certain amount of 16 ppg cement slurry was mixed prior to each experiment. The design, which was based on Table 2, and rheological data can be seen below.

100% Cement slurry		
<b>Total Volume [ml]</b>	<b>1800</b>	
	<i>Cement</i>	<i>Mud</i>
<b>Volume [ml]</b>	1800	/
<b>Density [ppg]</b>	16	/
<b>Initial Temperature [°C]</b>	25,1	/

Table 6: Cement slurry design experiment 2

The Fann Viscometer was used to measure the rheological data of the slurry.

Rheological Data		
<i>Shear Rate [1/s]</i>	<i>Shear Stress [lb/100ft<sup>2</sup>]</i>	
5,11	13,85	
10,22	15,98	
51,09	20,24	
102,18	25,56	
170,3	33,02	
340,6	55,38	
510,9	68,16	
1021,8	106,5	
<b>Plastic Viscosity [cp]</b>	<b>27,55</b>	
10 seconds / 10 minutes Gel Strength		
<b>Rotational Speed [rpm]</b>	<i>10 sec Gel Strength [lb/100ft<sup>2</sup>]</i>	<i>10 min Gel Strength [lb/100ft<sup>2</sup>]</i>
3	1	30

Table 7: Rheological data of cement slurry experiment 2.1

As already discussed, the rheological model of a concrete fits best the Bingham Plastic model.

Experiment 2: Different mud-cement ratios

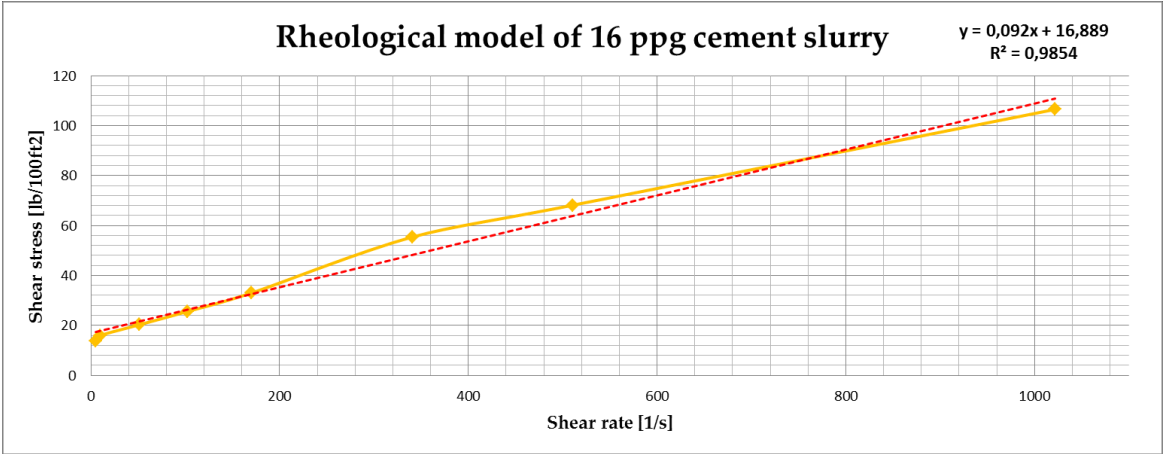


Figure 41: Rheological model of 16 ppg cement slurry

The plastic viscosity is equal to the slope k and can be read off the linear function of the plot.

$$\tau = \tau_{\gamma} + \mu_p * \gamma = 0,092x + 16,889 \tag{13}$$

To change  $\left[ \frac{lb}{100 ft^2} \right]$  to  $[cp]$  the following conversion is necessary:

$$\left[ \frac{lb}{100 ft^2} \right] * \left( \frac{1,065 * 47886}{100 * 1,703} \right) = [cp] \tag{14}$$

$$0,092 * 299,46 = 27,55 [cp]$$

### 6.2.3 Experiment 2.1: 100% Cement slurry

The first experiment was performed with 100% of cement slurry, and therefore, no contamination was induced. The conductivity measurement was run for 24 hours for each test.



Figure 42: Experiment 2.1: Left side view - back view - top view

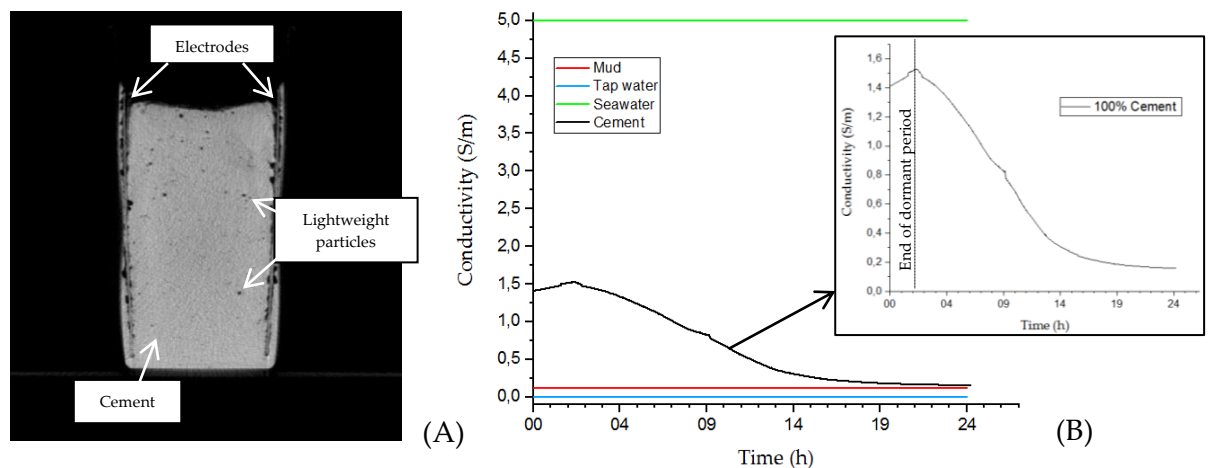


Figure 43: Experiment 2.1: CT-Scan (A), conductivity vs. time (B)

As expected, in Figure 42, a uniform cement sample can be seen. The CT-scan proves the homogeneity of the slurry. The electrodes, located on the side of the beaker, are visible. Moreover, the small dark marks can be identified as tiny, lightweight particles.

The conductivity curve of cement shows the anticipated location between the mud (~0,12 S/m) and seawater (~5 S/m) line, whereas tap water, represents the line furthest down (~5 mS/m) (Figure 43 (B)).

By comparing the conductivity vs. time curve of 100% cement with the curvature from the literature (Figure 19), conformity can be validated. Furthermore, the temperature reading from the fiber-optics was added to illustrate the conductivity/temperature behavior (Figure 44). According to expectations, a decrease in conductivity can be recognized at the end of the dormant period, while the temperature starts to increase.

## Experiment 2: Different mud-cement ratios

The rapid rise of conductivity in the dormant phase, due to the dissolution process, is not visible since the data logging was started after the rheology test were performed.

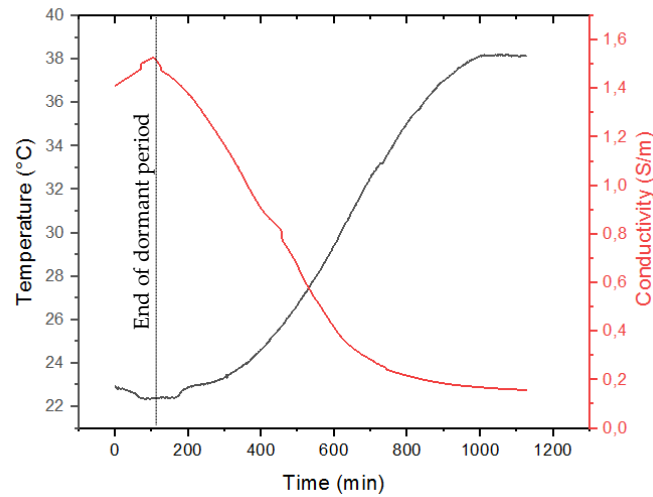


Figure 44: Visualization of change in conductivity compared to temperature over time

### 6.2.4 Experiment 2.2: 100% cement slurry + 0,6% of cement mass starch

It is well known that the setting time and workability of cement increase by adding starch to the initial slurry. Commonly, starch admixtures are utilized as a retarder in the cement industry since this additive is locally available and cheaper compared to other chemicals.

(Akindehinde Akindahunsi, et al. 2013),(Joseph and Xavier 2014),(Peschard et al. 2004)

To visualize the retarding effect of starch, 0,6% of cement mass was added to 1800 ml of the pure cement slurry.

100% Cement slurry + 0,6% of Cement mass starch		
Total Volume [ml]	1800	
	<u>Cement</u>	<u>Starch</u>
Volume	1800 ml	12 g

Table 8: Slurry design experiment 2.2



Figure 45: Experiment 2.2: Left side view - back view - top view

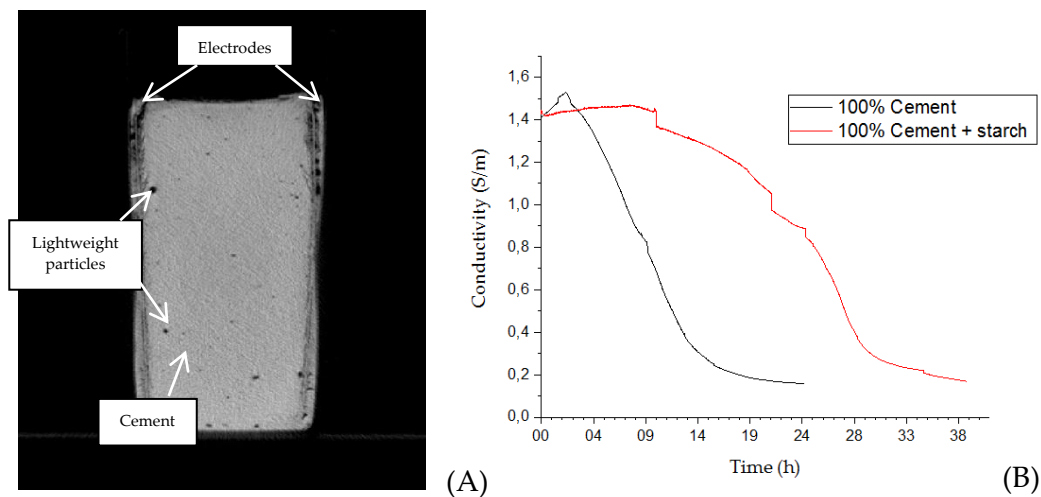


Figure 46: Experiment 2.2: CT-Scan (A), conductivity vs. time compared to experiment 2.1 (B)

Discoloration of the hydrated cement can be recognized at the bottom of the beaker (Figure 45). Pure cement slurry shows a lighter shade compared to cement with specific additives. For example, an admixture that contains calcium ions can cause darkening of the cement color.

(“Dark Discoloration of Flatwork| Concrete Construction Magazine” n.d.).

The dissimilarity of the color over the sample refers to inadequate mixing of the cement slurry with the starch. By squeezing the sample on the top and the bottom, a slight difference in texture can be recognized. The lower part is a little bit softer compared to the upper part since the cement-starch mixture accumulated on the bottom. Nevertheless, the slurry seems homogenous on the CT-scan since this device is not able to differentiate between pure cement and cement-starch mixture due to the similar absorption of the radiation.

The retarding effect of starch is shown by plotting the conductivity change of pure cement versus cement with starch. After approximately 12 hours, the slurry started to hydrate. Therefore, this test was performed for 39 hours. The irregularities in the red line are a result of the LCR-Meter software malfunctions. Due to an inexplicable reason, the data logging stops after different periods.

Experiment 2: Different mud-cement ratios

### 6.2.5 Experiment 2.3: 90% Cement slurry + 10% Mud

In experiment 2.3, the first test with a contaminated slurry was performed.

90% Cement slurry + 10% Mud		
Total Volume [ml]	1800	
	<i>Cement</i>	<i>Mud</i>
Volume	1620 ml	180 ml

Table 9: Slurry design experiment 2.3



Figure 47: Experiment 2.3: Left side view - back view - top view

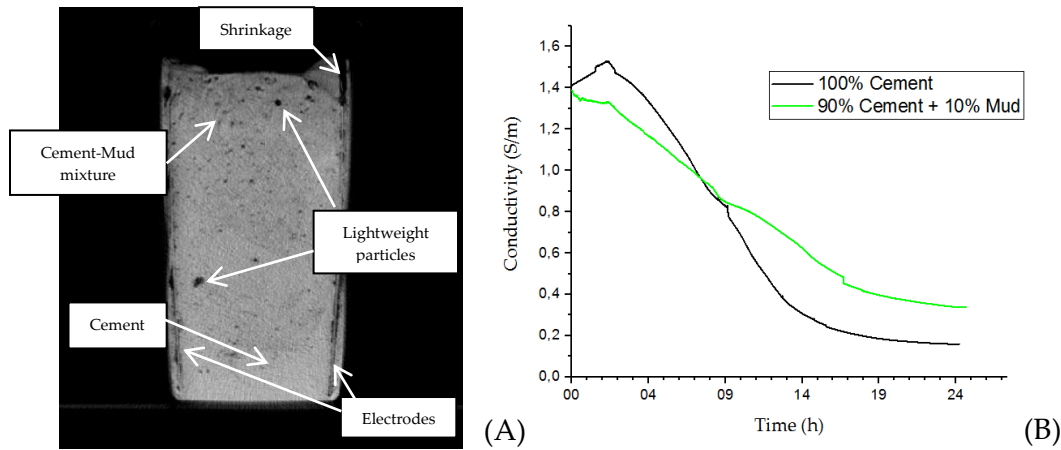


Figure 48: Experiment 2.3: CT-Scan (A), conductivity vs. time compared to experiment 2.1 (B)

On the bottom of the beaker, an accumulation of the denser cement can be detected which turned dark due to the presence of  $\text{Ca}^{2+}$  ions from the mud. The lighter cement-mud mixture moved to the top indicated by the brighter color (Figure 47).

By looking at the CT-scan, a difference in color can be recognized which verifies the contamination. The denser cement slurry is detected on the bottom ( in the CT-scan more brighter), and the lighter mixture can be seen on the top (in the CT-scan darker). If we compare the CT-scan with the one from experiment 2.1, we can see that the color of the sample not uniform anymore. Shrinkage is already present due to the water in the mud (Figure 47 and Figure 48). The green line differs from the black curve as expected, but unfortunately, due to a lot of LCR-Meter software malfunctioning during this test, the data were mainly interpolated and therefore not used for the investigation.

## 6.2.6 Experiment 2.4: 70% cement slurry + 30% mud

Next test was performed with 30% contamination.

70% Cement Slurry + 30% mud		
<b>Total Volume [ml]</b>	<b>1800</b>	
	<i>Cement</i>	<i>Mud</i>
<b>Volume</b>	1260 ml	540 ml

Table 10: Slurry design experiment 2.4

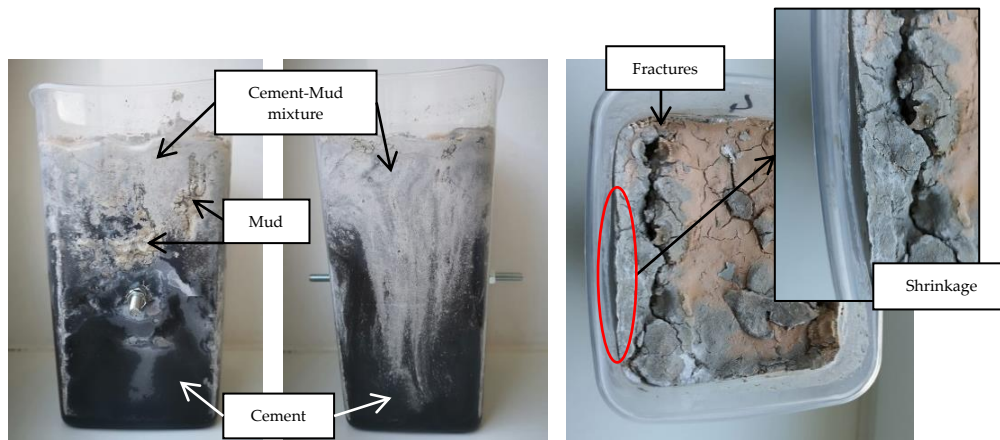


Figure 49: Experiment 2.4: Left side view - back view - top view

## Experiment 2: Different mud-cement ratios

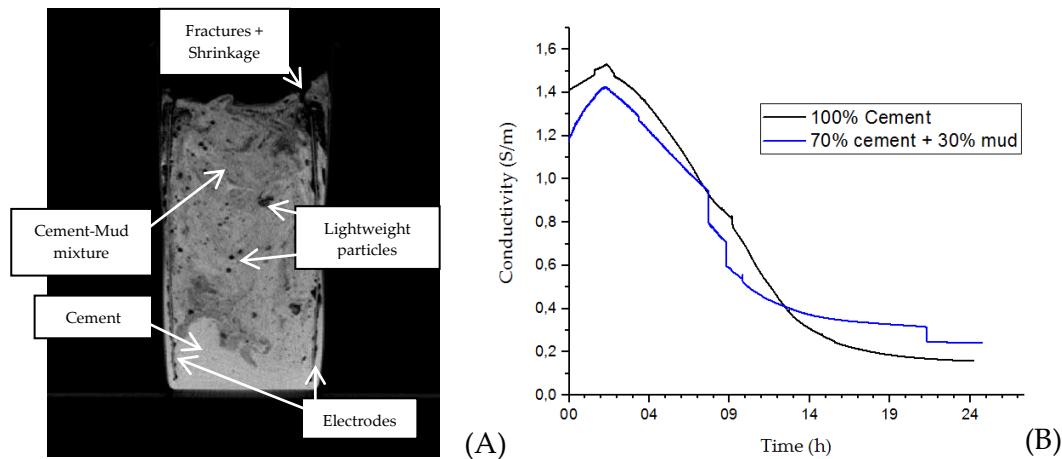


Figure 50: Experiment 2.4: CT-Scan (A), conductivity vs. time compared to experiment 2.1 (B)

Since more volume of mud was added, the amount of discoloration of the cement slurry increased. In Figure 49, pure mud particles are already visible. The cement, which was not contaminated, moved to the bottom and can be detected on the CT-scan (bright). The darkest area is located on the top and indicates high contaminated cement.

In the beginning, the conductivity is lower compared to the pure cement slurry. However, after approximately 12 hours, the decline of the curve is less, and the values remain higher. The conductivity decrease in pure cement due to the formation of compounds. Hence, if the cement is contaminated, not all ions can compound, and therefore, the conductivity remains higher in the final stage.

### 6.2.7 Experiment 2.5: 50% cement slurry + 50% mud

50% Cement Slurry + 50% mud		
Total Volume [ml]	1800	
	<i>Cement</i>	<i>Mud</i>
Volume	900 ml	900 ml

Table 11: Slurry design experiment 2.5



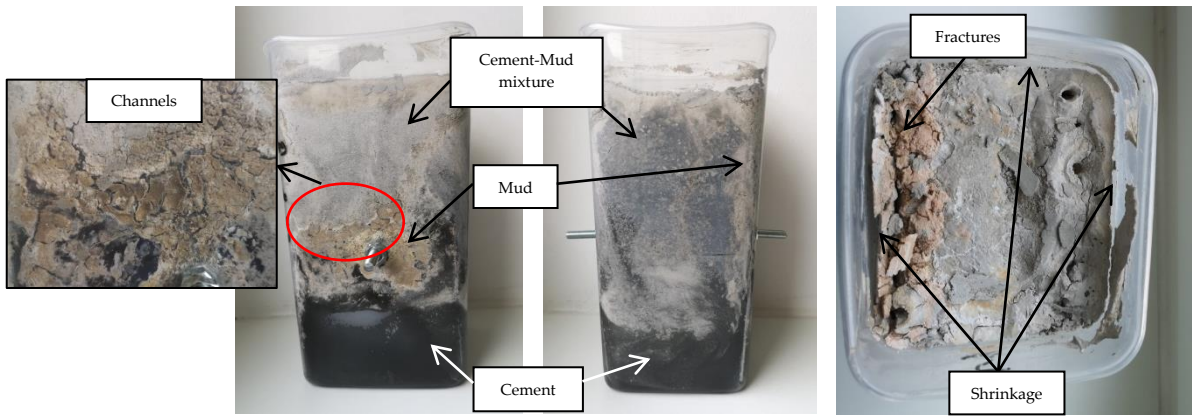


Figure 51: Experiment 2.5: Left side view - back view - top view

By mixing 50% of cement with 50 % of mud, a significantly smaller amount of cement is visible on the bottom. The bright color on the top indicates the cement-mud mixture. Channels can be noted in the area where mud has concentrated.

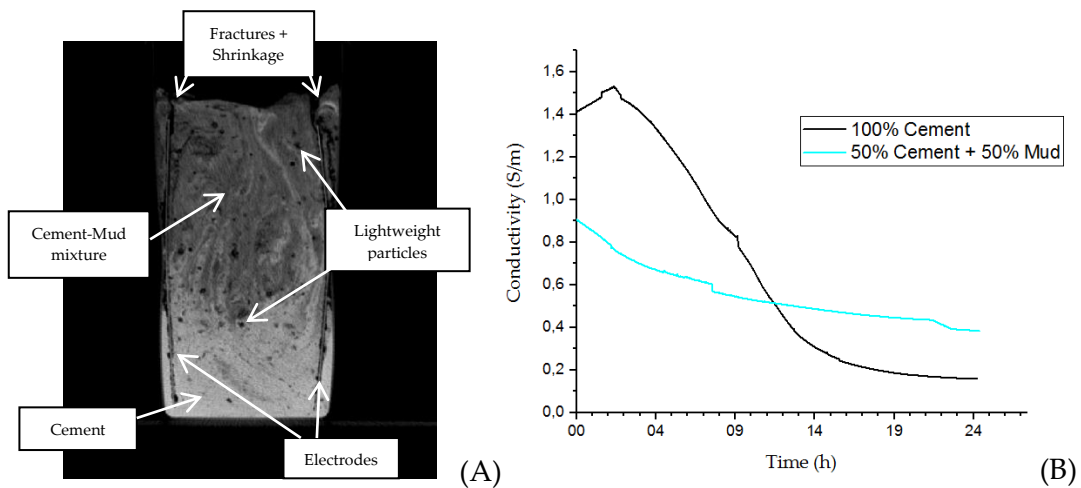


Figure 52: Experiment 2.5: CT-Scan (A), conductivity vs. time compared to experiment 2.1 (B)

The CT-scan proves the statements about Figure 51, and the conductivity is lower compared to experiment 2.4, as expected. Unfortunately, a lot of malfunctions of the device made this test inconclusive.

Experiment 2: Different mud-cement ratios

6.2.8 Experiment 2.6: 30% cement slurry + 70% mud

30% Cement Slurry + 70% mud		
Total Volume [ml]	1800	
	<i>Cement</i>	<i>Mud</i>
Volume	540 ml	1260 ml

Table 12: Slurry design experiment 2.6

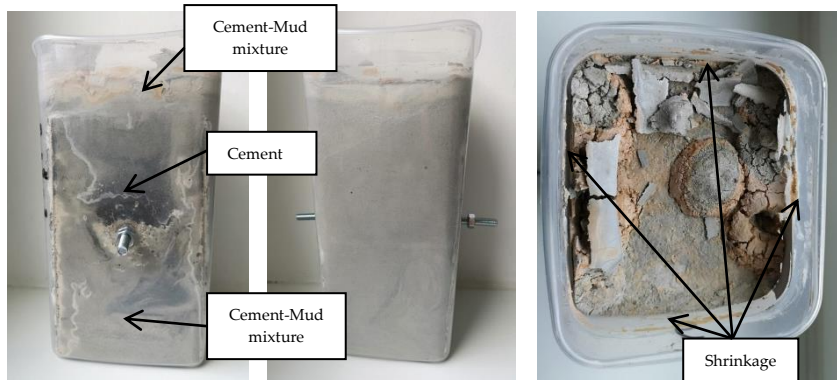


Figure 53: Experiment 2.6: Left side view - back view - top view

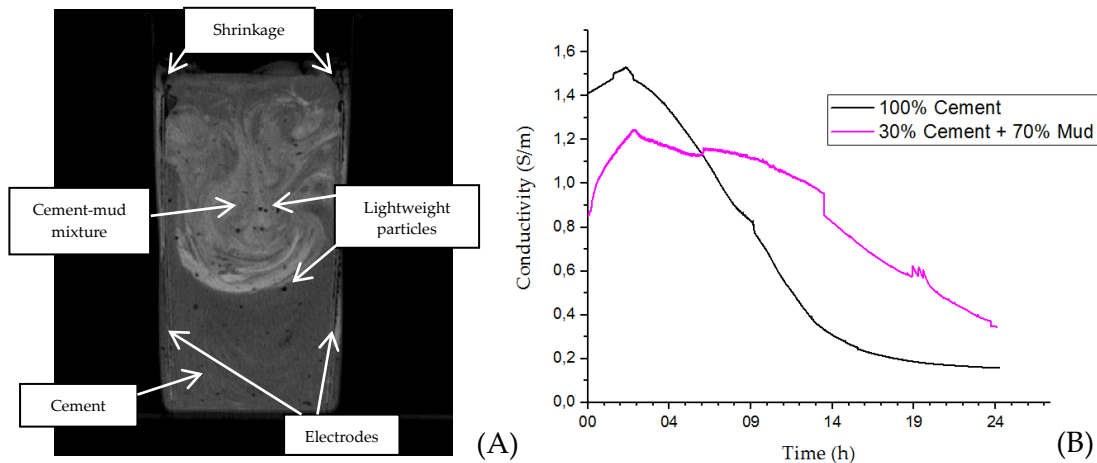


Figure 54: Experiment 2.6: CT-Scan (A), conductivity vs. time compared to experiment 2.1 (B)

The CT-scan proves the location of the cement visible in Figure 53. The slurry remains mainly soft as not enough cement is present to harden. The conductivity is lower compared to experiment 2.4 at the beginning but remains higher at the end.

### 6.2.9 Experiment 2.7: 10% cement slurry + 90% mud

10% Cement Slurry + 90% mud		
Total Volume [ml]	1800	
	<i>Cement</i>	<i>Mud</i>
Volume	180 ml	1620 ml

Table 13: Slurry design experiment 2.7

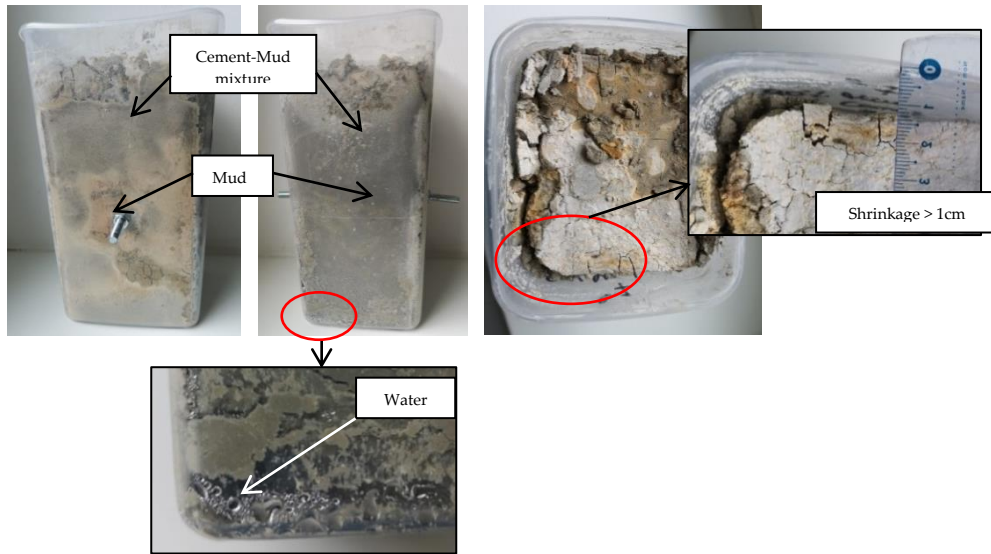


Figure 55: Experiment 2.7: Left side view - back view - top view

At 90% contamination, the slurry remains extraordinarily soft and wet. Water drops can be recognized on the bottom of the beaker, and the shrinkage is significantly high.

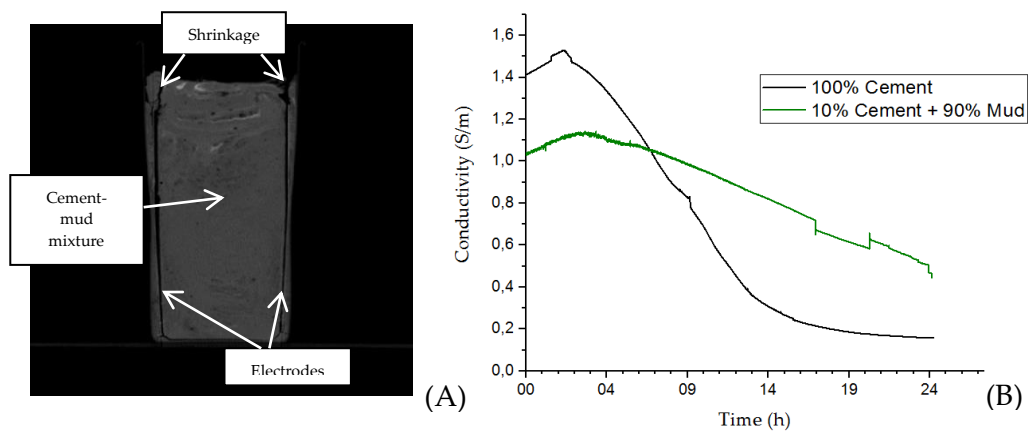


Figure 56: Experiment 2.7: CT-Scan (A), conductivity vs. time compared to experiment 2.1 (B)

Experiment 2: Different mud-cement ratios

The CT-scan demonstrate the overall contamination of the cement. We see a difference in conductivity compared to pure cement, but the data is again not meaningful.

6.2.10 Experiment 2.8: 100% mud

The last test was performed with 100 % of mud.

100% mud		
Total Volume [ml]		1800
	<i>Cement</i>	<i>Mud</i>
Volume	-	1800 ml

Table 14: Slurry design experiment 2.8



Figure 57: 100% mud



Figure 58: 100% mud after resting one week

A massive shrinkage and formation of channels can be recognized after one week.

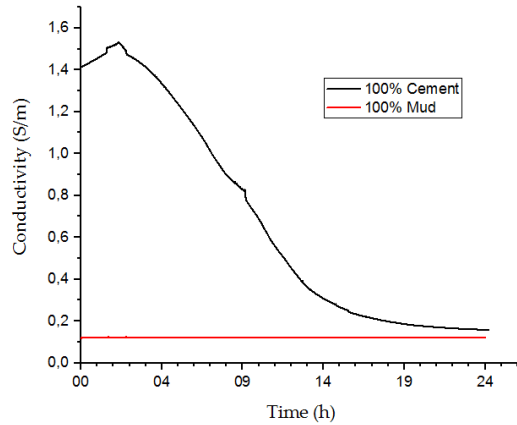


Figure 59: Experiment 2.7: conductivity vs. time compared to experiment 2.1

As expected, the conductivity measurement of 100% cement is lower as pure cement ever reaches and remains stable over 24h.

### 6.2.11 Result

Figure 60 shows the eight different samples with various mud contamination. On this picture, the contamination is already clearly visible with the naked eye. The images from the CT-scan prove the impure cement.

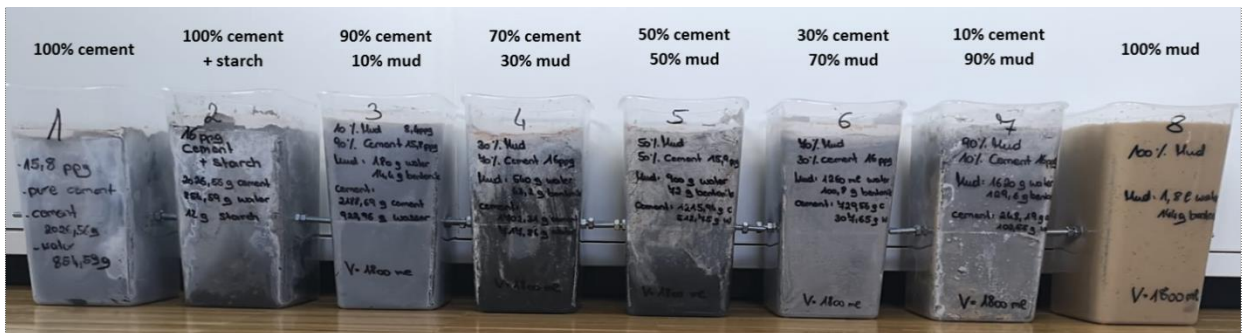


Figure 60: Samples with different level of mud contamination

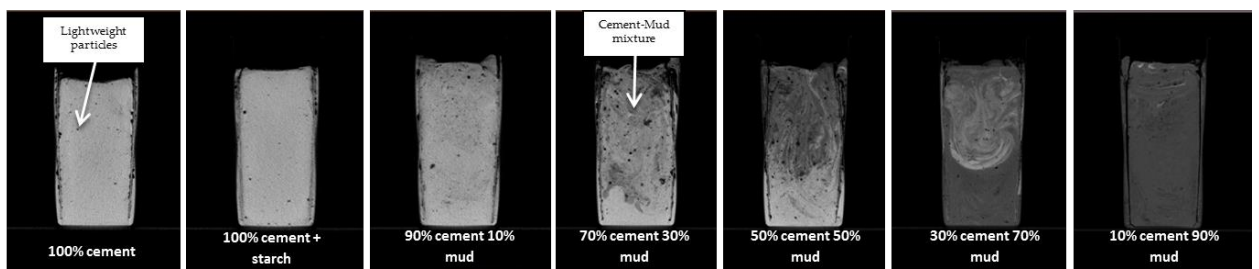


Figure 61: CT-scan of Samples with varying degrees of mud contamination

Experiment 2: Different mud-cement ratios

The figure below shows the comparison of sample 4 with sample 6. As a reference, the curve of sample 1 and the mud line are as well visible.

The conductivity decreases significantly with the increasing degree of mud contamination. This diagram proves that measuring conductivity can identify contaminated and unhydrated cement.

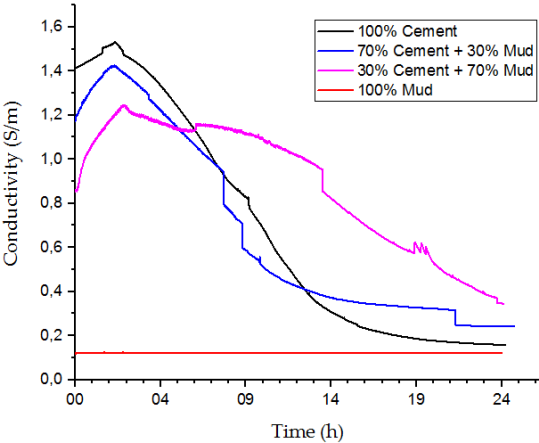


Figure 62: Comparison of different samples.

## 6.3 Experiment 3: Fiber optic cable measurement

### 6.3.1 Equipment

- Scale, Kern FCB
- Constant Speed Mixer, Chandler Engineering
- Heidolph RZR 2051 electronic Mixer
- Pressurized Gravity Balencometer
- Baroid Mud Balance
- Fann Rational Viscometer, Chandler Engineering
- Fiber-optics

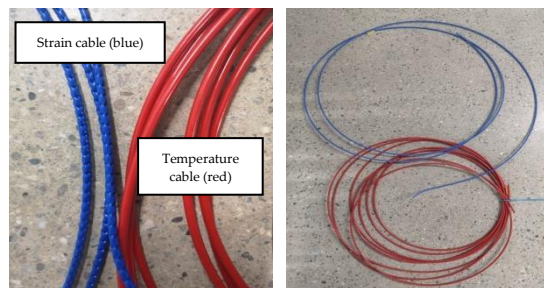


Figure 63: Fiber-optics

- Minirig

The Minirig can be seen below and is operated through the control unit.

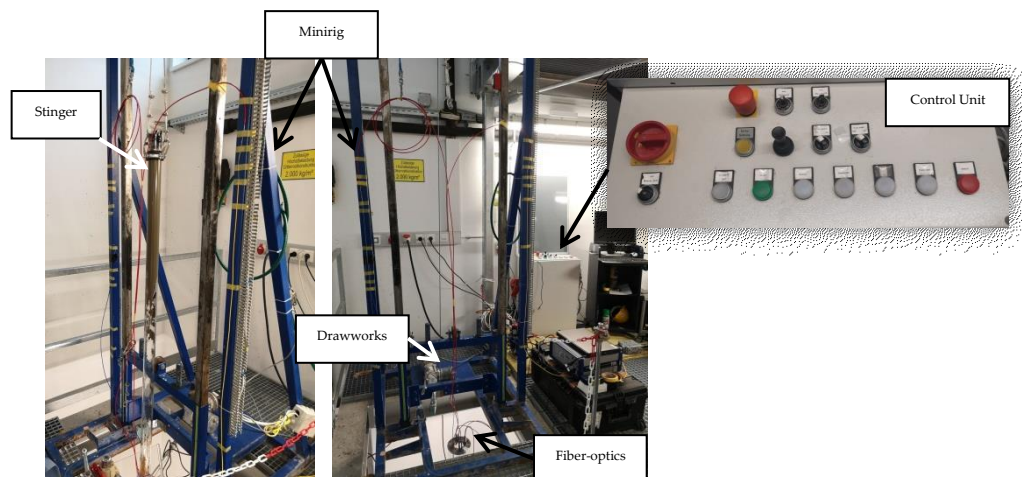


Figure 64: Minirig

### Experiment 3: Fiber optic cable measurement

- Construction to hold the pipe in place

The construction in Figure 65 was designed by Emanuel Hofer, which can be seen in more detail in his thesis ("Master Thesis by Emanuel Hofer.Pdf" n.d.), and will support the stability of the pipe during the test.



Figure 65: Pipe holding construction, designed by Emanuel Hofer

- Test tube

These experiments were conducted in a plexiglass tubing with a length of two meters. The outer pipe represents the casing or borehole and has an outside diameter of 150mm. The outside diameter of the stinger, illustrated by the inner tube, is 55mm. The ratio of the diameters represents a downscaled cement plug setting scenario with a 12,5" borehole and a 5" drill pipe.

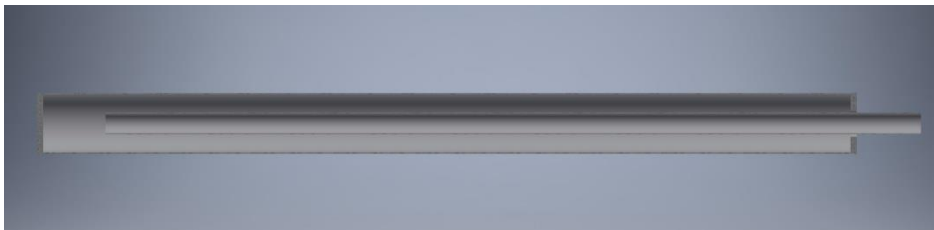


Figure 66: Tubing design



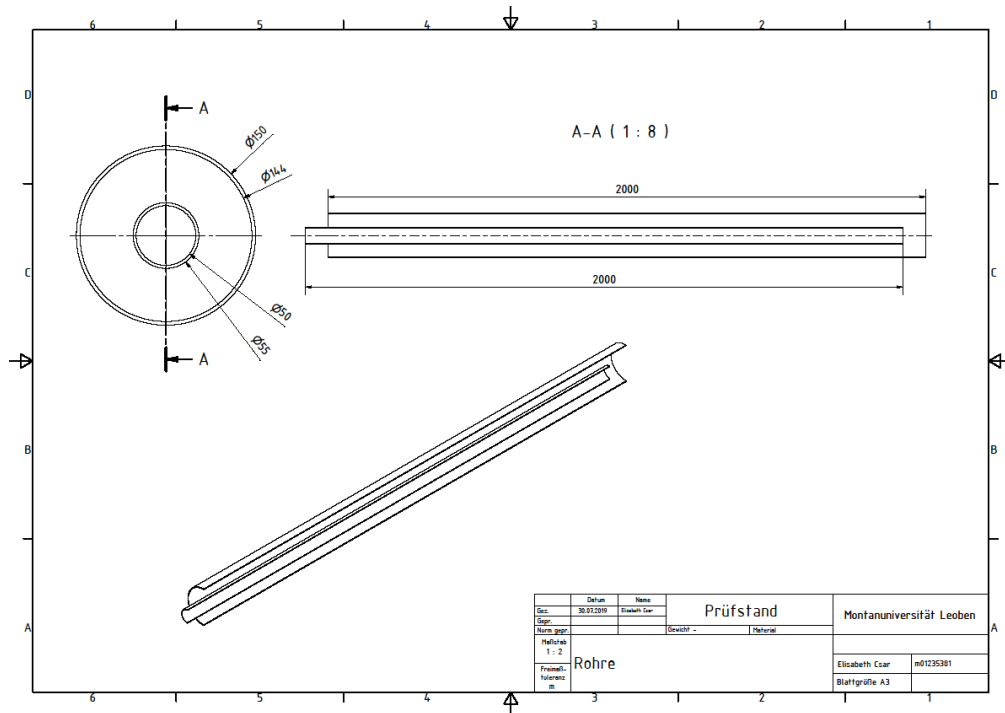


Figure 67: Dimensions of tubing

- Construction to hold fiber-optics in place

To install the fiber-optics in the tube, a structure to maintain the cables in place was necessary to be designed.

The bottom-plate can be seen in Figure 68. The dimensions of all components are attached in the appendix.



Figure 68: Bottom-plate design



Figure 69: Top-plate design

Experiment 3: Fiber optic cable measurement



Figure 70: Cylinders to clamp fiber-optics

6.3.2 Experiment 3.1: Stable base fluid – competent cement plug

As already mentioned, fiber-optic cables are a perfect solution to measure temperature and strain in a concrete. These cables are cheap, uncomplicated to install and can remain in the cured cement without any problems.

To prove the validity of these parameters, the following tests were performed.

6.3.2.1 Slurry design

The cement plug slurry design was based on the master thesis of Emanuel Hofer. The best practice scenario was used to create a stable and competent cement plug.

The polymer mud was mixed 10 hours previous to the test and represented the drilling fluid. The quantity of the chemicals was calculated by the mud slurry preparation table (Table 3).

<b>Polymer Mud (10 liters)</b>	
<i>Water</i>	<i>10 l</i>
<i>K2CO3 (weight agent and inhibitor)</i>	<i>800 g</i>
<i>S-ES Bio XG- Xanthan Gum (viscosity agent)</i>	<i>30 g</i>
<i>S-ES Pac LV (fluid loss agent)</i>	<i>140 g</i>
<i>Citric Acid (pH control)</i>	<i>10 g</i>

Table 15: Experiment 3.1: Polymer mud design

<b>Rheological Data</b>	
<i>Density</i>	<i>8,7 ppg</i>
<i>Initial Temperature</i>	<i>22 °C</i>
<i>Shear rate [1/s]</i>	<i>Shear Stress [lb/100ft<sup>2</sup>]</i>
5,11	4

10,22	6	
51,09	15	
102,18	23	
170,3	31	
340,6	47	
510,9	60	
1021,8	90	
<b>Flow behavior index</b>	<b>0,5882</b>	
<b>10 seconds / 10 minutes Gel Strength</b>		
<b>Shear rate [1/s]</b>	<u>10 sec Gel Strength</u> [lb/100ft <sup>2</sup> ]	<u>10 min Gel Strength</u> [lb/100ft <sup>2</sup> ]
5,109	4	4

Table 16: Experiment 3.1: Rheological data of the polymer mud

As expected for mud, the Power-Law model fits best. The flow behavior index  $n$  can be read off the exponential equation.

$$\tau = K * \gamma^n = 1,617 * \gamma^{0,5882} \quad (15)$$

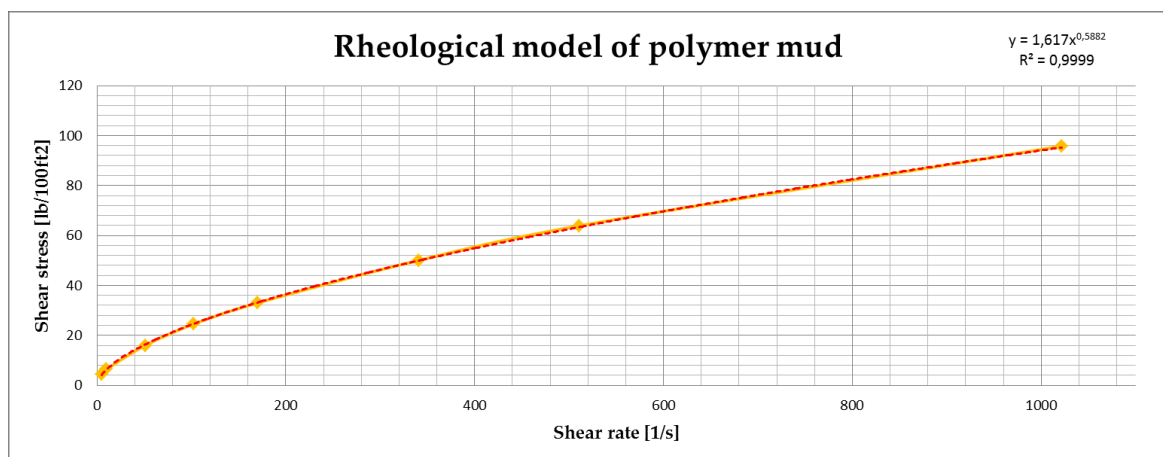


Figure 71: Experiment 3.1: Rheological model of polymer mud

Relatively low shear stress values and no change during the 10 sec gel strength and 10 min gel strength test, characterize the slurry as low flat gel.

The base fluid consisted of bentonite mud and was as well prepared 10 hours in advance.

Experiment 3: Fiber optic cable measurement

<b>Bentonite Mud (10 liters)</b>	
<i>Water</i>	<i>10 l</i>
<i>Bentonite</i>	<i>800 g</i>

Table 17: Experiment 3.1: Bentonite mud design

The measured density was 8,8 ppg. Therefore the mud had to be weighed up since the required density for the base fluid was 13,2 ppg.

<i>+ Barite (weight agent)</i>	<i>8,5 kg</i>
--------------------------------	---------------

Table 18: Experiment 3.1: Weight agent

<b>Rheological Data</b>		
<b>Density</b>	<b>13,2 ppg</b>	
<b>Initial Temperature</b>	<b>21,2 °C</b>	
<i>Shear rate [1/s]</i>	<i>Shear Stress [lb/100ft<sup>2</sup>]</i>	
5,11	115	
10,22	136	
51,09	138	
102,18	169	
170,3	202	
340,6	232	
510,9	262	
1021,8	>300 (not on the scale anymore)	
<b>Flow behavior index</b>	<b>0,1893</b>	
<b>10 seconds / 10 minutes Gel Strength</b>		
<b>Shear rate [1/s]</b>	<i>10 sec Gel Strength</i> <i>[lb/100ft<sup>2</sup>]</i>	<i>10 min Gel Strength</i> <i>[lb/100ft<sup>2</sup>]</i>
5,109	108	115

Table 19: Experiment 3.1: Rheological data of the base fluid

Again a type of mud was investigated, the expectations of a Power-Law model have been met. The flow behavior index is shown below.

$$\tau = K * \gamma^n = 81,276 * \gamma^{0,1893} \quad (16)$$

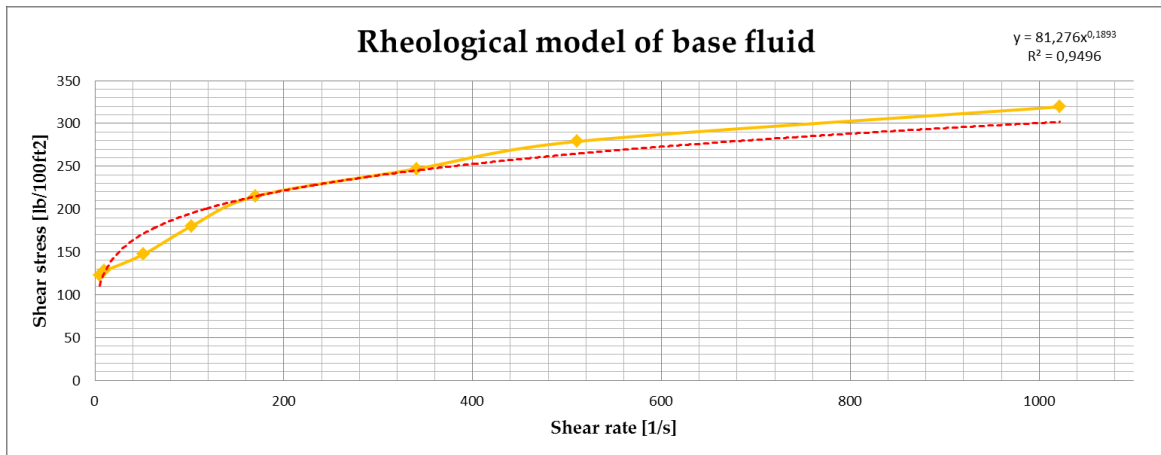


Figure 72: Experiment 3.1: Rheological model of base fluid

The fluid is characterized as a high flat gel due to the extremely high shear stress values and the slight decrease during the 10 sec gel strength and 10 min gel strength test.

The cement slurry was mixed 30 minutes before the cement plug was set.

<b>Cement Slurry</b>	
<i>Total Volume</i>	<i>10 l</i>
<i>Cement</i>	<i>9118,2 g</i>
<i>Water</i>	<i>7088,3 g</i>

Table 20: Experiment 3.1: Cement slurry design

<b>Rheological Data</b>	
<i>Density</i>	<i>13,4 ppg</i>
<i>Initial Temperature</i>	<i>21,7°C</i>
<i>Shear rate [1/s]</i>	<i>Shear Stress [lb/100ft²]</i>
5,11	1,5
10,22	1
51,09	3
102,18	4
170,3	6
340,6	9
510,9	15
1021,8	26
<b>Plastic Viscosity [cp]</b>	<b>7,79</b>

### Experiment 3: Fiber optic cable measurement

10 seconds / 10 minutes Gel Strength		
Shear rate [1/s]	10 sec Gel Strength [lb/100ft <sup>2</sup> ]	10 min Gel Strength [lb/100ft <sup>2</sup> ]
5,109	1	2

Table 21: Experiment 3.1: Rheological data of the cement slurry

The rheological data of cement can be best described by the Bingham Plastic model. The plastic viscosity can be read off of the linear equation below.

$$\tau = \tau_{\gamma} + \mu_p * \gamma = 0,026x + 1,5306 \quad (17)$$

Conversion for the plastic viscosity:

$$\left[ \frac{lb}{100 ft^2} \right] * \left( \frac{1,065 * 47886}{100 * 1,703} \right) = [cp] \quad (18)$$

$$0,026 * 299,46 = 7,79 [cp]$$

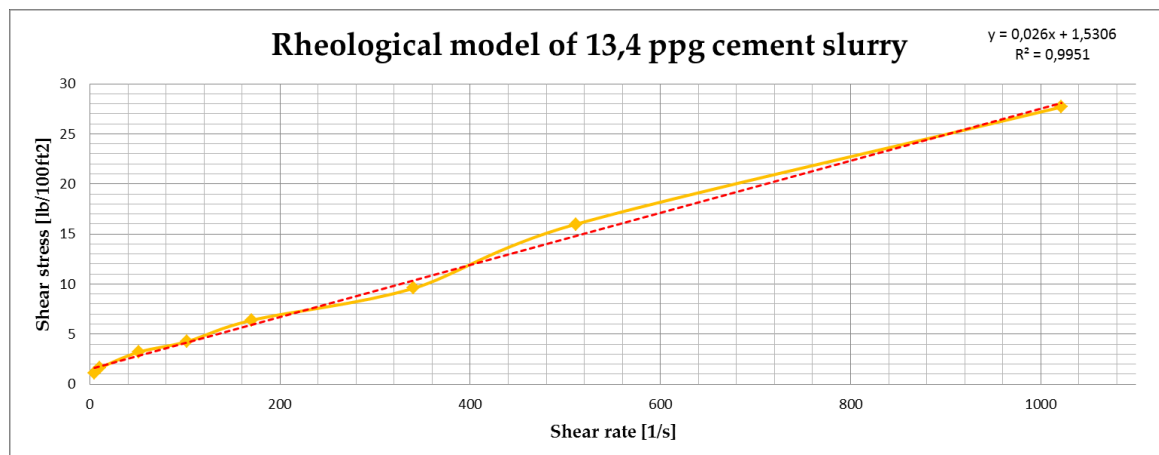


Figure 73: Experiment 3.1: Rheological model of 13,4 ppg cement slurry

This cement slurry can as well be classified as a low flat gel due to the low shear stress and similar values for during the 10 sec/10 min gel strength test.

#### 6.3.2.2 Planned fiber-optics installation

In the picture below the planned fixing procedure will be explained. One fixation point is located at the top and the other one at the bottom. The cable will be run down from the top towards the bottom and then back again. Finally, each cable will make four loops.

Unfortunately, the cables were too stiff. Therefore we could not build the curvature at the bottom plate. For this reason, the bottom-plate had to be modified.

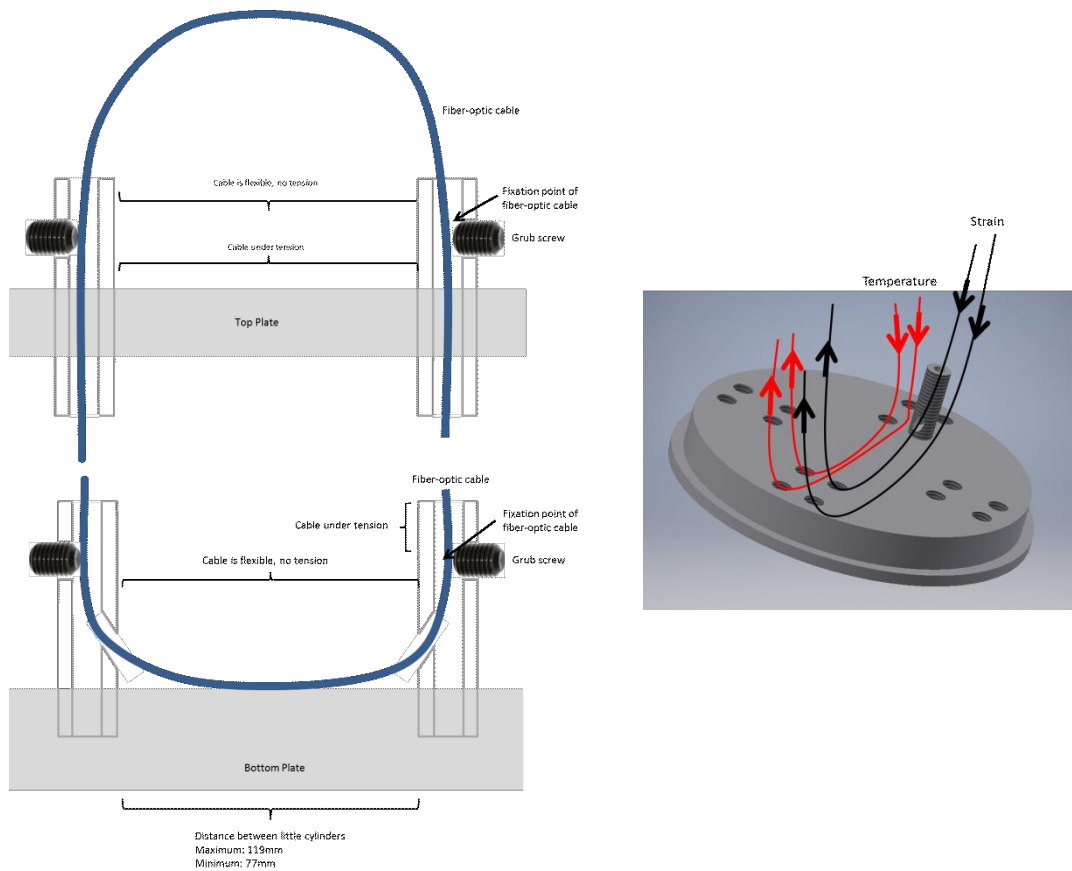


Figure 74: Fiber-optic installation plan

### 6.3.2.3 Final installation

Figure 75 shows the final installation. Due to the experience of the TU-Graz, we decided to only install two loops per cable as the space between the cables is very small. The bottom-plate was as well modified as can be seen in Figure 77. Through bores were created and sealed with silicone. It was necessary to place the little cylinders at the bottom to protect the cables from being crushed by the tube.

Experiment 3: Fiber optic cable measurement

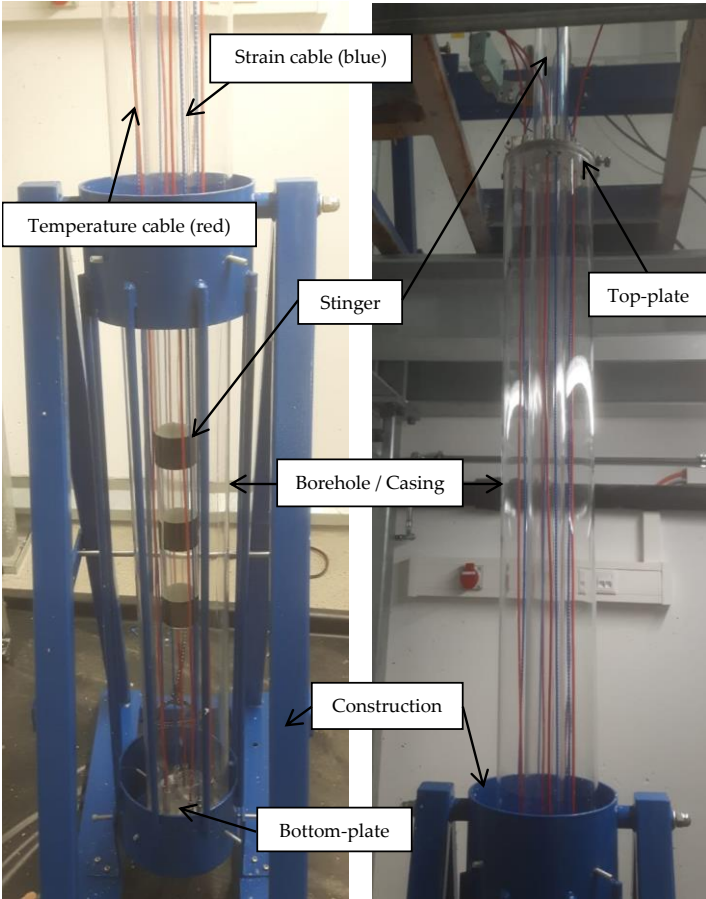


Figure 75: Final installation



Figure 76: Top-plate installation





Figure 77: Bottom-plate installation

#### 6.3.2.4 Setting procedure

As already mentioned, the slurries were prepared previous to the test. After the fiber-optic installation the tube was placed into the mounting support, and the stinger was installed inside the pipe (A). Afterward, the polymer fluid was filled through a funnel which was connected at the top of the stinger into the tube (B). The next step was to place the base fluid at the bottom of the pipe (C). Finally, the stinger was lifted with the rig to the top of the cement base, and there, the cement slurry was positioned (D). The base fluid was stable as expected, and the data logging was run for 36 hours.

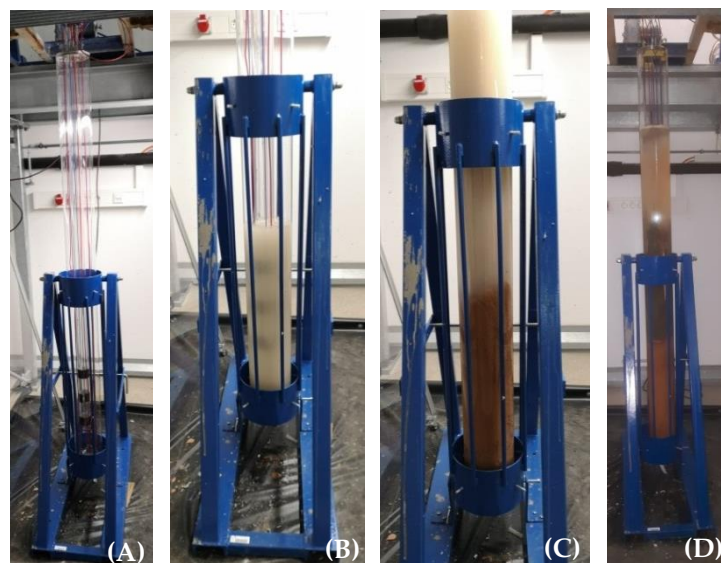


Figure 78: Setting procedure of competent cement plug

### 6.3.2.5 Results

#### Temperature

The results of the fiber-optic measurement can be seen in the images below.

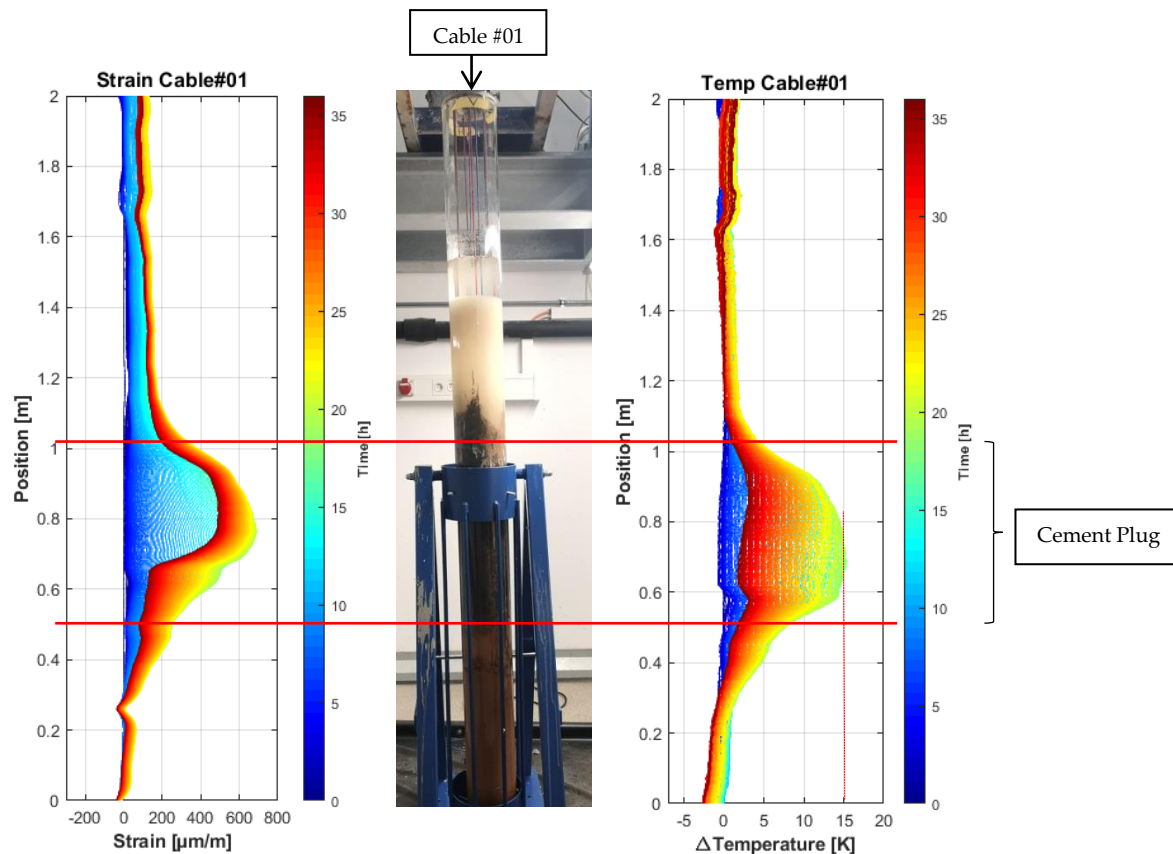


Figure 79: Experiment 3.1: Cement plug position, visible in strain and temperature profile

From 1,6 m to 2 m, the tubing is empty, which means the temperature change can be referred to the temperature change in the room. The polymer fluid is located at approximately 1,13 m to 1,6 m, and the slight difference in temperature is again a result of the surrounding temperature change. The same counts for the base fluid which is located at the bottom of the tube. The identification of the position of the cement plug is exact since a significant temperature increase due to the chemical reaction during the hydration process can be recognized. After approximately 17 hours, the most substantial increase in temperature is recorded.

By comparing the four temperature cables with each other difference in height of the bottom of the cement, plug can be identified (Figure 80 and Figure 81). By measuring the depth in the laboratory the unconformity of the temperature measurements is proven. This temperature test not only defines the exact location of the cement but verifies the preciseness of the fiber-optics.

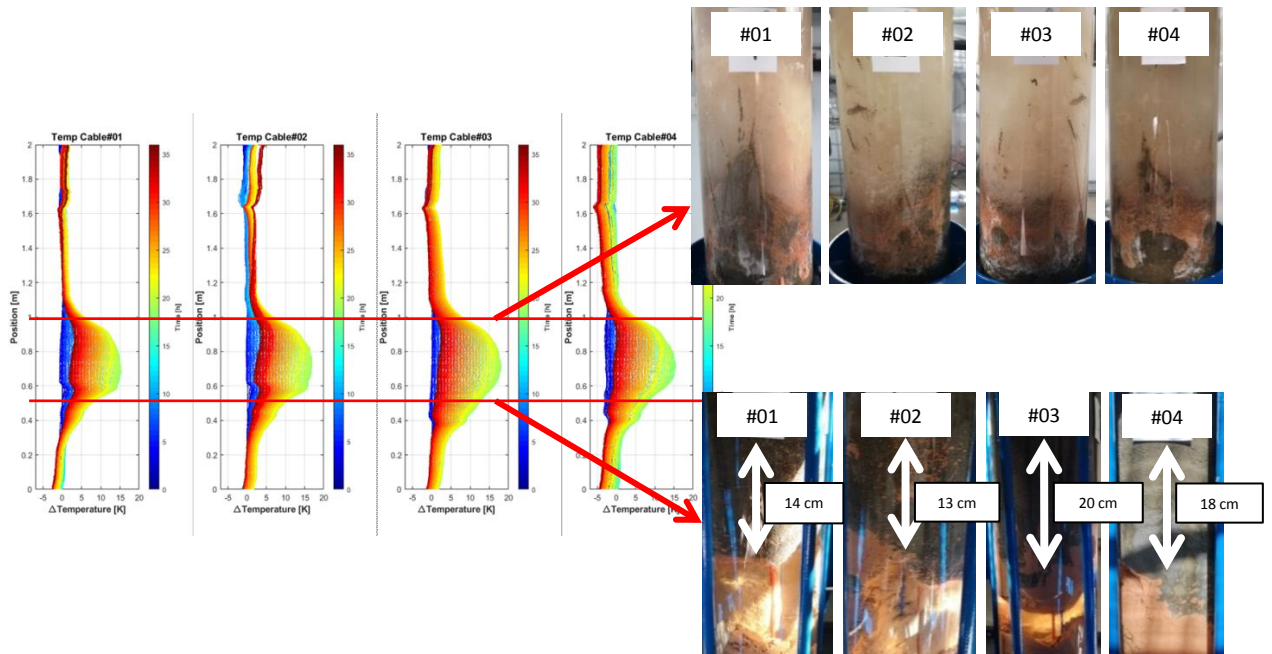


Figure 80: Experiment 3.1: Depth vs. temperature change for each cable

The temperature change vs. time plots illustrate even better the increase and later on the decrease in temperature due to the hydration process.

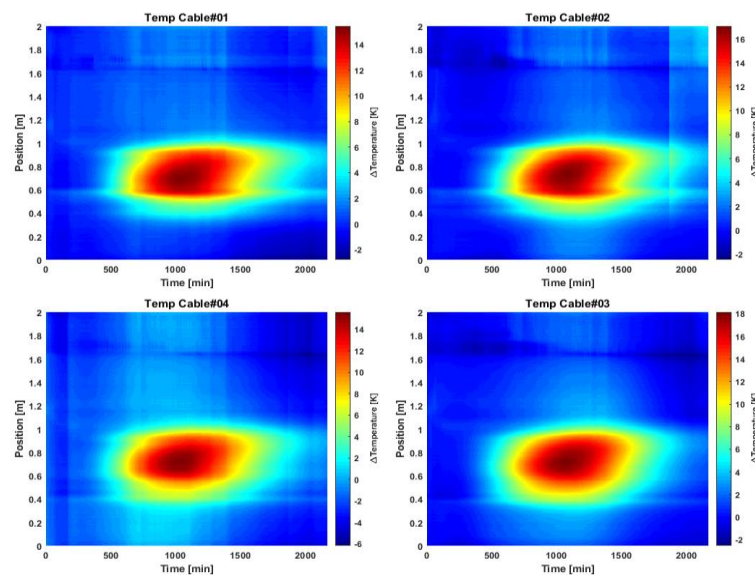


Figure 81: Experiment 3.1: Temperature change over time

Experiment 3: Fiber optic cable measurement

**Strain**

The results of the strain measurement can be seen below and as well confirms the position of the cement plug. Since the cable was not bonded with the cement at the beginning, the change in strain is a result of temperature change. After the cable is combined with the cement, the values can be linked to the increased compressive strength of the cement due to the hydration process.

A crack in the cement shaft would result in a strain peak (Winkler et al., n.d.). Therefore, no cracks occurred during the hardening process as can be seen in the picture below.

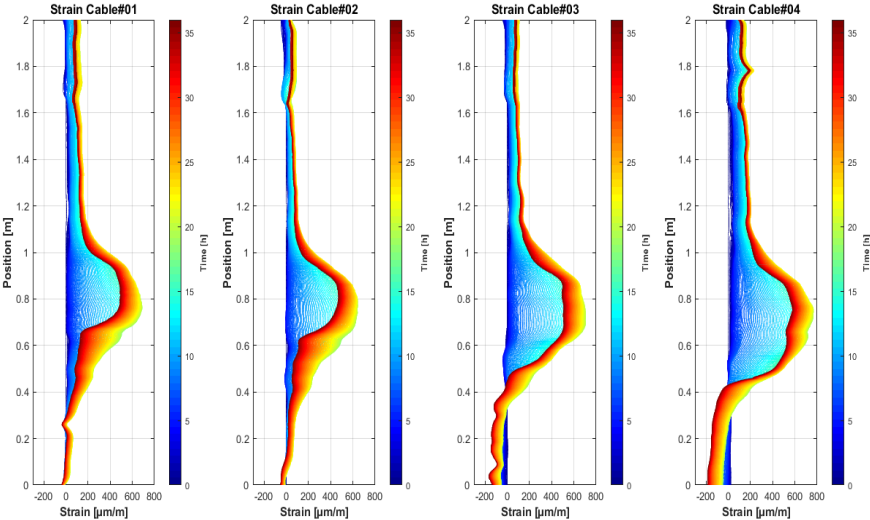


Figure 82: Experiment 3.1: Depth vs. strain for each cable

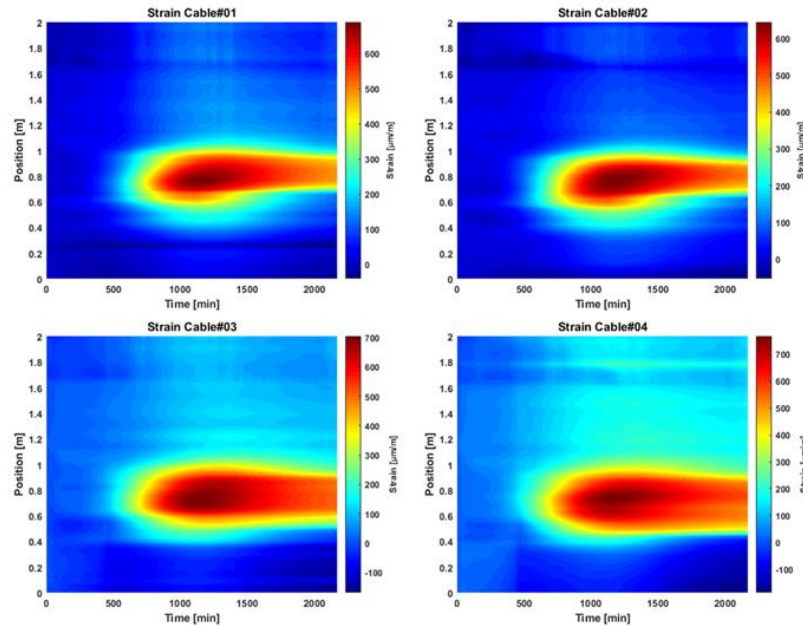


Figure 83: Experiment 3.1: Strain over time

To discuss the strain measurement in more detail, a time versus strain plot with different compensation factors were created. To identify the pure strain behavior due to the influence of shrinkage and creepage, the temperature-related changes of the object must be compensated. Usually, for cement, the compensation factor equals  $12 \mu\text{m/m per K}$  and for the cable  $35 \mu\text{m/m per K}$ .

For the picture below, the position at 0,8 m was analyzed. The blue line represents the data without any temperature compensation. The yellow line describes the temperature compensation of the cement and the red line of the cable. In the beginning, we have to follow the behavior of the cable until it starts to bond with the cement. Since the red and yellow curve starts to separate after approximately 350 minutes, we can assume the beginning of the hydration process and the development of the strain at this time. This statement matches the temperature over time plot as an increase in temperature can be seen after approximately 400 minutes which indicates the start of the hydration process. Though, we cannot define the exact time where the cable finally bonds with the cement. We can only assume that it happens after approximately 1200 minutes since this is the highest point of the yellow curve. Therefore, between 350 and 1200 minutes, a mixing zone of cable and cement compensation can be expected since we are in the transition zone of cement hydration. Afterward, the compensation curve of cement can be referred to the strain behavior. Moreover, the onset of bonding and shrinkage of the cement equals to  $60 \mu\text{m/m}$  at this specific position and is visualized in the plot.

### Experiment 3: Fiber optic cable measurement

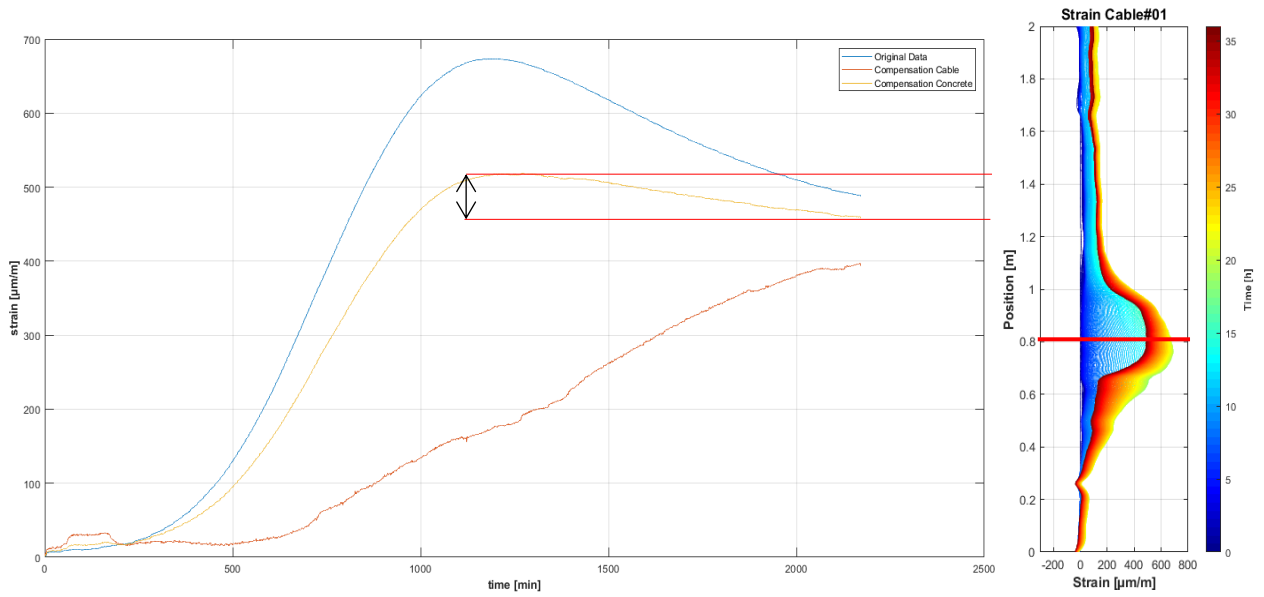


Figure 84: Time vs. strain for different compensation at position 0,8 m

Figure 85 shows the compensation curves at position 1,8 m. Since no cement is present at this level, cable compensation is valid over the entire measured time. Comparing the behavior of the yellow and red lines with Figure 84, a different build-up can be recognized. This analyzes whether cement or other slurry is present.

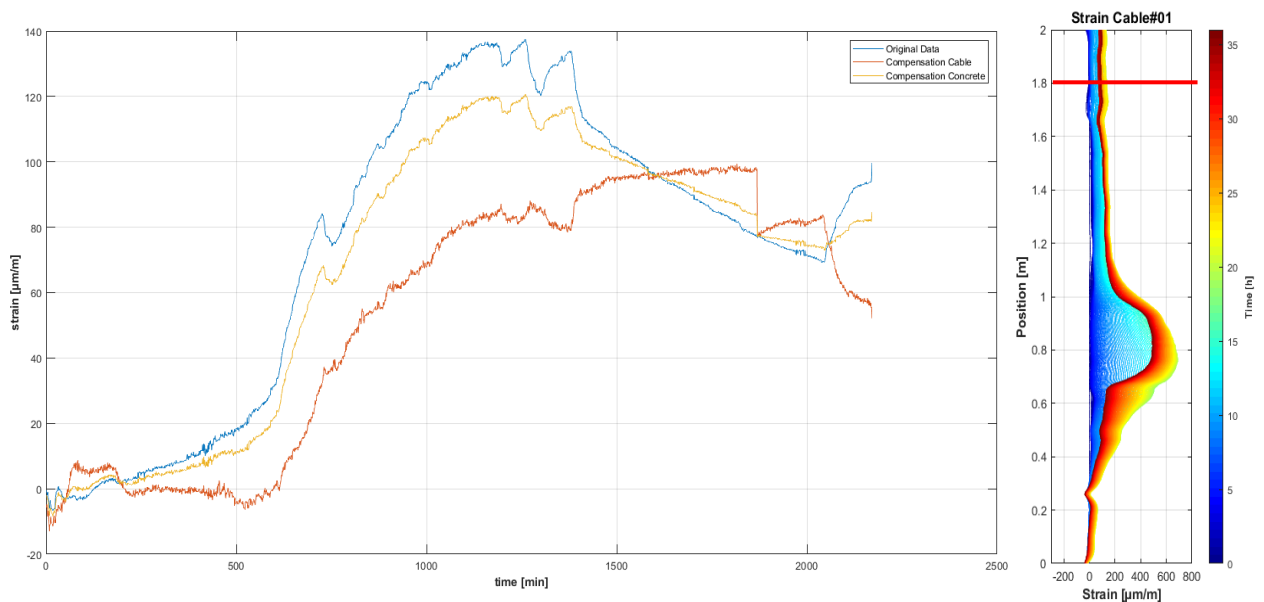


Figure 85: Time vs. strain for different compensation at position 1,8m

3D-plots of the temperature change and strain development are attached in appendix A.

## CT-scan

CT-scans of experience 3.1 were created and analyzed.

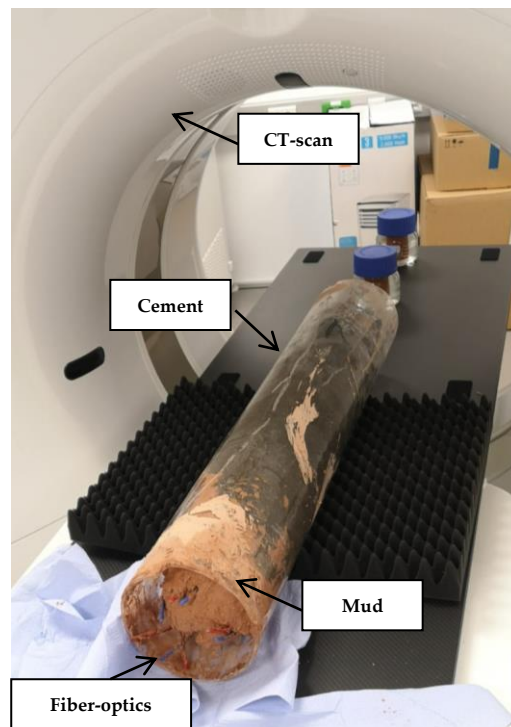


Figure 86: Performing CT-scan of competent cement plug

In contrast to the CT-scans from experiment 2, the brighter color represents the mud due to the added barite since the iron from the barite absorbs the radiation better compared to the cement. The small dark points represent lightweight particles, and the fiber-optic cables can be identified.

Figure 87 verifies the competent cement plug. And some bentonite mud, weighted with barite can be seen at the bottom of the plug. The temperature cable is more visible compared to the strain cable due to the higher stiffness, which is a result of more strengthening material.

Experiment 3: Fiber optic cable measurement

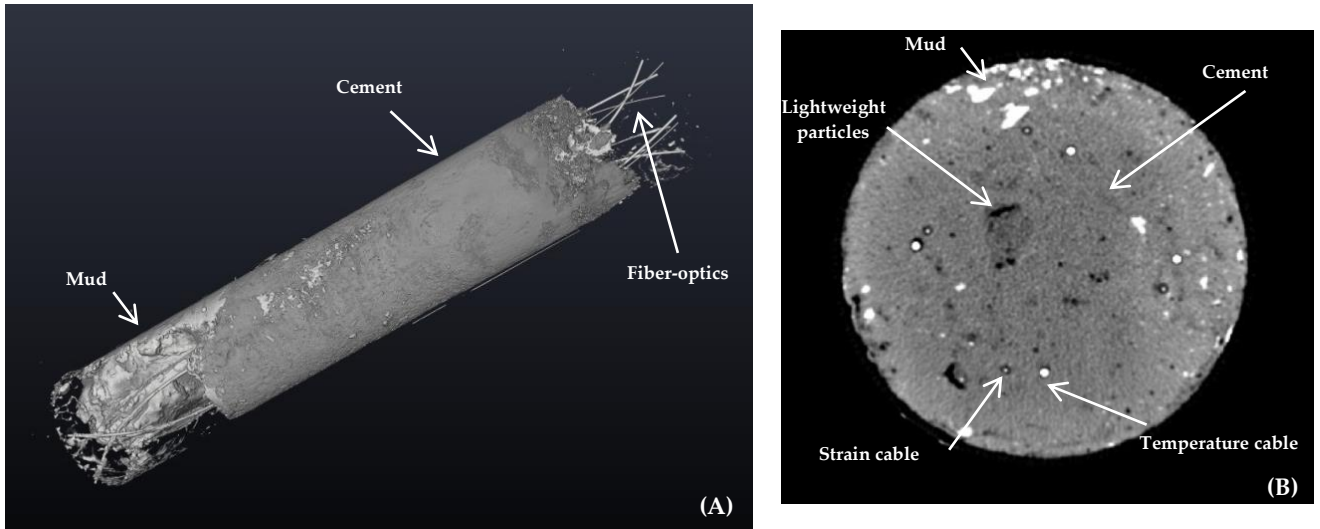


Figure 87: CT-scan of competent cement plug; 3D view (A); radial cross section (B)

The different heights of cement level, as already discussed in Figure 80, are verified by the CT-scan below. At cable#3 (C) and cable#4 (D), the slurry reached a lower depth.

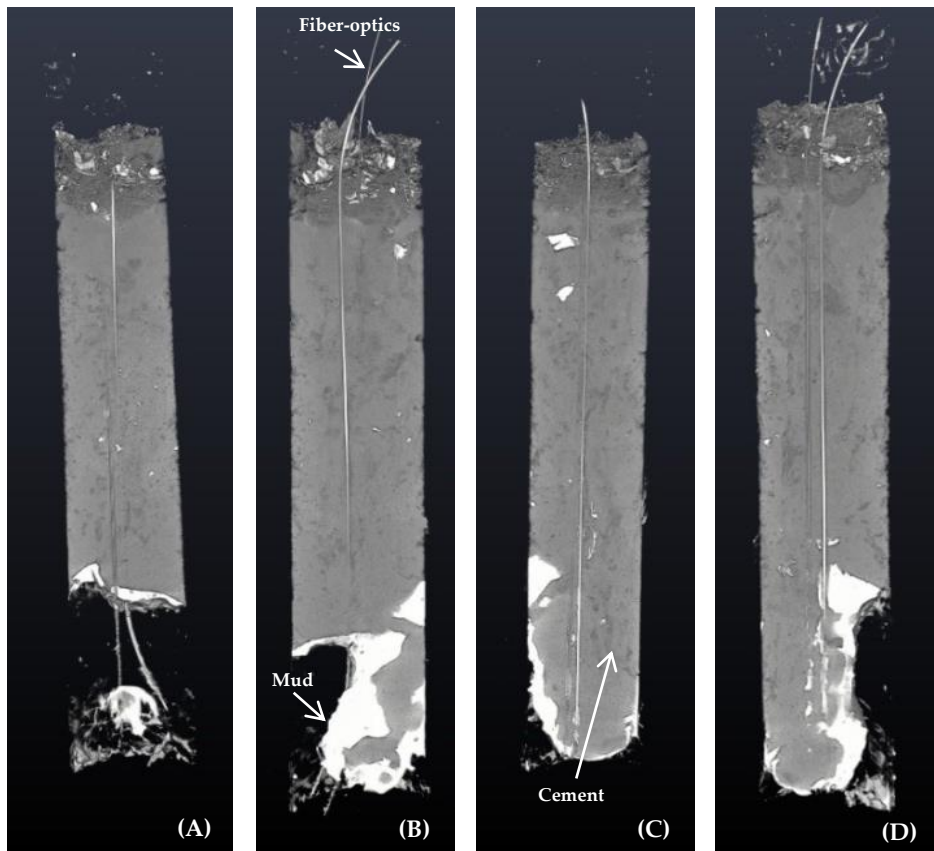


Figure 88:CT-scan: cable#1 (A); cable#2 (B); cable#3 (C); cable#4 (D)



### 6.3.3 Experiment 3.2: Unstable base fluid – contaminated cement plug

#### 6.3.3.1 Slurry design

For the second experiment with the fiber-optics, a cement plug with an unstable base was simulated. The polymer mud was mixed 10 hours in advance to the test, and its design and the rheological data can be seen below. The mixture was the same as for the first test, and the slight difference between the data is a result of inaccuracy while taking the readings.

<b>Polymer Mud (10 liters)</b>	
<i>Water</i>	<i>10 l</i>
<i>K<sub>2</sub>CO<sub>3</sub> (weight agent and inhibitor)</i>	<i>800 g</i>
<i>S-ES Bio XG- Xanthan Gum (viscosity agent)</i>	<i>30 g</i>
<i>S-ES Pac LV (fluid loss agent)</i>	<i>140 g</i>
<i>Citric Acid (pH control)</i>	<i>10 g</i>

Table 22: Experiment 3.2: Polymer mud design

<b>Rheological Data</b>		
<b>Density</b>	<b>8,6 ppg</b>	
<b>Initial Temperature</b>	<b>24,6°C</b>	
<i>Shear rate [1/s]</i>	<i>Shear Stress [lb/100ft<sup>2</sup>]</i>	
5,11	5,33	
10,22	7,46	
51,09	18,11	
102,18	26,63	
170,3	35,15	
340,6	53,25	
510,9	67,1	
1021,8	101,18	
<b>Flow behavior index</b>	<b>0,5569</b>	
<b>10 seconds / 10 minutes Gel Strength</b>		
<b>Shear rate [1/s]</b>	<i>10 sec Gel Strength</i> <i>[lb/100ft<sup>2</sup>]</i>	<i>10 min Gel Strength</i> <i>[lb/100ft<sup>2</sup>]</i>
5,109	5	5

Table 23: Experiment 3.2: Rheological data of the polymer mud

Experiment 3: Fiber optic cable measurement

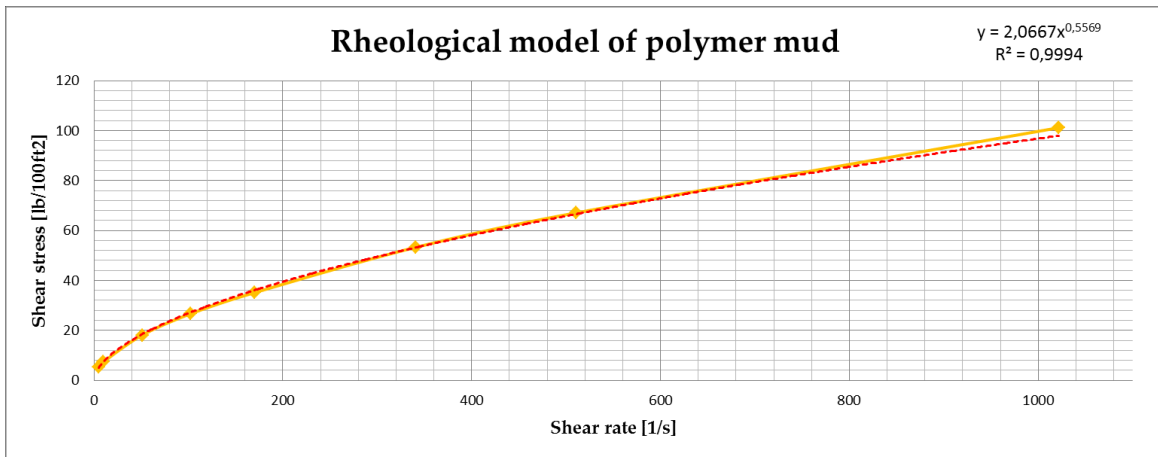


Figure 89: Experiment 3.2: Rheological model of polymer mud

Power-Law model:

$$\tau = K * \gamma^n = 2,0667 * \gamma^{0,5569} \quad (19)$$

The design of the bentonite mud was changed since the required density was 10 ppg.

Bentonite Mud (10 liters)	
Water	10 l
Bentonite	800 g

Table 24: Experiment 3.2: Bentonite mud design

+ Barite (weight agent)	2 kg
-------------------------	------

Table 25: Experiment 3.2: Weight agent

Rheological Data	
Density	9,9 ppg
Initial Temperature	23,2°C
Shear rate [1/s]	Shear Stress [lb/100ft²]
5,11	47,93
10,22	61,77
51,09	87,33
102,18	102,24
170,3	117,15
340,6	146,43
510,9	167,21

1021,8	223,65
<b>Flow behavior index</b>	<b>0,2732</b>
<b>10 seconds / 10 minutes Gel Strength</b>	
<b>Shear rate [1/s]</b>	<u>10 sec Gel Strength</u> [lb/100ft <sup>2</sup> ]
5,109	35
	<u>10 min Gel Strength</u> [lb/100ft <sup>2</sup> ]
	40

Table 26: Experiment 3.2: Rheological data of the base fluid

The slurry is as well characterized as a high flat gel due to its high shear stress values and the slight increase during the 10 sec/10 min gel strength test.

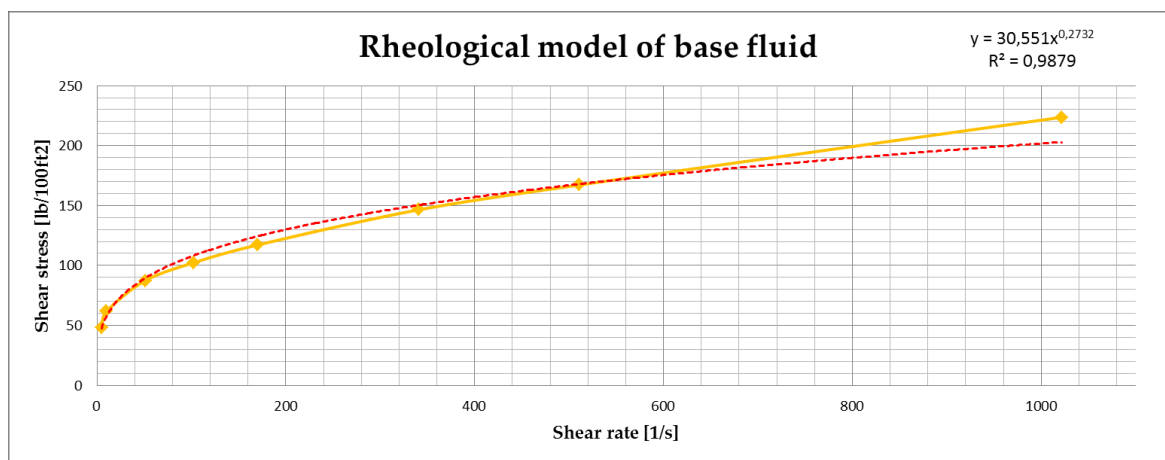


Figure 90 Experiment 3.2: Rheological model of the base fluid

The Power-LawModel is proven, and the equation can be seen below

$$\tau = K * \gamma^n = 30,551 * \gamma^{0,2732} \tag{20}$$

The density of the cement slurry was increased to 16 ppg compared to the previous experiment.

<b>Cement Slurry</b>	
Total Volume	10 l
Cement	13,51 kg
Water	5,7 kg

Table 27: Experiment 3.2: Cement slurry design

Experiment 3: Fiber optic cable measurement

Rheological Data		
<b>Density</b>	<b>16 ppg</b>	
<b>Initial Temperature</b>	<b>24,3°C</b>	
<i>Shear rate [1/s]</i>	<i>Shear Stress [lb/100ft<sup>2</sup>]</i>	
5,11	21,3	
10,22	26,63	
51,09	41,54	
102,18	51,12	
170,3	63,9	
340,6	87,33	
510,9	111,83	
1021,8	170,4	
<b>Plastic Viscosity [cp]</b>	<b>42,49</b>	
<b>10 seconds / 10 minutes Gel Strength</b>		
<i>Shear rate [1/s]</i>	<i>10 sec Gel Strength [lb/100ft<sup>2</sup>]</i>	<i>10 min Gel Strength [lb/100ft<sup>2</sup>]</i>
5,109	9	13

Table 28: Experiment 3.2: Rheological data of the cement slurry

Due to the high density, the mud tends to act like a high flat gel. Tough, the increase during the 10 sec/10 min test is not significant.

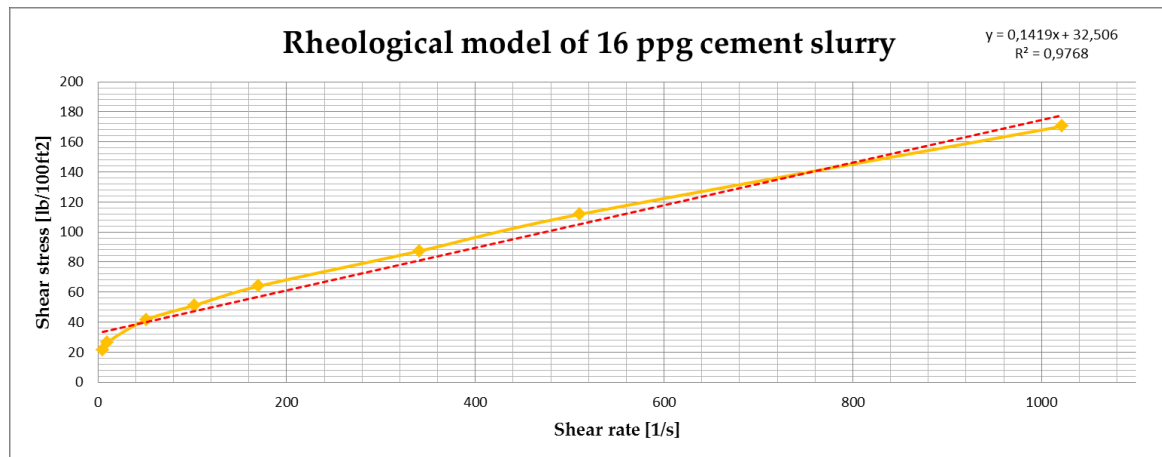


Figure 91 Experiment 3.2: Rheological model of 16 ppg cement slurry

The Bingham Plastic model fits best.

$$\tau = \tau_{\gamma} + \mu_p * \gamma = 0,1419x + 32,506 \quad (21)$$

Conversion for the plastic viscosity:

$$\left[ \frac{lb}{100 ft^2} \right] * \left( \frac{1,065 * 47886}{100 * 1,703} \right) = [cp] \quad (22)$$

$$0,092 * 299,46 = 42,49 [cp]$$

### 6.3.3.2 Fiber-optic installation

In Figure 92, the modified bottom plate is shown, and the fiber-optics were installed as already described in experiment 3.1.

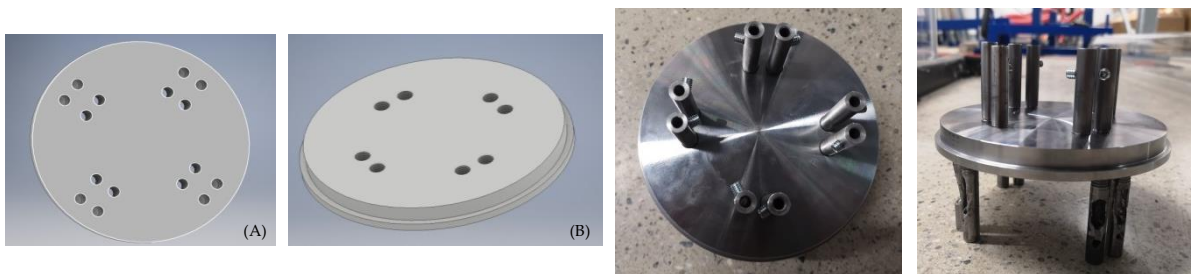


Figure 92: Modified bottom-plate, bottom view (A) – top view (B)

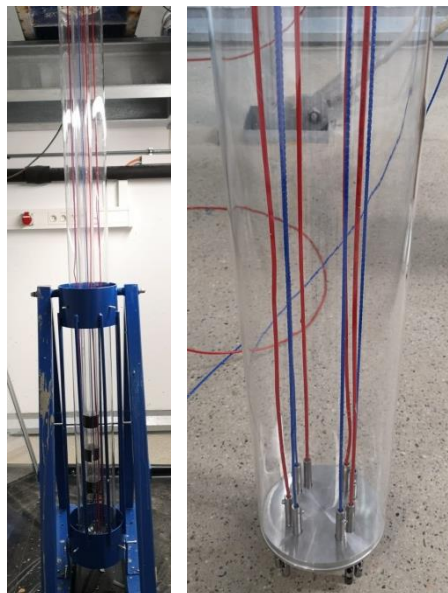


Figure 93: Fiber-optic installation experiment 3.2

### 6.3.3.3 Setting procedure

The failed cement plug was placed with the same method as for the previous experiment. The tube was filled up with the polymer fluid (A), the base fluid (B) and finally, with the cement slurry (C). As expected, the cement fell through the cement base and accumulated at the bottom of the tube. As a result, most of the cement slurry was contaminated as can be seen on the image below.

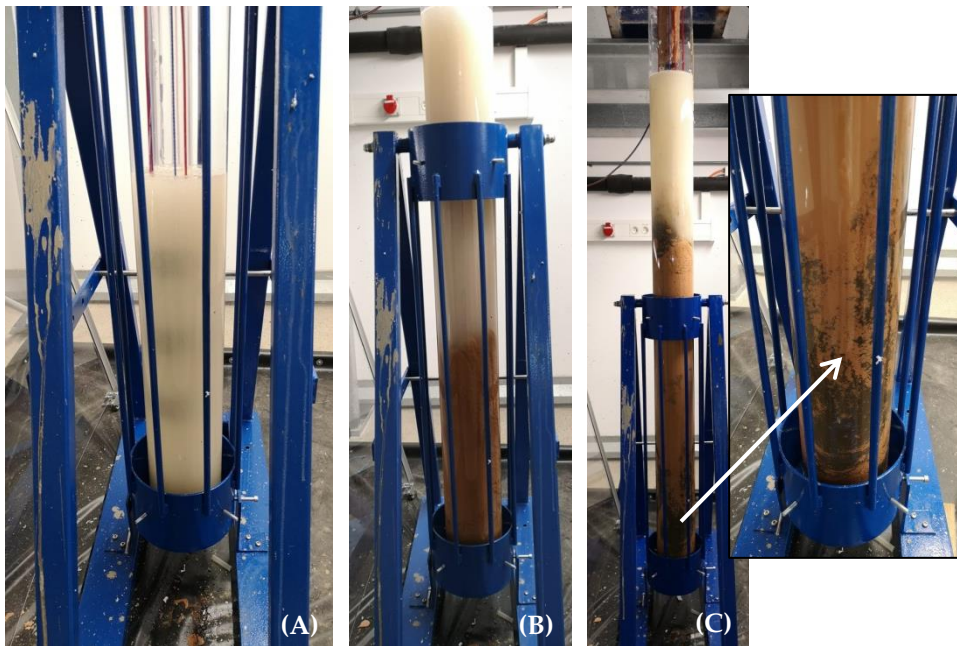


Figure 94: Setting procedure of failed cement plug

### 6.3.3.4 Results

#### Temperature

The depth vs. temperature plot proves the failed cement plug, which accumulated at the bottom of the tube. Compared to the previous test, the cement plug is now spread over a longer distance which is visualized in Figure 95. The TOC can be assumed at 0,8 m. From 0,4 m to 0,8 m, the temperature increase is less compared to the bottom of the tube. This phenomenon can be referred to the contamination of the cement since the cement accumulated on the bottom whereas the cement-mud mixture remained above. The temperature increase is higher ( $\sim 23$  K) compared to experiment 3.1, and the top temperature is already reached after 13 hours. The greater quantity of cement and higher room temperature are responsible for the earlier start of the hydration. Moreover, the heat generated during the exothermic reaction accelerates the cement reaction. Therefore, the reaction takes place faster and the result is a higher temperature increase.

The temperature reduction at the beginning of cable #1 can be explained due to slurry sticking on the cable during filling.

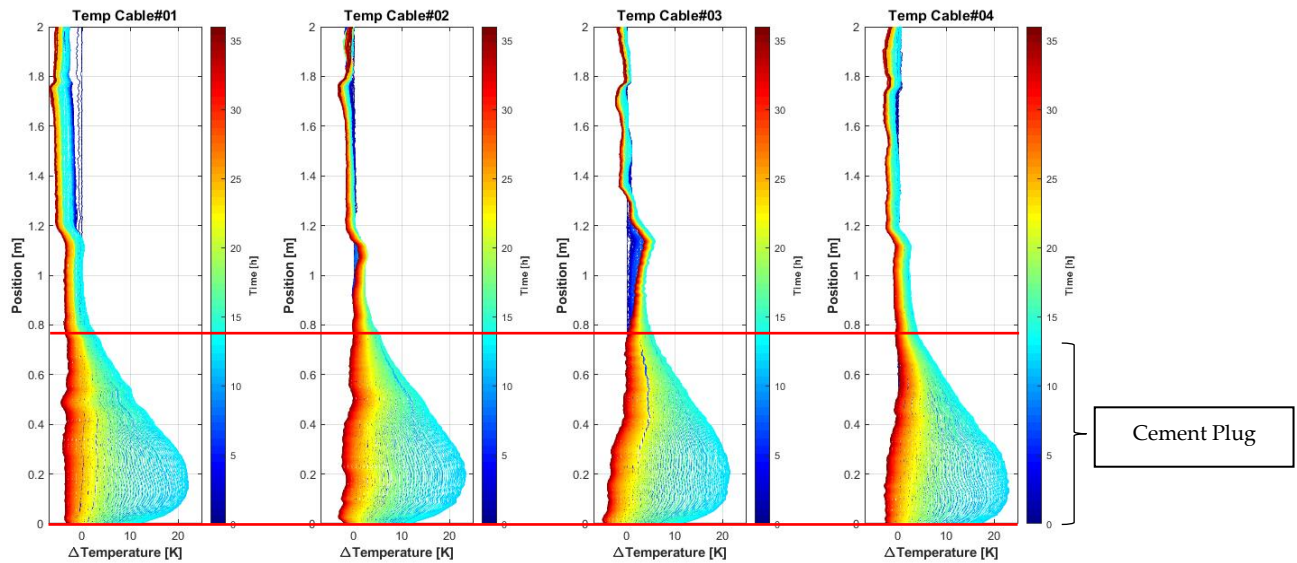


Figure 95: Depth vs. temperature change for each cable

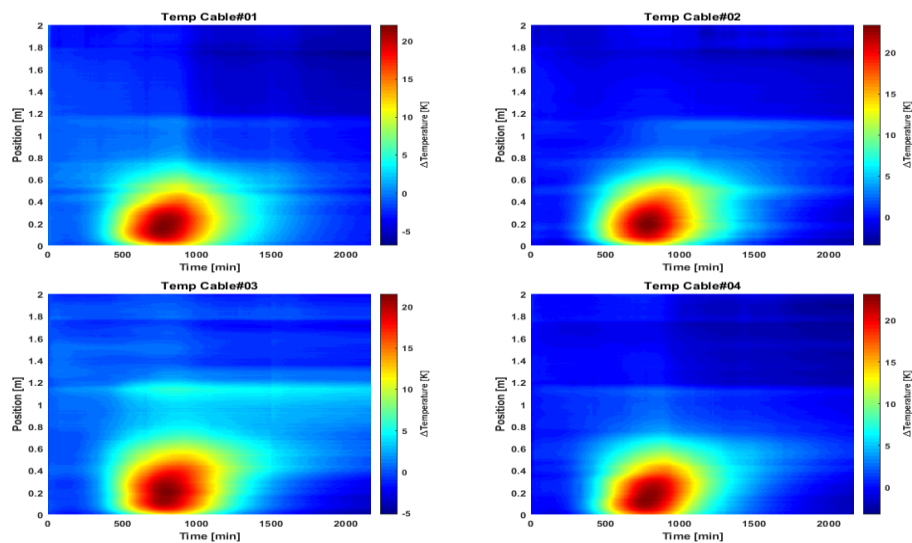


Figure 96: Time vs. temperature change

### Strain

The fiber-optics are very precise in detecting the location of the cement plug. The increase in strain is the same compared to experiment 3.1. This plot does not show a steady increase and decrease over the length of the tube, which can be related to the contaminated cement.

### Experiment 3: Fiber optic cable measurement

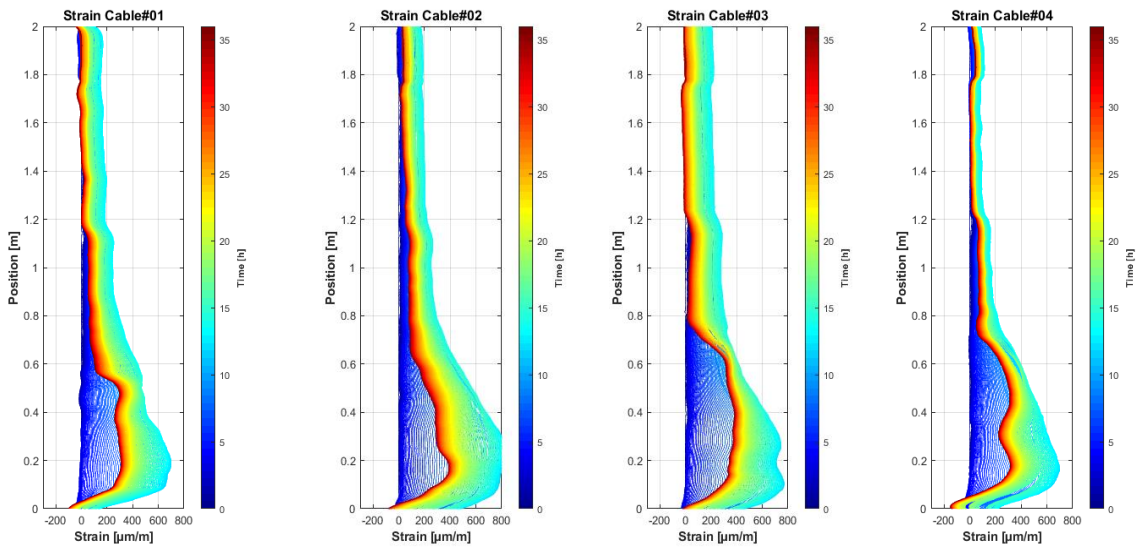


Figure 97: Strain vs. depth for each cable

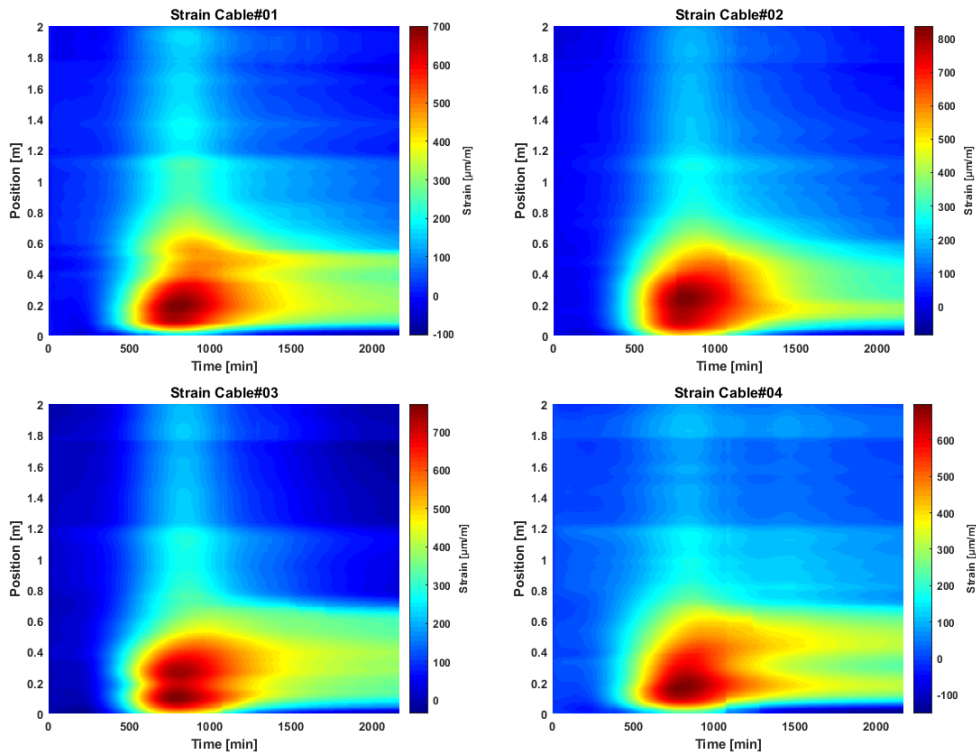


Figure 98: Time vs. Strain

Again, temperature compensation was performed and plotted for a better understanding of the strain behavior. (Figure 99)



The hydration process and strain development started a little bit earlier compared to the previous test as already discussed above. The separation of the yellow and red line can be detected at approximately 230 minutes. The final bond can be assumed at 820 minutes.

Compared to experiment 3.1 the compensation curve for the cable developed faster due to the greater quantity of cement and the onset of bonding and shrinkage is significantly higher ( $\sim 110 \mu\text{m/m}$ ) which can also be referred to the higher cement density (Figure 99).

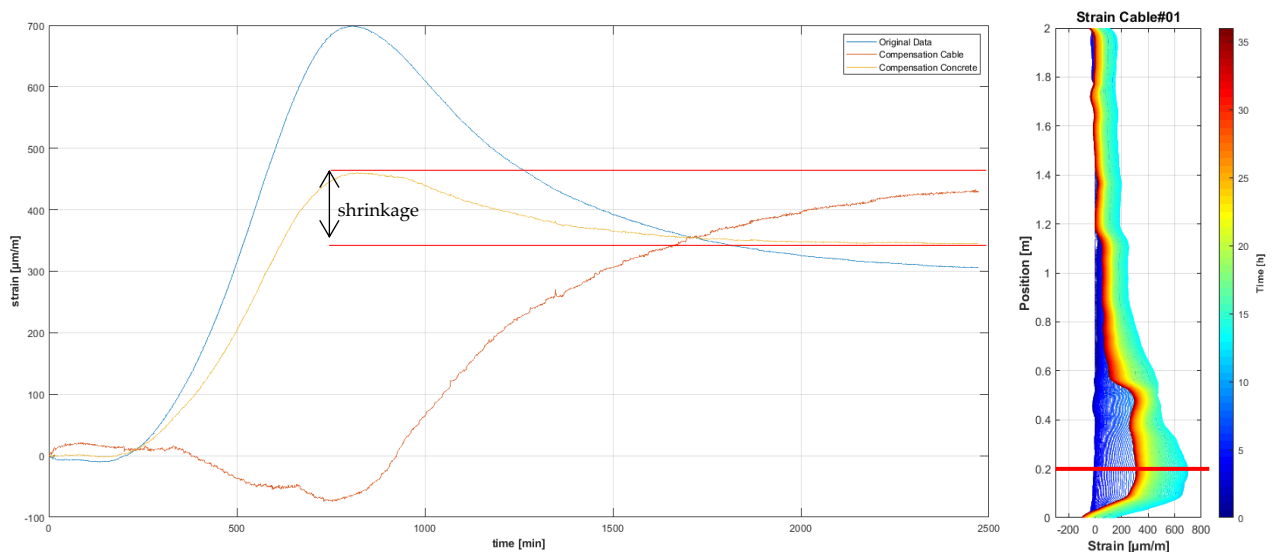


Figure 99: Time vs. strain for different compensation at position 0,2 m

3D-plots of the temperature change and strain development are attached in appendix A.

### CT-scan

CT-scans were as well performed for the contaminated cement plug.

### Experiment 3: Fiber optic cable measurement

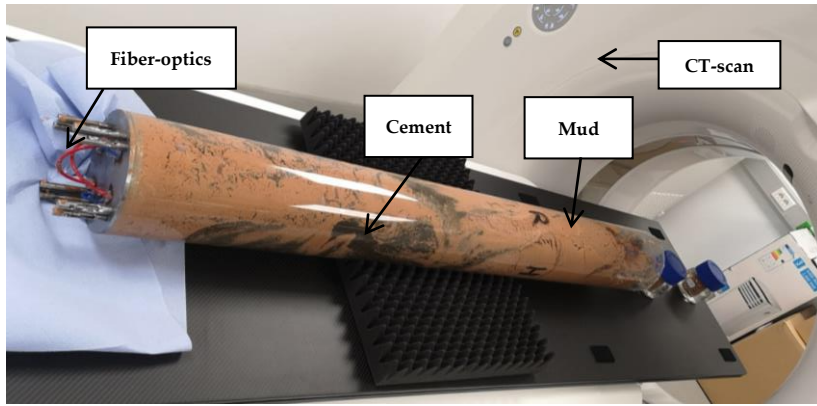


Figure 100: Performing CT-scan of contaminated cement plug

Figure 101 proves the accumulation of the cement on the bottom of the tube. The cross-section of the top (C) indicates the cement-mud mixture, whereas the cross-section on the bottom (B) verifies the settled cement. The mud-cement mixture over the whole pipe is visualized (A).

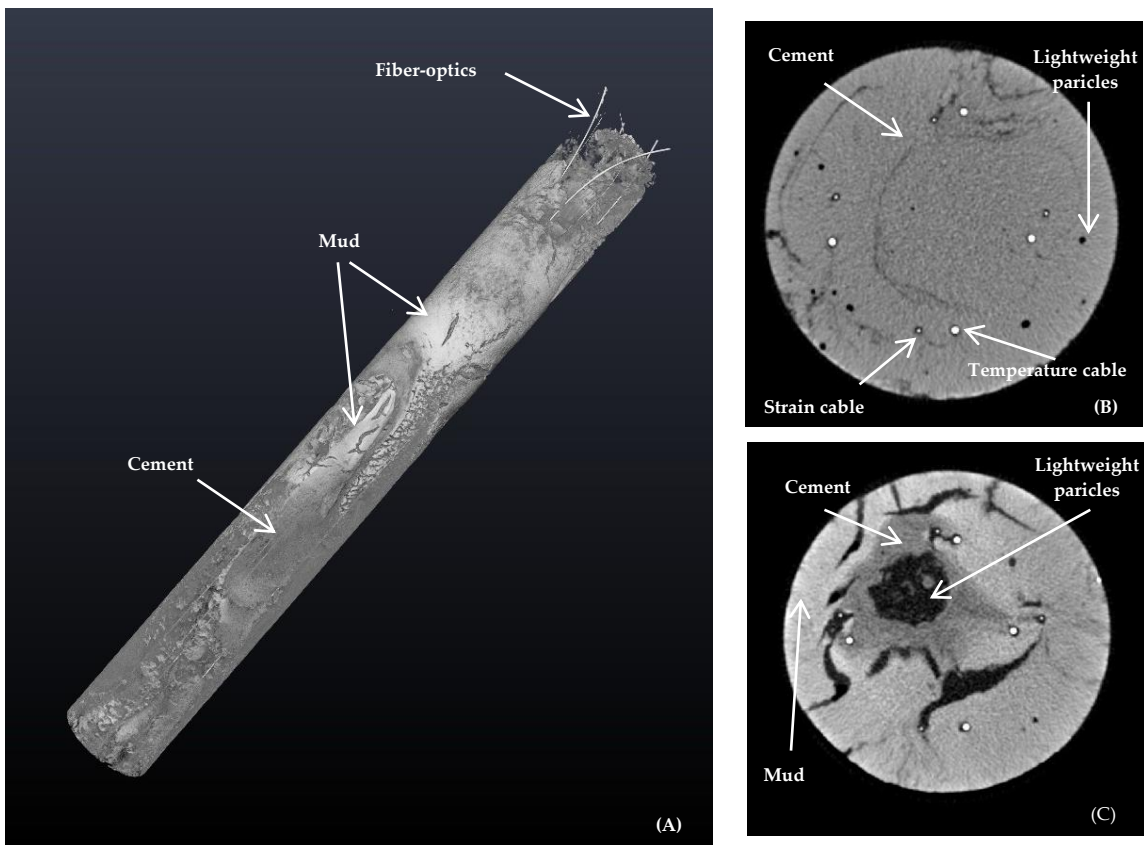


Figure 101: CT-scan of contaminated cement plug; 3D view (A); radial cross-section bottom (B); radial cross-section top (C)

The contamination is even better demonstrated by analyzing each side of the tube. The darker slurry, which indicates the cement is located on the bottom. No homogeneity can be recognized.

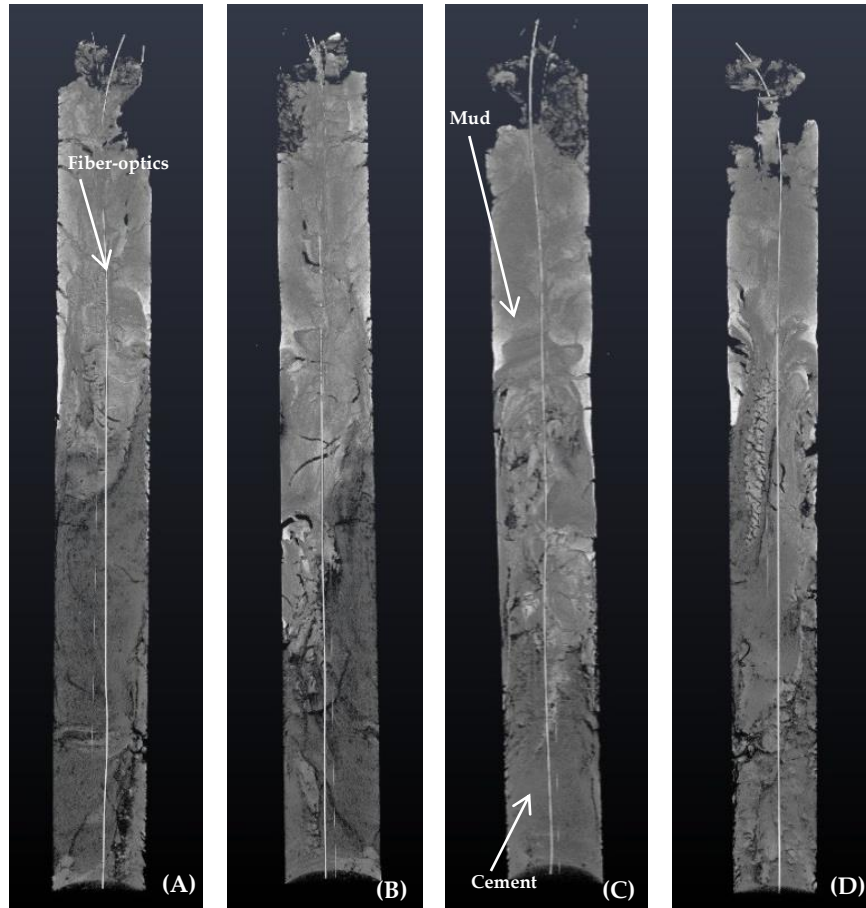


Figure 102: CT-scan: cable#1 (A); cable#2 (B); cable#3 (C); cable#4 (D)



## Chapter 7 Recommendations for future work

Electrical conductivity measurements could be another measure of how the cement slurry is hydrating and annulus/well integrity as already proved in this thesis. These generated values can identify contaminated and unhydrated cement. Due to the malfunctions of the LCR-Meter, the data logging was not precise, and moreover, the tests were not performed under the same conditions. Therefore, the experiments should be repeated with improved LCR-Meter and software. Afterward, a more accurate analysis can be done to prove the significance of measuring electrical conductivity during the hydration process of cement. Once the electrical conductivity test is improved it is recommended to run the measurement simultaneously to the fiber-optic data logging and evaluate and compare the different readings.

Moreover, the tests with the fiber-optics should be continued to study different levels of contamination of cement slurry to obtain a better understanding of the generated data. Additionally, it is recommended to analyze the strain measurement in more detail and investigate any correlation with the hydration volume change, static gel strength development, and potential gas migration. Strain data logging could also provide information about generated cracks in the cement sheath. An interesting approach would also be to evaluate resins behavior with fiber-optics. These sensors are as well usable to perform an interface evaluation during the placement of cement slurry while displacing mud.

Fiber-optics are as well able to recognize and record noises. Therefore a distributed acoustic study should as well be performed since mud, spacer and cement show distinct acoustic signatures. Not only the location of the different slurries could be identified, but also a crack in the cement sheath can be established.

Besides, using the same setup, the fiber-optics could be replaced by a wire and sensors where the cable can be used to send power and transmit data.

Finally, the focus should be on the future field application and not only on how we can install the fiber-optics downhole but also consider what the generated data mean and how can we use them.



## Chapter 8 Conclusion

Well plugs are being used for several different operations in the oil and gas industry, such as lost circulation control, formation testing, directional/sidetrack drilling, zonal isolation, and well abandonment. A cement plug placed off-bottom in a wellbore is often too soft or not in the planned location due to contamination and hence fail to provide a hydraulic seal and lead to well integrity and safety issues. To avoid any incidents and future problems related to well integrity a perfect and intact well barrier is crucial. An imperfect cement barrier will lead to the additional time needed to drill the next section and will, therefore, result in a delay in kick-off. In addition, setting several plugs before a competent plug is obtained will require extra time that will undoubtedly result in increased costs.

Therefore, methods to determine the phase of hydration process, define the exact location of the cement, establish contaminated parts of cement and prove a competent/imperfect well barrier were analyzed and tested in this thesis.

Monitoring the cement hardening process gives us an insight into the level of contamination and the right placement of the cement slurry. Data monitoring is more and more common in the oil and industry since setting an impeccable cement plug is essential for well integrity, safety, and cost decrease.

For this thesis, eight conductivity tests with different levels of mud contamination were performed and analyzed. Electrical conductivity measurement could be a possibility to identify the hydration process of the cement slurry, establish unhydrated cement, discover contaminated cement, and provide information about the well integrity.

Two different experiments with fiber-optic sensing were performed, analyzed, and compared in detail. Furthermore, the precise measurement of the cables to identify the exact location of the cement was demonstrated. Besides the verification of the absence of cracks in the cement sheath, the strain measurement gives us as well information about the shrinkage of the cement. Therefore, fiber-optic sensing will significantly improve the accuracy of cement plugs and operational performance in the oil and gas industry.

In conclusion, data logging of conductivity, temperature, and strain during the hydration process of cement is a vital topic to investigate further since it is an excellent opportunity for long term monitoring to guarantee safety, well integrity and environmental protection. Furthermore, the ultimate abandon of the well can be ensured. Reducing remedial jobs means maximizing effective productive time and will result in significant cost savings.





# Appendix A

## Dimensions

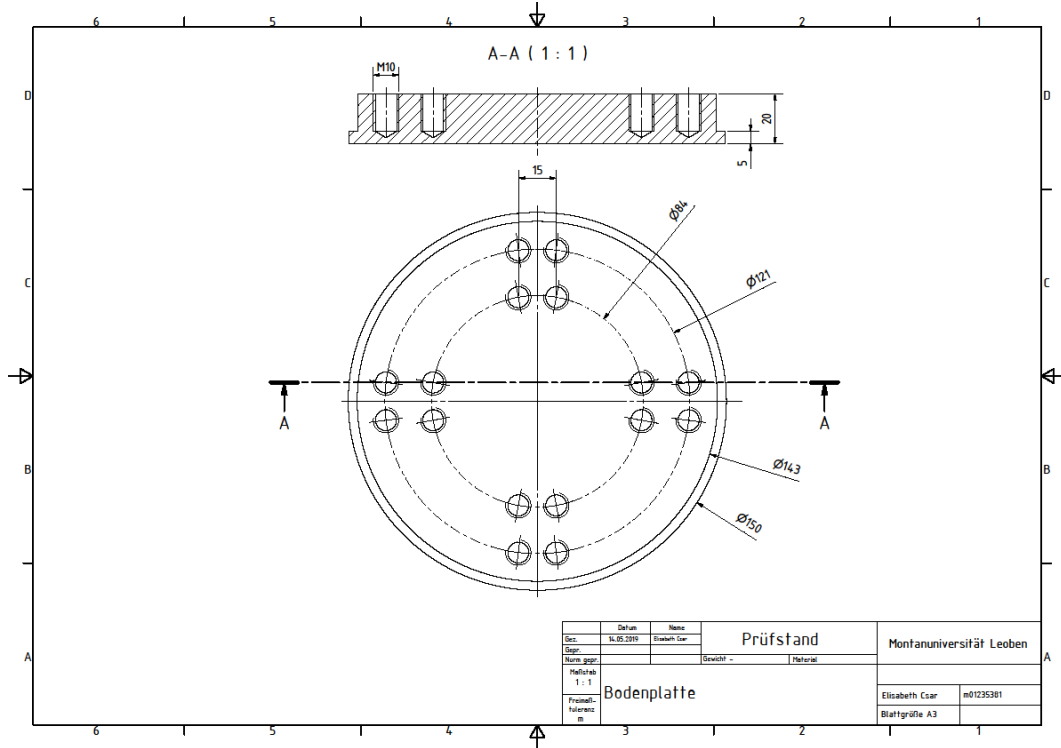


Figure 103: Bottom-plate dimensions

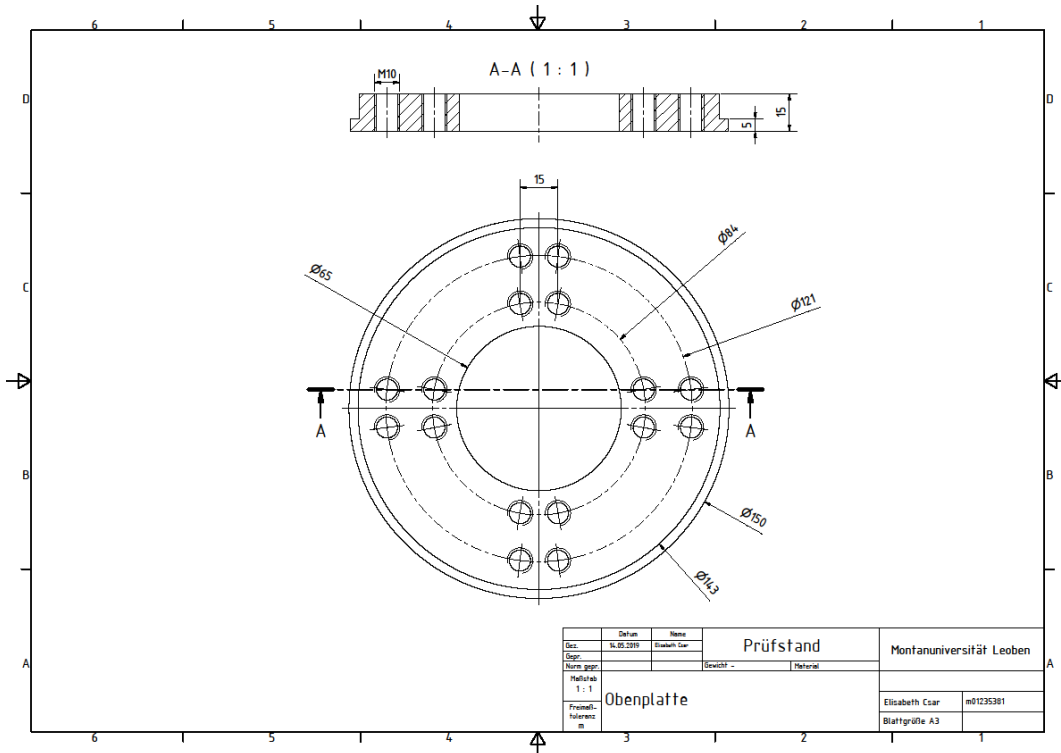


Figure 104: Top-plate dimensions

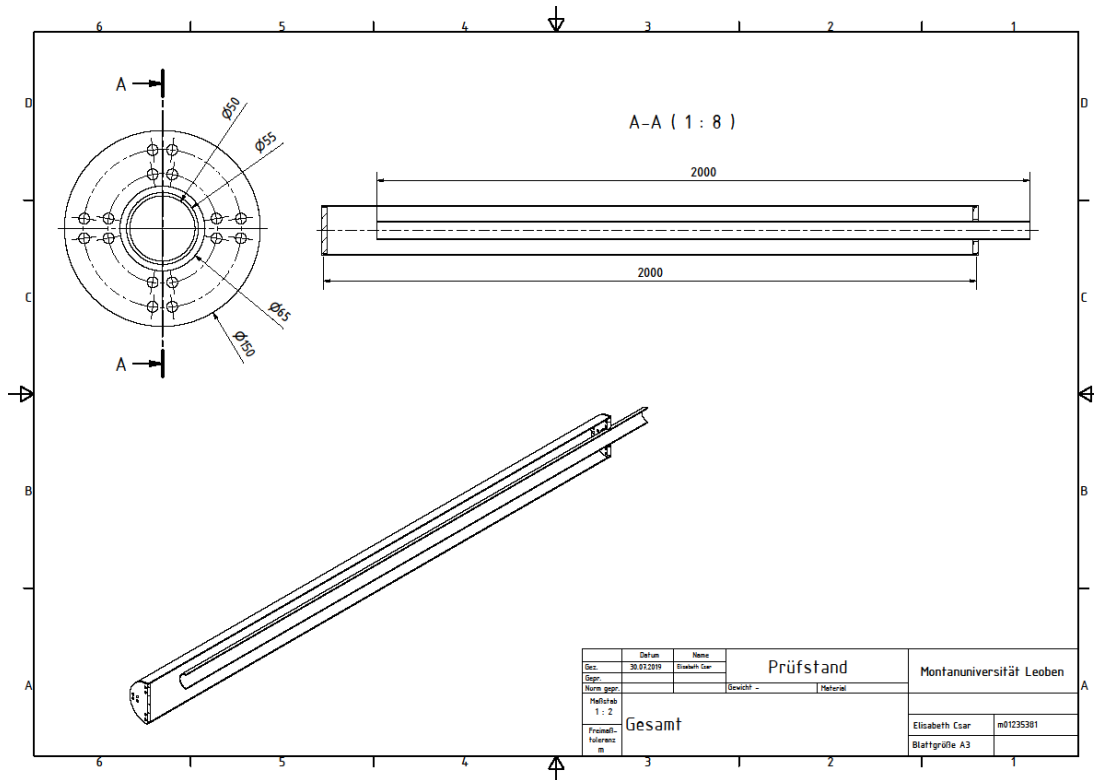


Figure 105: Overall design

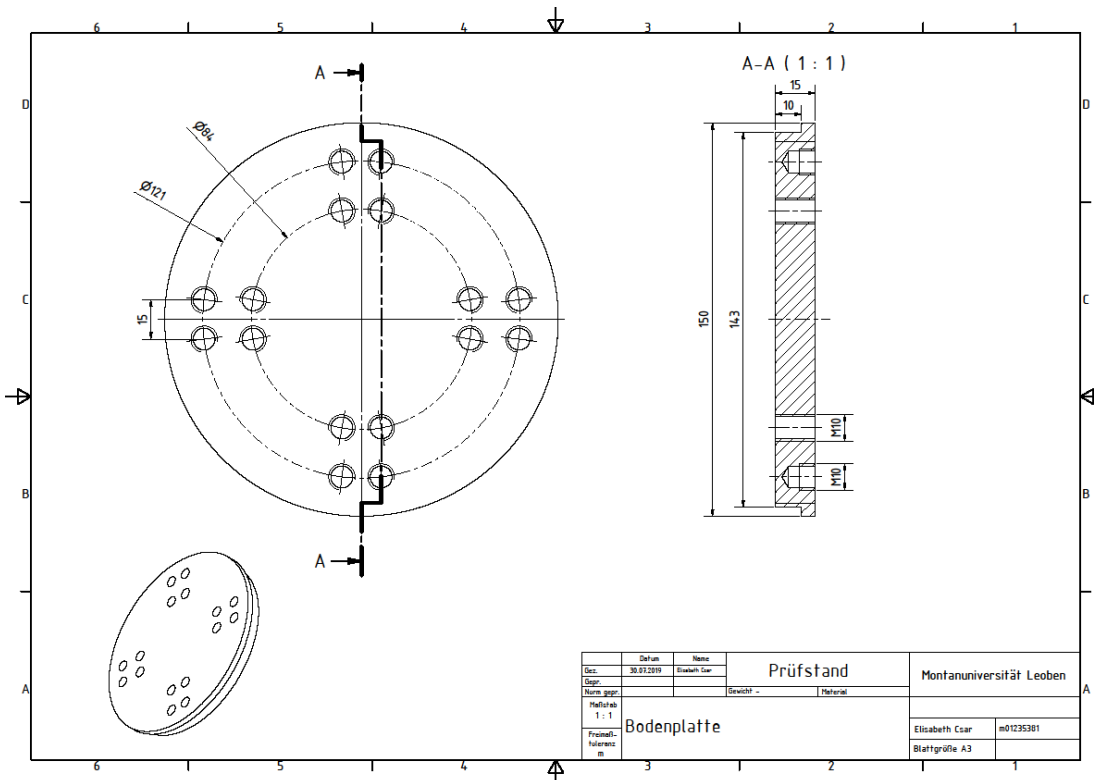


Figure 106: Modified bottom-plate dimensions

3D-plots temperature and strain

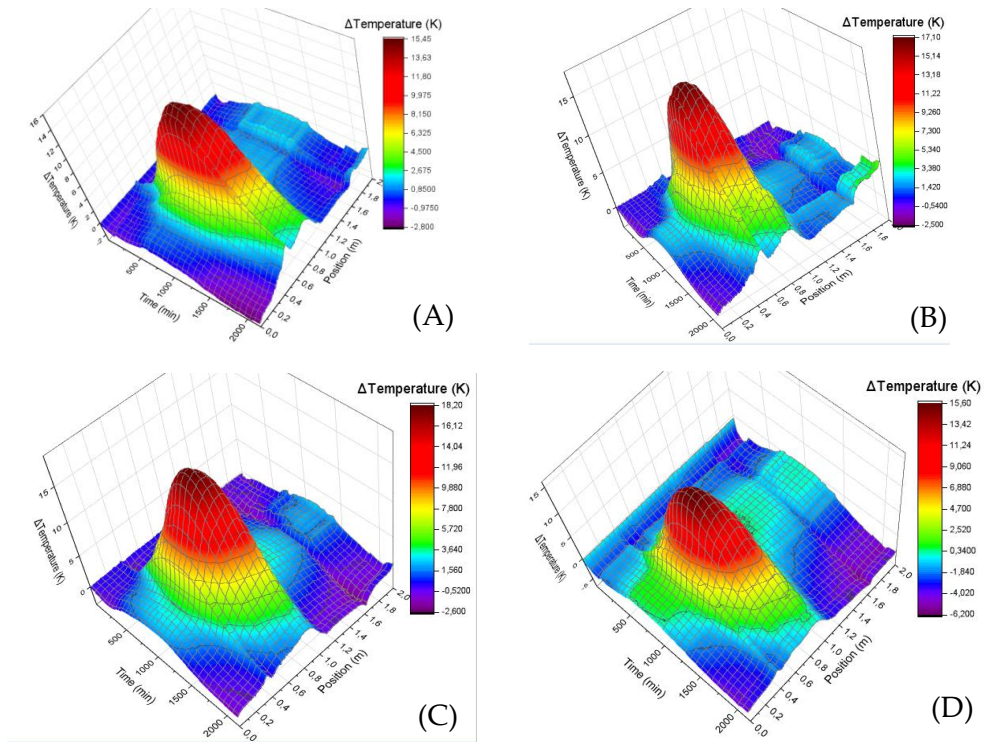


Figure 107: Experiment 3.1: 3D-plot of temperature change, cable #1 (A), cable #2 (B), cable #3 (C), cable #4 (D)

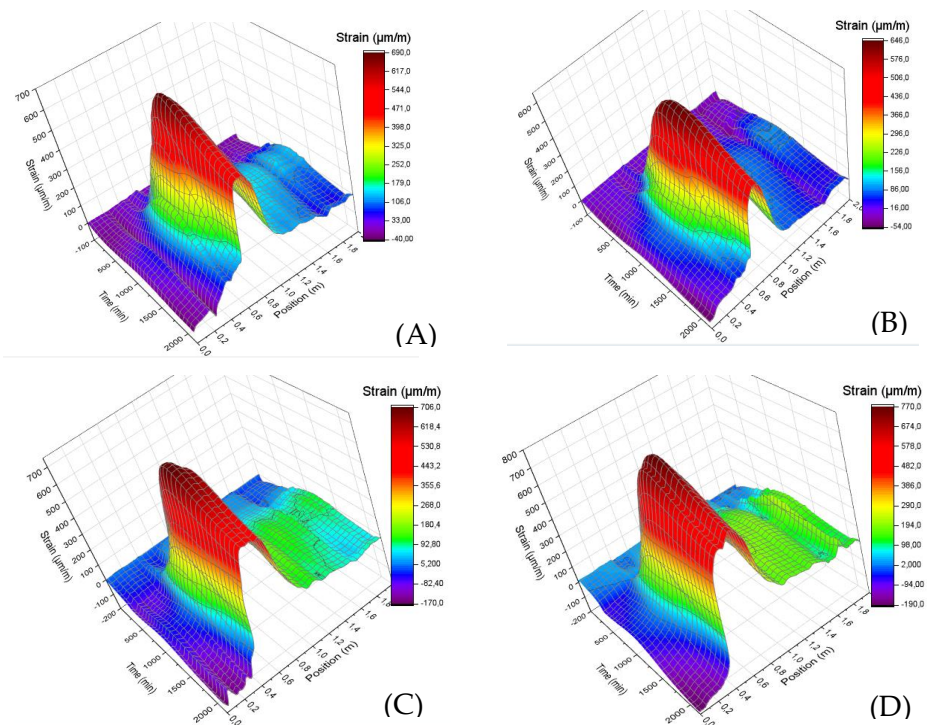


Figure 108: Experiment 3.1: 3D-plot of strain, cable #1 (A), cable #2 (B), cable #3 (C), cable #4 (D)

Appendix A

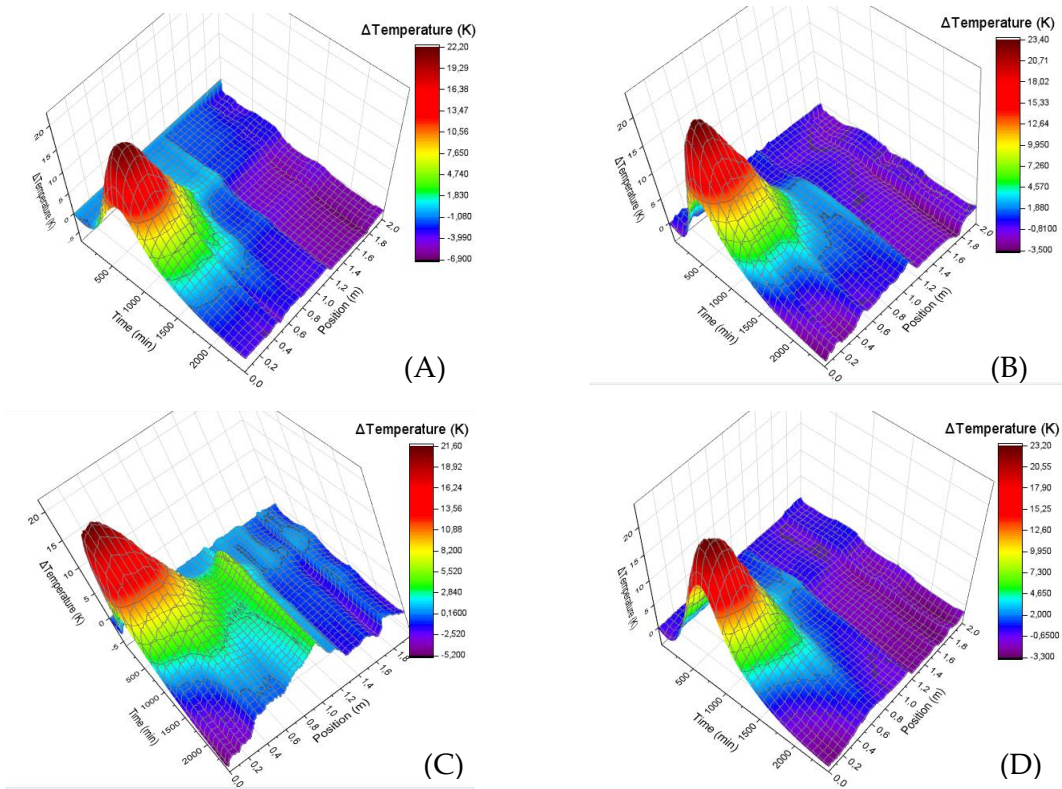


Figure 109: Experiment 3.2: 3D-plot of temperature change, cable #1 (A), cable #2 (B), cable #3 (C), cable #4 (D)

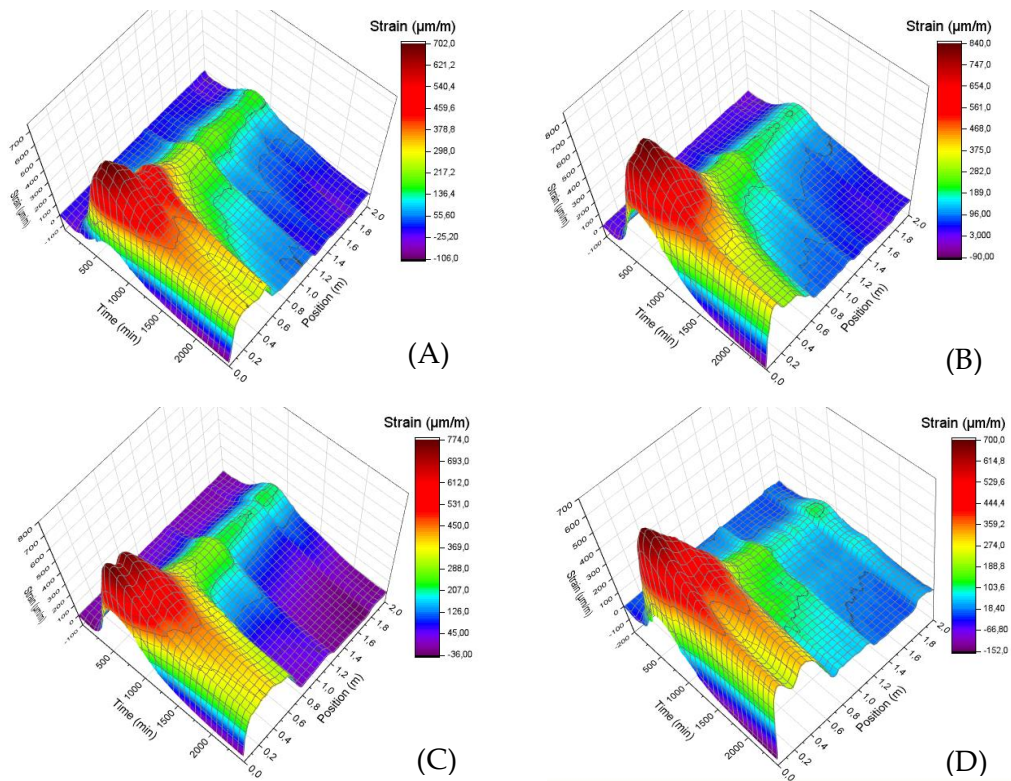


Figure 110: Experiment 3.2: 3D-plot of strain, cable #1 (A), cable #2 (B), cable #3 (C), cable #4 (D)

# Bibliography

- Aïtcin. 2016. "Hydration Reaction - an Overview | ScienceDirect Topics." 2016. <https://www.sciencedirect.com/topics/materials-science/hydration-reaction>.
- Akindehinde Akindahunsi, Sunny E. Iyuke, Wolfram Schmidt, and Sunny E. Iyuke. 2013. "(PDF) The Influence of Starches on Some Properties of Concrete." 2013. [https://www.researchgate.net/publication/264052500\\_The\\_Influence\\_of\\_Starches\\_on\\_some\\_Properties\\_of\\_Concrete](https://www.researchgate.net/publication/264052500_The_Influence_of_Starches_on_some_Properties_of_Concrete).
- Årebråt, Per Arild. n.d. "6 Causes for Contaminated Cement (and How to Avoid Them)." Accessed May 27, 2019. <http://www.perigon.no/blog/6-causes-of-contaminated-green-cement-and-how-to-avoid-them>.
- "Balanced-Plug Method. Basic Calculations." 2019. Better Well Cementing for ALL. April 19, 2019. <https://better-cementing-for-all.org/balanced-plug-method-calculations>.
- Bruton, Greg, Jimmy Land, David Moran, Shantanu Swadi, Ryan Strachan, and Ketil Tørge. 2014. "Historically, Drillers Have Relied on Openhole Cement Plugs or Cased Hole Whipstocks for Sidetracking Wells. By Incorporating an Innovative Downhole Anchor with a Whipstock Assembly, Drillers Can Set Whipstocks in Open Holes without Concern for Cement Plug Integrity. Advances in Whipstock and Mill Design Are Also Significantly Reducing the Time Required to Initiate Cased Hole Sidetracks." *Oilfield Review*, 10.
- "C01bc.Pdf." n.d. Accessed July 11, 2019. [https://www.praktikumphysik.uni-hannover.de/fileadmin/praktische-physik/AP/Versuche/Neue/B\\_C/C01bc.pdf](https://www.praktikumphysik.uni-hannover.de/fileadmin/praktische-physik/AP/Versuche/Neue/B_C/C01bc.pdf).
- "Cement Hydration." n.d. Accessed July 22, 2019. <https://www.understanding-cement.com/hydration.html>.
- "Cementing Operations -." 2018. January 15, 2018. [https://petrowiki.org/Cementing\\_operations](https://petrowiki.org/Cementing_operations).
- "Clear Directional - Tools." n.d. Accessed June 7, 2019. <http://www.landmarkgs.com/Clear/site6/sidetrack.html>.
- "Concrete: Scientific Principles." n.d. Accessed July 22, 2019. <http://matse1.matse.illinois.edu/concrete/prin.html>.
- "Dark Discoloration of Flatwork | Concrete Construction Magazine." n.d. Accessed August 16, 2019. [https://www.concreteconstruction.net/how-to/dark-discoloration-of-flatwork\\_o](https://www.concreteconstruction.net/how-to/dark-discoloration-of-flatwork_o).
- Diaz, Miguel. 2017. "Cement Plugging: A Nightmare Waiting to Happen?" September 21, 2017. <https://blog.wellcem.com/cement-plugging-a-nightmare-waiting-to-happen>.
- Dosky, St von, W. Ens, H. Grieb, M. Hilsendegen, and H. Schorb. 2013. "D6.3 - Optical Fiber Temperature Measurement for Process Industry." *Proceedings SENSOR 2013*, May, 578–82. <http://dx.doi.org/10.5162/sensor2013/D6.3>.
- DrillingFormulas.Com |. 2011. "Balanced Cement Plug." *Drilling Formulas and Drilling Calculations* (blog). 2011. <http://www.drillingformulas.com/balanced-cement-plug/>.

## Bibliography

- — —. 2014. "Lost Circulation and Well Control." *Drilling Formulas and Drilling Calculations* (blog). December 8, 2014. <http://www.drillingformulas.com/lost-circulation-and-well-control/>.
- — —. n.d. "Types of Flow and Rheology Models of Drilling Mud." *Drilling Formulas and Drilling Calculations* (blog). Accessed August 7, 2019. <http://www.drillingformulas.com/types-of-flow-and-rheology-models-of-drilling-mud/>.
- Fidan, E., T. Babadagli, and E. Kuru. 2004. "Use of Cement as Lost-Circulation Material: Best Practices." In *Canadian International Petroleum Conference*. Calgary, Alberta: Petroleum Society of Canada. <https://doi.org/10.2118/2004-090>.
- FPrimeC. 2017. "Electrical Resistivity of Concrete." FPrimeC Solutions. January 20, 2017. <https://www.fprimec.com/electrical-resistivity-of-concrete/>.
- Franus, Wojciech, Rafał Panek, and Magdalena Wdowin. 2015. "SEM Investigation of Microstructures in Hydration Products of Portland Cement." In . [https://doi.org/10.1007/978-3-319-16919-4\\_14](https://doi.org/10.1007/978-3-319-16919-4_14).
- FS.COM. 2014. "A Guide on Fiber Optic Cable." FS - Fiberstore. September 10, 2014. <https://www.fs.com/a-guide-on-fiber-optic-cable-aid-340.html>.
- Govind Balaji. 2018. "Electrochemistry - Why Is AC Current Used Rather than DC Current for Calculating the Conductance of a Solution(See Body)? - Chemistry Stack Exchange." 2018. <https://chemistry.stackexchange.com/questions/93917/why-is-ac-current-used-rather-than-dc-current-for-calculating-the-conductance-of>.
- Gupta, Nadish, Martijn Bogaerts, and Umar Arshad. 2014. "Off-Bottom Plug and Abandonment Operations in Deepwater Caribbean: Challenges and Solutions," 8.
- Gupta, Nupur Das, Martijn Bogaerts, Umar Arshad, and Hans G. Schlumberger. 2014. "AADE-14-FTCE-53 Off-Bottom Plug and Abandonment Operations in Deepwater Caribbean : Challenges and Solutions." In .
- Halliburton. n.d. "Plug Cementing - Halliburton." Accessed May 20, 2019. <https://www.halliburton.com/en-US/ps/cementing/cementing-solutions/plug-cementing/default.html>.
- Harestad, Kristian. 2018. "Download Free Paper: Different Types of Bases for Setting Balanced (off Bottom) Cement Plugs." 2018. <http://www.perigon.no/white-paper-different-types-of-bases-for-setting-balanced-off-bottom-cement-plugs-lp>.
- "How Does an Optical Strain Gauge Work?" 2018. HBM. March 28, 2018. <https://www.hbm.com/en/6827/article-how-does-an-optical-strain-gauge-actually-work/>.
- "IGMS - Distributed Fiber Optic Sensing in Tunneling." n.d. Accessed June 24, 2019. <https://www.tugraz.at/en/institutes/igms/projects/current-projects/distributed-fiber-optic-sensing-in-tunneling/>.
- "IGMS - Fiber Optic Sensors." n.d. Accessed June 18, 2019. <https://www.tugraz.at/en/institutes/igms/research/fiber-optic-sensors/>.
- jesseyang. 2017. "Applications of Fiber Optic Cable." *Jesseyang* (blog). September 8, 2017. <https://medium.com/@fsjoanna/applications-of-fiber-optic-cable-1c5d799b1f3a>.

- Joseph, Shilu Kurian, and Annie Sonia Xavier. 2014. "Effect of Starch Admixtures on Fresh and Hardened Properties of Concrete" 4 (3): 4.
- "Lost Circulation -." 2015. PetroWiki. June 30, 2015. [https://petrowiki.org/Lost\\_circulation](https://petrowiki.org/Lost_circulation).
- "Lost Circulation - Schlumberger Oilfield Glossary." n.d. Accessed June 6, 2019. [https://www.glossary.oilfield.slb.com/en/Terms/l/lost\\_circulation.aspx](https://www.glossary.oilfield.slb.com/en/Terms/l/lost_circulation.aspx).
- "Master Thesis by Emanuel Hofer.Pdf." n.d. Accessed August 28, 2019. <https://pure.unileoben.ac.at/portal/files/3947223/AC15407198n01.pdf>.
- Mohan Doshi. 2014. "LOST CIRCULATION - THE BASICS." *Technologie*, March 8. <https://de.slideshare.net/mohan153doshi/lost-circulation-the-basics-md-slideshare>.
- Montgomery, Carl. 2013. "Fracturing Fluids." *Effective and Sustainable Hydraulic Fracturing*, May. <https://doi.org/10.5772/56192>.
- Narendra Kumar Dewangan. 2015. "Cementation." *Engineering*, March 23. <https://www.slideshare.net/narendrakumard/cementation-46169143>.
- Ng'ang'a, Samuel Ikinya. 2014. "CEMENTING PROCESSES IN GEOTHERMAL WELL DRILLING: APPLICATION AND TECHNIQUES," 37.
- Obla, Karthik, R Hong, S Sherman, D Bentz, and Scott Jones. 2018. "Relating the Electrical Resistance of Fresh Concrete to Mixture Proportions." *Advances in Civil Engineering Materials* 7 (March). <https://doi.org/10.1520/ACEM20170126>.
- Peschard, A., A. Govin, P. Grosseau, B. Guillhot, and R. Guyonnet. 2004. "Effect of Polysaccharides on the Hydration of Cement Paste at Early Ages." *Cement and Concrete Research* 34 (11): 2153–58. <https://doi.org/10.1016/j.cemconres.2004.04.001>.
- "Pre-Flushes and Spacers | Trican Well Service." n.d. Accessed July 7, 2019. <https://www.tricanwellservice.com/cementing/pre-flushes-and-spacers>.
- "Preview-Ceme.Pdf." n.d. Accessed May 20, 2019. <http://www.iadc.org/wp-content/uploads/2015/08/preview-ceme.pdf>.
- "Progressive Gels - Schlumberger Oilfield Glossary." n.d. Accessed August 7, 2019. [https://www.glossary.oilfield.slb.com/en/Terms/p/progressive\\_gels.aspx](https://www.glossary.oilfield.slb.com/en/Terms/p/progressive_gels.aspx).
- "Rak-82\_3131\_cement\_hydration\_-\_new.Pdf." n.d. Accessed July 23, 2019. [https://mycourses.aalto.fi/pluginfile.php/130982/mod\\_resource/content/1/Rak-82\\_3131\\_cement\\_hydration\\_-\\_new.pdf](https://mycourses.aalto.fi/pluginfile.php/130982/mod_resource/content/1/Rak-82_3131_cement_hydration_-_new.pdf).
- "Remedial Cementing -." 2015. June 25, 2015. [https://petrowiki.org/Remedial\\_cementing](https://petrowiki.org/Remedial_cementing).
- "Resistivity and Electrical Conductivity." 2017. *Basic Electronics Tutorials* (blog). April 16, 2017. <https://www.electronics-tutorials.ws/resistor/resistivity.html>.
- Rommetvedt, Petter. 2018. "Setting Off-Bottom Cement Plugs: What Is Your Success Rate?" 2018. <http://www.perigon.no/blog/setting-off-bottom-cement-plugs-what-is-your-success-rate>.
- Salahub, W.F., and H.E. Ripley. 1980. "Obtaining Open-Hole Cement Plugs On The First Attempt." *Journal of Canadian Petroleum Technology* 19 (01). <https://doi.org/10.2118/80-01-06>.
- Sebastian, Sebastian. 2013. "Messaufbau: Spezifische Leitfähigkeit von Flüssigkeiten mit LabView messen." 2013. <http://sebastians-space.blogspot.com/2013/06/messaufbau-spezifische-leitfahigkeit.html>.

## Bibliography

- Souza, Leonardo, Alejandro De La Cruz Sasso, and Hector Munoz. 2017. "Tailored and Reliable Method for Cement Plug Improves Times in Deep Water." In *OTC Brasil*. Rio de Janeiro, Brazil: Offshore Technology Conference. <https://doi.org/10.4043/28060-MS>.
- "Spacers and Flushers in Cementing - PetroWiki." n.d. Accessed July 7, 2019. [https://petrowiki.org/Spacers\\_and\\_flushers\\_in\\_cementing](https://petrowiki.org/Spacers_and_flushers_in_cementing).
- "Spacers and Flushes - Halliburton." n.d. Accessed July 7, 2019. <https://www.halliburton.com/en-US/ps/cementing/materials-chemicals-additives/spacers-and-flushes/default.html>.
- Swaddiwudhipong, S, D Chen, and Min-Hong Zhang. 2002. "Simulation of the Exothermic Hydration Process of Portland Cement." *Advances in Cement Research - ADV CEM RES* 14 (January): 61–69. <https://doi.org/10.1680/adcr.2002.14.2.61>.
- "Table 1 . Chemical Composition of Ordinary Portland Cement." n.d. ResearchGate. Accessed August 20, 2019. [https://www.researchgate.net/figure/Chemical-Composition-of-Ordinary-Portland-Cement\\_tbl1\\_274845006](https://www.researchgate.net/figure/Chemical-Composition-of-Ordinary-Portland-Cement_tbl1_274845006).
- "TREX-06235.Pdf." n.d. Accessed July 16, 2019. <http://www.mdl2179trialdocs.com/releases/release201303141200012/TREX-06235.pdf>.
- "Viscometer\_Info2.Pdf." n.d. Accessed August 7, 2019. [https://www.fann.com/content/dam/fann/Brochures/Viscometer\\_Info2.pdf](https://www.fann.com/content/dam/fann/Brochures/Viscometer_Info2.pdf).
- "Water Conductivity - Lenntech." n.d. Accessed August 13, 2019. <https://www.lenntech.com/applications/ultrapure/conductivity/water-conductivity.htm>.
- Wei, Xiaosheng. 2004. "Interpretation of hydration process of cement-based materials using resistivity measurement - ProQuest." 2004. <https://search.proquest.com/openview/2d4b8c19ec0999afe4494a047dca35f3/1?cb1=18750&diss=y&pq-origsite=gscholar>.
- Winkler, Madeleine, Christoph Martin Monsberger, Werner Lienhart, Alois Vorwagner, and Maciej Kwapisz. n.d. "Assessment of Crack Patterns along Plain Concrete Tunnel Linings Using Distributed Fiber Optic Sensing," 8.
- Woodford, Chris. 2018. "How Does Fiber Optics Work?" Explain That Stuff. September 26, 2018. <http://www.explainthatstuff.com/fiberoptics.html>.



# Acronyms

<i>OBCP</i>	Off-Bottom Cement Plugs
<i>LCM</i>	Loss Circulation Materials
<i>KOP</i>	Kick-Off Point
<i>BHA</i>	Bottom Hole Assembly
<i>WOC</i>	Waiting On Cement
<i>OBM</i>	Oil-Based Mud
<i>SBM</i>	Synthetic-Based Mud
<i>POOH</i>	Pull Out Of Hole
<i>POF</i>	Plastic Optical Fiber
<i>FBG</i>	Fiber Bragg Grating
<i>OBR</i>	Optical Backscatter Reflectometry
<i>OFDR</i>	Optical Frequency Domain Reflectometry
<i>OTDR</i>	Optical Time Domain Reflectometry
<i>API</i>	American Petroleum Institution
<i>NPT</i>	Non-productive time



# Symbols

$\rho$	specific electrical resistivity	$[\Omega m]$
$R$	electrical resistance	$[\Omega]$
$l$	length	$[m]$
$A$	cross-sectional area	$[m^2]$
$d$	diameter	$[m]$
$\mu_p$	plastic viscosity (PV)	$[cp]$
$\tau$	shear stress	$\left[\frac{lb}{100ft^2}\right]$
$\gamma$	shear rate	$[s^{-1}]$
$\sigma$	conductivity	$\left[\frac{s}{m}\right]$
$\Delta Q$	Energy	$[U]$
$m$	Mass	$[kg]$
$c$	Specific heat capacity	$\left[\frac{J}{kg * K}\right]$
$\Delta T$	Temperature change	$[K]$
$\tau_y$	yield point	$\left[\frac{lb}{100ft^2}\right]$
$\theta_{600}$	shear stress reading a 600 rpm	$\left[\frac{lb}{100ft^2}\right]$
$\theta_{300}$	shear stress reading a 300 rpm	$\left[\frac{lb}{100ft^2}\right]$
$K$	consistency index	$\left[\frac{lb * s}{100ft^2}\right]$
$n$	flow behavior index	$[-]$
$\theta_1$	shear stress at 300rpm	$\left[\frac{lb}{100ft^2}\right]$
$\theta_2$	shear stress at 600rpm	$\left[\frac{lb}{100ft^2}\right]$
$\omega_1$	shear rate at 300 rpm	$\left[\frac{1}{s}\right]$
$\omega_2$	shear rate at 600 rpm	$\left[\frac{1}{s}\right]$
$\theta_0$	shear stress at 3 rpm	$\left[\frac{lb}{100ft^2}\right]$



# List of Figures

Figure 1: NPT hours for several operations (Souza, Sasso, and Munoz 2017) .....	1
Figure 2: Under displaced balanced cement plug (DrillingFormulas.Com   2011).....	3
Figure 3: Ideal case of OBCP versus fluid mixing due to the unstable base and lighter mud underneath (N. Gupta, Bogaerts, and Arshad 2014) .....	4
Figure 4: OBCP in deviated well –reduced effective length of competent cement and slump angle (N. Gupta, Bogaerts, and Arshad 2014) .....	5
Figure 5: Cement plug at thief zone (Narendra Kumar Dewangan 2015) .....	6
Figure 6: Balanced plug method and drift plug method (Ng’ang’a 2014) .....	7
Figure 7: Cement plug for directional drilling and sidetracking/whipstocking (Narendra Kumar Dewangan 2015) .....	8
Figure 8: Cement plug for zonal isolation for testing operation (Narendra Kumar Dewangan 2015) .....	9
Figure 9: Cement plug for well abandonment (Narendra Kumar Dewangan 2015).....	10
Figure 10: Downward movement of cement slurry (Diaz 2017) .....	12
Figure 11: Internal construction of fiber-optic cable (Woodford 2018).....	16
Figure 12: Total internal reflection of light (Woodford 2018) .....	16
Figure 13: Single-mode optical-fiber (FS.COM 2014).....	17
Figure 14: Multi-mode optical fiber (FS.COM 2014) .....	17
Figure 15: Fiber Bragg Grating (“How Does an Optical Strain Gauge Work?” 2018).....	18
Figure 16: Fiber-optic sensors in civil infrastructure objects (“IGMS - Fiber Optic Sensors” n.d.) .....	20
Figure 17: Different phases of the hydration of Portland cement (Aïtcin 2016).....	24
Figure 18: Formed products of hydration of Portland cement (Franus, Panek, and Wdowin 2015) .....	24
Figure 19: Heat and electrical conductivity development during the hydration of cement (Aïtcin 2016) .....	28
Figure 20: First experiment setup .....	29
Figure 21: Test 1: Development of electrical resistance in a water and salt solution.....	30
Figure 22: Difference of using screws versus plates (Sebastian 2013) .....	31
Figure 23: Test 2: Development of electrical resistance in a water solution.....	32
Figure 24: Test 3: Development of electrical resistance in a water solution.....	32
Figure 25: Used screws compared to a new one.....	33
Figure 26: Test 4: Development of electrical resistance in a water solution.....	33
Figure 27: LCR Meter 879B .....	34
Figure 28: Development of electrical resistance in a water solution with LCR meter.....	34
Figure 29: Scale .....	36
Figure 30: Constant Speed Mixer, Chandler Engineering .....	37
Figure 31: Heidolph Mixer.....	37
Figure 32: Pressurized Gravity Balencometer .....	37
Figure 33: Baroid Mud Balance .....	38
Figure 34: Fann Rational Viscometer, Chandler Engineering.....	38
Figure 35: Rheological models (Montgomery 2013).....	41
Figure 36: Types of gel strengths in muds (“Progressive Gels - Schlumberger Oilfield Glossary” n.d.).....	42
Figure 37: Fann Rational Viscometer .....	42
Figure 38: Plastic container with electrodes .....	43
Figure 39: CT-scan .....	43

## List of Figures

Figure 40: Rheological model of bentonite mud .....	44
Figure 41: Rheological model of 16 ppg cement slurry.....	46
Figure 42: Experiment 2.1: Left side view - back view - top view .....	47
Figure 43: Experiment 2.1: CT-Scan (A), conductivity vs. time (B) .....	47
Figure 44: Visualization of change in conductivity compared to temperature over time.....	48
Figure 45: Experiment 2.2: Left side view - back view - top view .....	49
Figure 46: Experiment 2.2: CT-Scan (A), conductivity vs. time compared to experiment 2.1 (B) 49	
Figure 47: Experiment 2.3: Left side view - back view - top view .....	50
Figure 48: Experiment 2.3: CT-Scan (A), conductivity vs. time compared to experiment 2.1 (B) 50	
Figure 49: Experiment 2.4: Left side view - back view - top view .....	51
Figure 50: Experiment 2.4: CT-Scan (A), conductivity vs. time compared to experiment 2.1 (B) 52	
Figure 51: Experiment 2.5: Left side view - back view - top view .....	53
Figure 52: Experiment 2.5: CT-Scan (A), conductivity vs. time compared to experiment 2.1 (B) 53	
Figure 53: Experiment 2.6: Left side view - back view - top view .....	54
Figure 54: Experiment 2.6: CT-Scan (A), conductivity vs. time compared to experiment 2.1 (B) 54	
Figure 55: Experiment 2.7: Left side view - back view - top view .....	55
Figure 56: Experiment 2.7: CT-Scan (A), conductivity vs. time compared to experiment 2.1 (B) 55	
Figure 57: 100% mud .....	56
Figure 58: 100% mud after resting one week.....	56
Figure 59: Experiment 2.7: conductivity vs. time compared to experiment 2.1.....	57
Figure 60: Samples with different level of mud contamination .....	57
Figure 61: CT-scan of Samples with varying degrees of mud contamination .....	57
Figure 62: Comparison of different samples. ....	58
Figure 63: Fiber-optics .....	59
Figure 64: Minirig.....	59
Figure 65: Pipe holding construction, designed by Emanuel Hofer .....	60
Figure 66: Tubing design.....	60
Figure 67: Dimensions of tubing .....	61
Figure 68: Bottom-plate design .....	61
Figure 69: Top-plate design .....	61
Figure 70: Cylinders to clamp fiber-optics.....	62
Figure 71: Experiment 3.1: Rheological model of polymer mud .....	63
Figure 72: Experiment 3.1: Rheological model of base fluid .....	65
Figure 73: Experiment 3.1: Rheological model of 13,4 ppg cement slurry .....	66
Figure 74: Fiber-optic installation plan .....	67
Figure 75: Final installation.....	68
Figure 76: Top-plate installation .....	68
Figure 77: Bottom-plate installation .....	69
Figure 78: Setting procedure of competent cement plug .....	69
Figure 79: Experiment 3.1: Cement plug position, visible in strain and temperature profile .....	70
Figure 80: Experiment 3.1: Depth vs. temperature change for each cable.....	71
Figure 81: Experiment 3.1: Temperature change over time.....	71
Figure 82: Experiment 3.1: Depth vs. strain for each cable.....	72
Figure 83: Experiment 3.1: Strain over time .....	73
Figure 84: Time vs. strain for different compensation at position 0,8 m .....	74
Figure 85: Time vs. strain for different compensation at position 1,8m .....	74
Figure 86: Performing CT-scan of competent cement plug.....	75
Figure 87: CT-scan of competent cement plug; 3D view (A); radial cross section (B) .....	76
Figure 88:CT-scan: cable#1 (A); cable#2 (B); cable#3 (C); cable#4 (D) .....	76
Figure 89: Experiment 3.2: Rheological model of polymer mud .....	78
Figure 90 Experiment 3.2: Rheological model of the base fluid.....	79

Figure 91 Experiment 3.2: Rheological model of 16 ppg cement slurry .....	80
Figure 92: Modified bottom-plate, bottom view (A) – top view (B) .....	81
Figure 93: Fiber-optic installation experiment 3.2 .....	81
Figure 94: Setting procedure of failed cement plug .....	82
Figure 95: Depth vs. temperature change for each cable .....	83
Figure 96: Time vs. temperature change .....	83
Figure 97: Strain vs. depth for each cable .....	84
Figure 98: Time vs. Strain .....	84
Figure 99: Time vs. strain for different compensation at position 0,2 m .....	85
Figure 100: Performing CT-scan of contaminated cement plug .....	86
Figure 101: CT-scan of contaminated cement plug; 3D view (A); radial cross-section bottom (B); radial cross-section top (C).....	86
Figure 102: CT-scan: cable#1 (A); cable#2 (B); cable#3 (C); cable#4 (D) .....	87
Figure 103: Bottom-plate dimensions.....	93
Figure 104: Top-plate dimensions .....	93
Figure 105: Overall design .....	94
Figure 106: Modified bottom-plate dimensions.....	94
Figure 107: Experiment 3.1: 3D-plot of temperature change, cable #1 (A), cable #2 (B), cable #3 (C), cable #4 (D).....	95
Figure 108: Experiment 3.1: 3D-plot of strain, cable #1 (A), cable #2 (B), cable #3 (C), cable #4 (D) .....	95
Figure 109: Experiment 3.2: 3D-plot of temperature change, cable #1 (A), cable #2 (B), cable #3 (C), cable #4 (D).....	96
Figure 110: Experiment 3.2: 3D-plot of strain, cable #1 (A), cable #2 (B), cable #3 (C), cable #4 (D) .....	96





# List of Tables

Table 1: Compound specific heat of hydration (Swaddiwudhipong, Chen, and Zhang 2002),("Table 1 . Chemical Composition of Ordinary Portland Cement." n.d.) .....	25
Table 2: Cement slurry preparation table .....	35
Table 3: Mud slurry preparation table .....	36
Table 4: Mud design for experiment 2 .....	43
Table 5: Rheological data of mud for experiment 2 .....	44
Table 6: Cement slurry design experiment 2.....	45
Table 7: Rheological data of cement slurry experiment 2.1.....	45
Table 8: Slurry design experiment 2.2.....	48
Table 9: Slurry design experiment 2.3.....	50
Table 10: Slurry design experiment 2.4.....	51
Table 11: Slurry design experiment 2.5.....	52
Table 12: Slurry design experiment 2.6.....	54
Table 13: Slurry design experiment 2.7.....	55
Table 14: Slurry design experiment 2.8.....	56
Table 15: Experiment 3.1: Polymer mud design .....	62
Table 16: Experiment 3.1: Rheological data of the polymer mud.....	63
Table 17: Experiment 3.1: Bentonite mud design .....	64
Table 18: Experiment 3.1: Weight agent.....	64
Table 19: Experiment 3.1: Rheological data of the base fluid.....	64
Table 20: Experiment 3.1: Cement slurry design .....	65
Table 21: Experiment 3.1: Rheological data of the cement slurry .....	66
Table 22: Experiment 3.2: Polymer mud design .....	77
Table 23: Experiment 3.2: Rheological data of the polymer mud.....	77
Table 24: Experiment 3.2: Bentonite mud design .....	78
Table 25: Experiment 3.2: Weight agent.....	78
Table 26: Experiment 3.2: Rheological data of the base fluid.....	79
Table 27: Experiment 3.2: Cement slurry design .....	79
Table 28: Experiment 3.2: Rheological data of the cement slurry.....	80